University of Massachusetts Amherst
ScholarWorks@UMass Amherst

Doctoral Dissertations 1896 - February 2014

1-1-2005

Functionalized quantum dots for dispersion in polymers and cross-linking at interfaces.

Habib, Skaff
University of Massachusetts Amherst

Follow this and additional works at: https://scholarworks.umass.edu/dissertations_1

Recommended Citation
Skaff, Habib,, "Functionalized quantum dots for dispersion in polymers and cross-linking at interfaces." (2005). *Doctoral Dissertations 1896 - February 2014*. 1072.
https://scholarworks.umass.edu/dissertations_1/1072

This Open Access Dissertation is brought to you for free and open access by ScholarWorks@UMass Amherst. It has been accepted for inclusion in Doctoral Dissertations 1896 - February 2014 by an authorized administrator of ScholarWorks@UMass Amherst. For more information, please contact scholarworks@library.umass.edu.

UMASS/AMHERST
312066 0288 8678 7

FUNCTIONALIZED QUANTUM DOTS FOR DISPERSION IN POLYMERS AND CROSS-LINKING AT INTERFACES

A Dissertation Presented

By

HABIB SKAFF

Submitted to the Graduate School of the
University of Massachusetts Amherst in partial fulfillment
of the requirements for the degree of

DOCTOR OF PHILOSOPHY

February 2005

Polymer Science and Engineering

© Copyright by Habib Skaff 2005

All Rights Reserved

FUNCTIONALIZED QUANTUM DOTS FOR DISPERSION IN POLYMERS AND CROSS-LINKING AT INTERFACES

A Dissertation Presented

By

HABIB SKAFF

Approved as to style and content by:

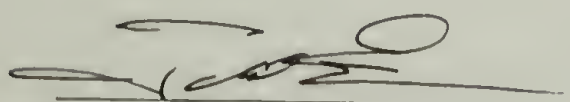

Todd S. Emrick, Chair

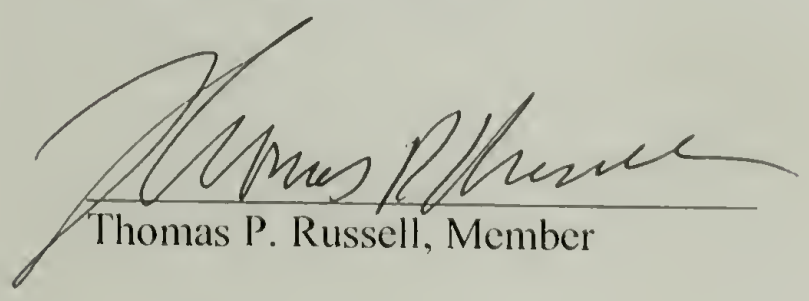

Thomas P. Russell, Member

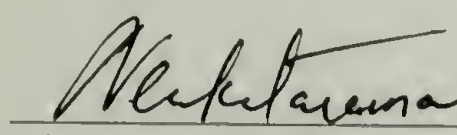

Dhandapani Venkataraman, Member

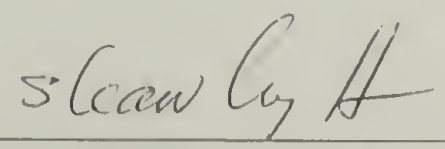

Shaw L. Hsu, Department Head
Polymer Science and Engineering

DEDICATION

In memory of Elias Skaff, Habib A. Skaff, and Farid J. Shaya

ACKNOWLEDGMENTS

I would like to thank my advisor, Todd Emrick, for taking a chance on an engineer and having the patience to guide me throughout my research career. Your friendship and guidance mean a great deal to me, and it will never be forgotten. I would also like to extend my gratitude to the other members of my committee, Thomas P. Russell and Dhandapani Venkataraman. You have been very helpful through all levels of my research, and I would like to thank you for your direction, helpful comments, and suggestions.

I want to thank the Eastman Kodak Company for providing funding for much of this research. I would especially like to thank John Pochan and Steve Switalski, whose expertise and guidance were invaluable to this work.

A special thanks to all my friends and family for their continual support and friendship which has helped me stay focused on this work and whose encouragement has made this journey worth doing.

ABSTRACT

FUNCTIONALIZED QUANTUM DOTS FOR DISPERSION IN POLYMERS AND CROSS-LINKING AT INTERFACES

FEBRUARY 2005

HABIB SKAFF, B.S., UNIVERSITY OF FLORIDA

M.S., UNIVERSITY OF MASSACHUSETTS AMHERST

Ph.D., UNIVERSITY OF MASSACHUSETTS AMHERST

Directed by: Professor Todd Emrick

Quantum dots are attractive potential components for next generation technologies such as light emitting diodes, sensors, and photovoltaic cells due to their unique and tunable electro-optical properties. The effective integration of quantum dots into devices requires a stable dispersion or self-assembly of the quantum dots in the solid-state. Such dispersions or assemblies are dictated by the interactions between the ligand environment of the quantum dots and the chosen polymer matrix. This thesis will highlight key contributions to the area of tailored cadmium selenide nanocrystals through the use of novel, functionalized ligands. This includes the utilization of ring-opening metathesis polymerization (ROMP), reversible addition fragmentation chain-transfer (RAFT) polymerization, and metal mediated couplings to control the polymer composition and molecular weight in radial polymerizations from CdSe nanocrystals. CdSe quantum dots were also found to assembly at the interface of immiscible fluids, and through appropriately functionalization these assemblies were effectively cross-linked. The key finding in this work is the retention of the inherent quantum dot fluorescence following these polymerization methods.

TABLE OF CONTENTS

ACKNOWLEDGMENTS ..... Page v

ABSTRACT vi

LIST OF TABLES ix

LIST OF FIGURES x

CHAPTER

1. INTRODUCTION 1

    1.1 Quantum Dot Synthesis and Their Incorporation into Composite materials. 3
    1.2 Synthesis of Cadmium Selenide Nanocrystals 7
        1.2.1 Room Temperature Synthetic Methods 7
        1.2.2 High Temperature Organometallic Syntheses 9
    1.3 Integration of Quantum Dots into Polymer Materials 12
        1.3.1 Polymer-Quantum Dot Blends 13
        1.3.2 Growth of Quantum Dots in Polymers 17
        1.3.3 Chain-End Attachment of Polymers to Quantum Dot Surfaces ... 18
        1.3.4 Radial Growth of Polymers From Quantum Dot Surfaces 21
        1.3.5 Self- and Directed-Assembly of Quantum Dots 22
    1.4 Summary and Future Outlook 23

2. DISPERSION OF QUANTUM DOTS IN POLYMER MATERIALS – A GRAFTING FROM APPROACH 26

    2.1 Introduction 26
    2.2 Ring-Opening Metathesis Polymerization (ROMP) From CdSe Nanocrystals 27
    2.3 Reversible Addition Fragmentation Chain Transfer (RAFT) Polymerization from CdSe Nanocrystals 37

3. WATER SOLUBLE CADMIUM SELENIDE NANOCRYSTALS PREPARED BY FUNCTIONALIZATION WITH PEG-SUBSTITUTED PYRIDINE 45

    3.1 Introduction 45
    3.2 Amphiphilic CdSe Nanocrystals 47
    3.3 Future Work 54

4. CONJUGATED POLYMER-QUANTUM DOT COMPOSITES 56

    4.1 Introduction 56
    4.2 CdSe Nanocrystals Tailored with Poly(phenylene vinylene) 58

4.3 Summary and Future Outlook 67

5. DIRECTED AND SELF-ASSEMBLY OF CdSe NANOCRYSTALS 70

5.1 Assembly of CdSe Nanocrystals in Polymer Templates 74
5.1.1 Directed-Assembly of CdSe Nanocrystals Using Diblock Copolymer templates 75
5.1.2 Simultaneous Self-Assembly of CdSe Nanocrystals and Block Copolymers 80
5.2 Interfacial Assembly of Nanocrystals in Immiscible Fluids 83
5.2.1 Cross-linked Nanocrystal Sheets by Radical Polymerization of the Fluid-Fluid Interfacial Assemblies 88
5.2.2 Cross-linking of CdSe Nanocrystals on Water Droplets to Give Robust Capsules 92
5.3 Future Outlook 98

6. EXPERIMENTAL 100

6.1 Chapter 2 Experimental 100
6.2 Chapter 3 Experimental 104
6.3 Chapter 4 Experimental 106
6.4 Chapter 5 Experimental 109

REFERENCES 113

BIBLIOGRAPHY 119

LIST OF TABLES

Table

Page

1. Polymers successfully grown from the quantum dot surface.....41

LIST OF FIGURES

Figure

Page

1.1 Exciton formation induced by the absorption of energy....3

1.2 Schematic comparison of the electronic states of bulk semiconductors *vs.* quantum dots....4

1.3 Size dependence of absorption for CdSe nanocrystals as a result of quantum confinement. As the nanocrystal diameter increases the bandgap decreases. Reprinted from *J. Phys. Chem. Solids* Volume 59, Brus, L, pp 459-465, Copyright 1998, with permission from Elsevier Science....5

1.4 Photoluminescence spectra illustrating the more narrow and symmetric emission of CdSe quantum dot (red) in relation to Rhodamine B (black) 6

1.5 Synthesis of high quality CdSe nanocrystals developed by Bawendi and coworkers.10

1.6 (a) Overcoating of CdSe nanocrystals core with a ZnS shell; (b) the larger bandgap ZnS shell provides a protective layer for the CdSe core....11

1.7 TEM micrograph of (a) CdSe nanocrystals/unfunctionalized poly(3-hexyl thiophene) blend cast from a binary solvent system,and (b) CdSe nanocrystals blended with amine functionalized poly(3-hexyl thiophene) 14

1.8 Synthesis of amine functionalized poly(3-hexyl thiophene) 15

1.9 Diblock copolymer architecture containing quantum dot-coordinating phosphine or phosphine oxide moieties....16

1.10 Dendrimer encapsulated CdSe nanocrystals with hydroxyl periphery 20

2.1 Synthesis of ligand **1** 28

2.2 Transmission electron micrograph of **1**-covered CdSe nanocrystals....29

2.3 Functionalization of catalyst 2 by ligand exchange with compound 1 30

2.4 Selected region of ^{1}H NMR spectra showing the ruthenium benzylidene proton of compound **2** (top); **2** and metathesis exchange product (middle); and the CdSe-poly(cyclooctene) composite (bottom) 31

2.5 Initially, TOPO-covered CdSe nanocrystals are stripped of their aliphatic periphery and replaced with ligand **1**. Addition of Ru catalyst yield macrointiator **5** and subsequent monomer addition gives composite material **6** 32

2.6 Absorbance and photoluminescence spectra of **1**-functionalized CdSe nanocrystals (left) and polycyclooctene functionalized CdSe nanocrystals (right).....35

2.7 (a) **1**-functionalized CdSe nanocrystals, (b) polycyclooctene covered CdSe nanocrystal composite material, (c) nanocrystal-polycyclooctene composite material after annealing at 95 °C for 17 hrs, (d) TOPO-covered CdSe nanocrystals in a polycyclooctene matrix 36

2.8 Procedure for the synthesis of ligand **10**. The first step depicts the hydrophosphorylation of DOPO to give **8**, and the second step depicts the CDI coupling of **8** and **9** to give ligand **10** 38

2.9 Absorption and fluorescence spectra of **(a) 10**-covered CdSe nanocrystals, **(b)** poly(methyl acrylate)-covered CdSe nanocrystals, and **(3)** poly(styrene)-covered CdSe nanocrystals in toluene 42

2.10 Transmission electron micrographs of **(a)** poly(styrene)-covered CdSe nanocrystals prepared by the RAFT technique in poly(styrene), and **(b)** TOPO-covered CdSe nanocrystals in poly(styrene) prepared by RAFT 43

3.1 Mitsunobu coupling of PEG and 4-hydroxy pyridine to yield of ligands **11** and **12**...48

3.2 Schematic representation of two different ligand exchange chemistries used to convert TOPO-covered CdSe nanocrystals to PEG-pyridine covered CdSe nanocrystals.....50

3.3 Absorbance and photoluminescence spectra of **11**-functionalized CdSe nanocrystals in (a) CH_2Cl_2 and (b) water.....51

3.4 Absorbance profiles of PEG-pyridine covered CdSe nanocrystals in water, showing little change in the first exciton absorbance over several days of irradiation. The spectra are not normalized; solvent evaporation results in the observed increase in absolute absorption 52

4.1 Synthesis of **13**-covered CdSe nanocrystals and their subsequent functionalization with PPV 58

4.2 a) Transmission electron micrograph of **13**-functionalized CdSe nanocrystals at 650 K magnification. The lattice structure observed, as well as the electron diffraction pattern (inset) illustrates the crystalline nature of the quantum dots; b) UV-Vis (blue curve, band-edge absorption at 550 nm) and photoluminescence spectra (red curve, emission maximum at 570 nm; FWHM 30 nm) of **13**-covered quantum dots 60

4.3 TEM micrographs and fluorescence spectra (excitation 330 nm; blue curve represents solution state fluorescence and red curve represents solid state fluorescence) of PPV-quantum dot hybrid materials. a) Pyridine-covered CdSe nanocrystals blended with PPV, b) **13**-functionalized CdSe nanocrystals blended with PPV, and c) composite CdSe nanocrystal-PPV, where PPV was grown from the nanocrystal surface. Each sample contained approximately 5 wt. % nanocrystal 63

4.4 The effect of **13**-functionalized CdSe nanocrystal loading (wt %) on the solid state fluorescence emission spectra of CdSe-PPV oligomer blends 64

4.5 Photoluminescence spectrum of PPV-CdSe nanocrystal composite material excited at 350 nm. Emission of the quantum dot observed at 555 and 600 nm and shows two emission maxima 65

4.6 (a) Photoluminescence (excitation at 400 nm) and (b) excitation (emission at 700 nm) spectra of PPV functionalized CdSe nanocrystals..... 67

5.1 A schematic representation of CdSe nanocrystal assembly at a water droplet-solution interface during formation of a "breath figure." (A) Initially a small droplet of water condenses on the nanocrystal/polystyrene solution and (B) Subsequent segregation of the nanocrystals to the interface and evaporation of the solvent traps the nanocrystal at the polymer-air interface, thereby functionalizing only the surface of the holes. (C) confocal fluorescence microscope images of a sample obtained from solvent casting a chloroform solution of 7 wt.% PS (76 k) and 1 wt.% 4 nm TOPO-covered CdSe nanocrystals at 80% relative humidity. Scale bars: 16μm. The inset in C shows a fluorescence intensity scan along the line indicated..... 74

5.2 (A) Procedure for the deposition of nanocrystals into nanoporous block copolymer template by withdrawal from a heptane solution of TOPO-covered CdSe nanocrystals. (B) The photoluminescence spectra of the CdSe nanocrystal filled templates demonstrating that higher solution concentration in the dipping process gave templates with stronger emission signals. Solutions 1, 2, and 3 are 65, 130, and 240 μg/ml, respectively..... 77

5.3 TEM micrographs showing the effects of solution concentration and withdrawal rate are shown above. The deposition of 5 nm particles solutions of (A) 240 μg/ml, (B) 130 μg/ml, and (C) 65 μg/ml (at ca. 20 cm/s). (D) 10 nm nanocrystals deposited into the polymer template illustrating the possibility of placing one particle per pore. The scale bar represents 20 nm..... 79

5.4 TEM image of **12**-covered CdSe nanocrystals dispersed in a PMMA matrix..... 81

5.5 (A) **12**-covered and (B) **11**-covered CdSe nanocrystals assembled in a P(S-*b*-PMMA) copolymer template..... 82

5.6 Confocal microscope image of TOPO-covered CdSe nanocrystal assembled at the interface of oil and water. (A) Confocal image of different size droplets, (inset) fluorescence image of nanocrystals assembled on a water droplet of sulforhodamine-B dye. Channel 1 represents fluorescence from the nanocrystals and channel 2 represents fluorescence from the dye. (B) Confocal cross-sectioning of a an individual droplet illustrating its spherical nature.....86

5.7 Three-dimensional reconstruction of confocal microscope image of 2-D phase separation of 2.8 nm particles (green) and 4.6 nm particles (red) assembled at the interface of oil and water. The scale bar, 16 μm.....87

5.8 Confocal microscope image of a sheet of cross-linked **1**-functionalized nanocrystals. The scale bar is 16 μm 89

5.9 Digital photographs of organic dye (red solution) (A) placed on top of a cross-linked interfacial assembly of CdSe nanocrystals, (B) additional dye is added, (C-D) diffusion of the dye through the membrane in a nonconvective fashion.....91

5.10 Confocal microscope image of **1**-covered nanocrystals cross-linked at the water-oil interface. The scale bar is 40 μm 92

5.11 Synthesis of norbornene ligand **15**.....93

5.12 (A) Procedure for cross-linking **15**-functionalized CdSe/ZnS core/shell nanocrystals using a water-soluble ruthenium catalyst to give cross-linked nanocrystal capsules. (B) Structure of water soluble ring-opening metathesis catalyst **16** 95

5.13 Confocal microscope images of cross-linked CdSe nanocrystals **(a)** assembled at the oil-water interface and **(b)** after the removal of the interface by addition of methanol (fragments of ruptures capsules can be seen in the background).....96

5.14 Transmission electron micrographs of cross-linked CdSe nanocrystal assemblies. **(a)** Low magnification image of a dried nanocrystal capsule showing the retention of the capsule shape after drying. **(b)** High magnification image of a region of the same capsule showing the liquid-like assembly of nanocrystals and the nanoporous nature of the capsule. The inset electron diffraction pattern in **(b)** confirms the presence of nanocrystals 97

CHAPTER 1

INTRODUCTION

The technological advances of our modern society are proceeding at an extraordinary pace that is possibly unmatched by any prior historical era. However, a continuation of such advances places enormous demands on research scientists in terms of the discovery and development of new technologies, materials, medicines, devices, and the like. The emerging fields of nanoscience and nanotechnology are focused especially on materials with dimensions less than 100 nm. This "nano" focus promises to continue delivering these rapid advances simply by the fabrication of devices with ever smaller, yet well defined features. These smaller sizes lead predictably to increased surface area to volume ratios of the nanostructured materials, in turn increasing interfacial surface area (*i.e.* more interface is formed).[1]

This increase in surface area of the nanostructured materials is very significant for many technological applications, *e.g.* light emitting diodes, microprocessors, and computer memory storage,[2] because these device surfaces are responsible for many of the salient functions and properties of the device. In the semiconductor industry, the fabrication of materials with ever smaller feature sizes increases the number of functional components over a given area, which allows processors to perform tasks more quickly, and leads to a massive increase in memory storage. Research in nanoscience and nanotechnology is focused in large part on reaching the lower limits of size that simultaneously provides the upper limits of device performance.

The two primary methods for preparing nanoscale structures are "bottom-up" and "top-down." The bottom-up approach uses small building blocks as starting materials and assembles them into larger structures. Examples of bottom-up methods include chemical synthesis,[3,4] laser-induced assembly (i.e., laser-trapping),[5,6] self-assembly,[7] colloidal aggregation,[8] and 2-photon confocal processing.[9,10] In the top-down approach large objects are modified to give smaller features by destruction of a portion of the original structure. Examples of the top-down approach include lithographic techniques[11] (e.g., UV, electron or ion-beam, scanning probe, optical near field), film deposition and growth,[12] laser-beam processing,[13,14] and mechanical techniques (e.g., machining, grinding, and polishing).[15] While the bottom-up method allow for the formation of structures that possess extremely fine features, there are complexities associated with this method that must be addressed in order to improve the practical aspects of the method. In contrast, the top-down technique has been successfully adapted to the industrial scale, and optimization of this method has produced well-defined structures on size scales previously thought reachable only by bottom-up methods. However, top-down techniques are expected to reach an inherent size limit that is larger than that of bottom-up techniques. Thus, future advances in fabrication of devices with extraordinarily fine detail will require the integration of bottom-up methods rather than top-down methods.

Nanotechnology holds tremendous promise for the semiconductor research field. Semiconductor materials have already revolutionized modern day computation and electronics, with applications ranging from computer chips to light emitting diodes, and sensors. This unique class of materials can assume the characteristic properties of both

metals and insulators. In the ground state, the valence band or the highest occupied molecular orbital (HOMO), is filled with electrons, and separated from the conduction band, or the lowest unoccupied molecular orbital (LUMO), by a narrow band gap (E_g). In the ground state, semiconductors exhibit properties of an insulator. Excitation of a semiconductor promotes an electron from the valence band to the conduction band, leading to exciton formation, defined as a neutral bound electron-hole pair. In the presence of an electric field, the exciton can dissociate by migration of the electron and hole in opposite directions in the conduction and valence bands, respectively (Figure 1.1).[1,2]

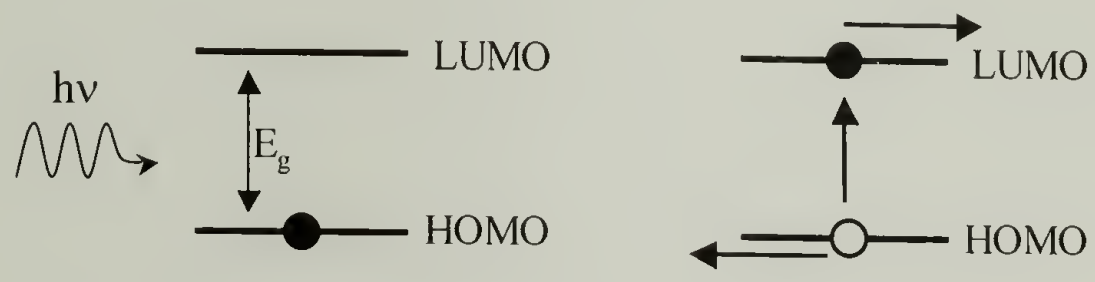

Figure 1.1: Exciton formation induced by the absorption of energy

1.1 Quantum Dot Synthesis and Their Incorporation into Composite Materials

Recent research focused on semiconductor materials with nanometer scale dimensions has led to the preparation of a fascinating class of novel materials that possess characteristics of both bulk and molecular semiconductors. These semiconductors are nanocrystalline materials, often spherical in shape, that exhibit properties of quantum confinement, and are thus often referred to as "quantum dots." Quantum confinement is observed in nanocrystals with radii smaller than the average distance between the electron and the hole, known as the bulk exciton Bohr radius. In the case of cadmium selenide semiconductor nanocrystals used extensively in this thesis, this distance is about 11 nm. The electronic states of spherical nanocrystals can

thesis, this distance is about 11 nm. The electronic states of spherical nanocrystals can be understood by the particle in a box model. The electron and hole are confined to a relatively small area by a potential that is infinite at the nanocrystal surface. As a result, semiconductors of nanoscopic dimensions have larger band gaps than bulk material, and have discrete energy levels (Figure 1.2).[16-27] Such features are characteristic of the molecular regime rather than the bulk. The intermediate nature of quantum dots, with characteristics of both bulk and molecular materials, explains the enthusiasm that drives the exploration of quantum dot based applications.

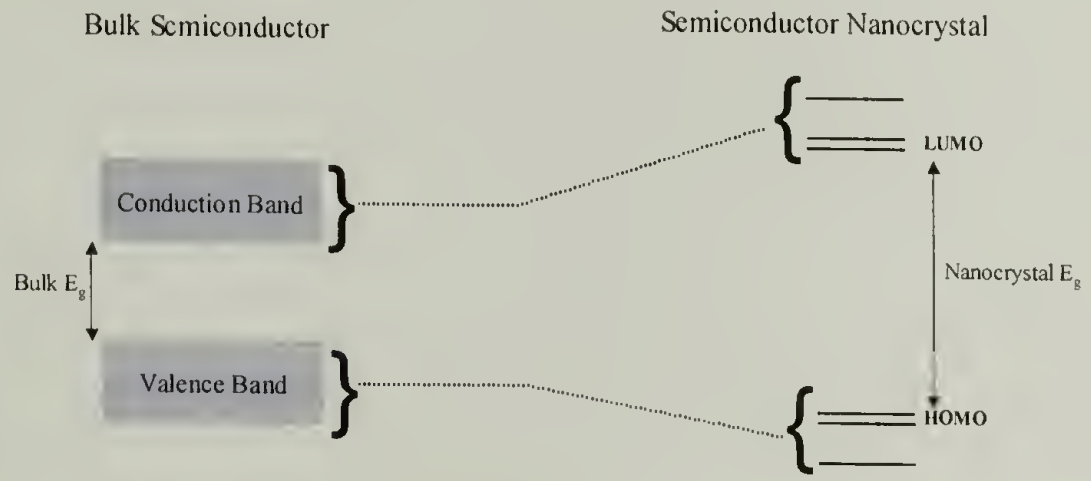

Figure 1.2: Schematic comparison of the electronic states of bulk semiconductors *vs.* quantum dots

The band gaps of quantum dots are strongly size-dependent, such that as the radius of the nanocrystal decreases, the band gap increases (Figure 1.3). This is a very exciting feature of quantum dots, as it allows for tunable absorption and photoluminescence emission wavelengths simply by adjusting nanocrystal size, within the quantum-confined regime.[20,28-35] This unique property affords a technological significance to semiconductor nanocrystals in areas ranging from light emitting diodes to cancer-detection devices. All of these prospective nanocrystal-based technologies

rely on the solubility and/or the processibility of the nanocrystals. Methods to control such nanocrystal properties will be addressed at multiple levels throughout this thesis.

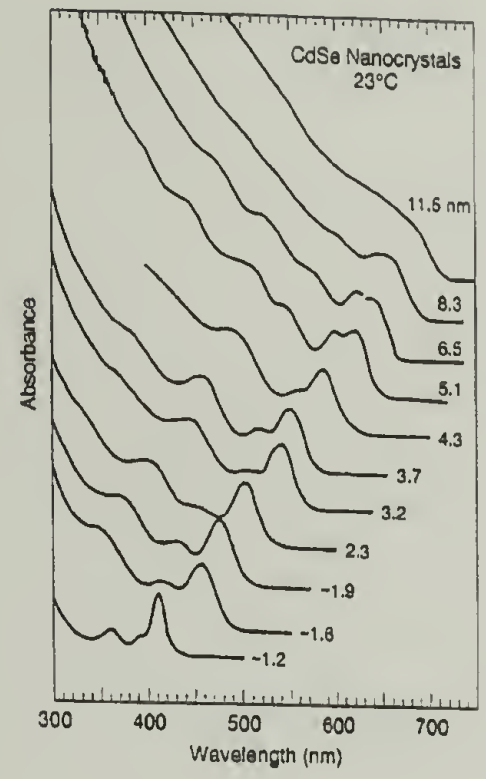

Figure 1.3: Size dependence of absorption for CdSe nanocrystals as a result of quantum confinement. As the nanocrystal diameter increases the bandgap decreases. Reprinted from *J. Phys. Chem. Solids* Volume 59, Brus, L, pp 459-465, Copyright 1998, with permission from Elsevier Science

Quantum dots of a variety of compositions have been prepared, including for example CdSe, CdS, Si, GaAs, PbSe, and InP. These are sp^3 hybridized structures that experience little lattice distortion upon exciton formation,[29] which limits the presence of defects and allows for fluid movement of charge carriers throughout the nanocrystal. In addition, radiationless internal conversion, or the conversion of electronic energy into heat, is slow. These factors, coupled with the quantum confined nature of the nanocrystals, afford a photoluminescence to quantum dots that is quite unlike that found in bulk semiconductors or organic molecules (Figure 1.4). Despite these unique and impressive features, quantum dots are far from ideal, as they suffer from problems that must be addressed in current research efforts. Their photoluminescence intensity is

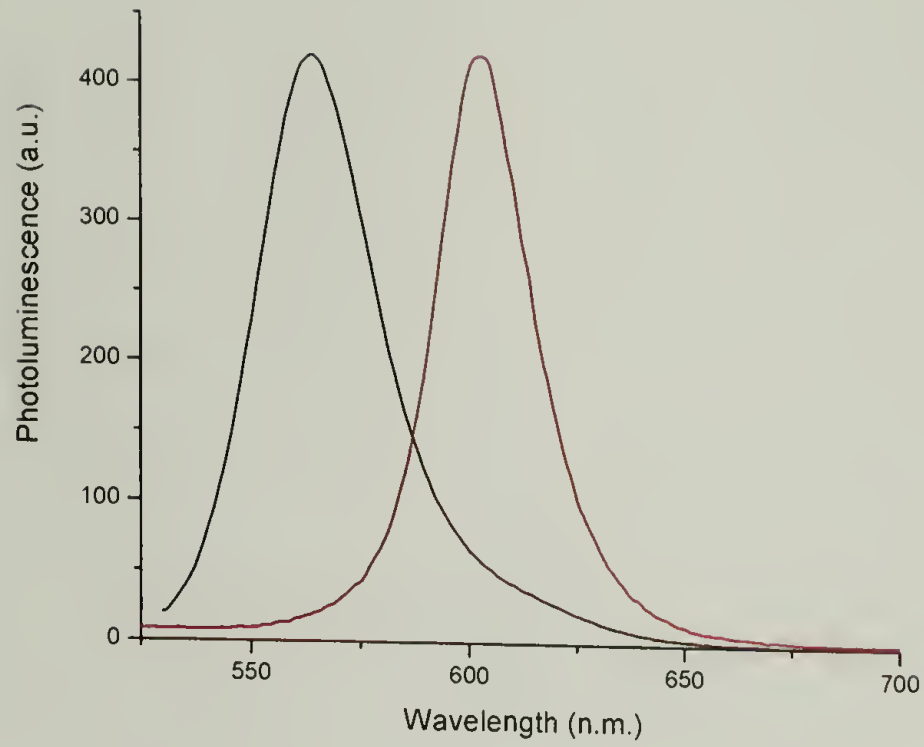

Figure 1.4: Photoluminescence spectra illustrating the more narrow and symmetric emission of CdSe quantum dot (red) in relation to Rhodamine B (black)

reduced by internal and surface defects that arise from their syntheses. These defects function as electron and hole traps, and lead to non-radiative emission and reduced photoluminescence. Typical solution quantum yields of high quality, organically passivated semiconductor nanocrystals prepared by methods described in the literature are in the range of 5-15%.

This introductory chapter describes the synthesis of CdSe nanocrystals from early procedures to state-of-the-art methods. The integration of quantum dots into polymers will be described, evolving from simple techniques such as blending the two components, to the more sophisticated "grafting-to" and "grafting-from" approaches. Finally, the directed-assembly of quantum dots in polymer materials will be introduced. The use of polymers offers great potential in manipulating the spatial arrangement and properties of nanocrystals, where the interplay between the polymeric and nanocrystal components, in terms of nanocrystal surface chemistry and particle-particle interfacial

interaction is key. Much of the work in this thesis on polymer-nanocrystal composite preparation will be of great importance for the future of the composite directed-assembly field.

1.2 Synthesis of Cadmium Selenide Nanocrystals

In general, nanocrystal syntheses have been performed by both top-down and bottom-up approaches. While the top-down approach has long been the favored technique for large scale commercial materials for its simplicity, scalability, and cost-effectiveness, the bottom-up approach is evolving into the favored approach in the academic as well as the newer industrial environment in part as a result of continual improvements in synthetic protocols over the past twenty years. Synthetic improvements for CdSe nanocrystals have been pursued with particular vigor, and their extraordinary properties have become better understood as better syntheses developed, from early examples of room temperature methods, to state-of-the-art high temperature procedures in use today.

1.2.1 Room Temperature Synthetic Methods

Seminal contributions in the area of CdSe quantum dots were provided by Brus and coworkers at Bell laboratories in the 1980's. Their initial work focused on room temperature nanocrystal preparations in inverse micelles, with an organic solvent (*e.g.*, heptane) as the major phase, and water as the minor phase. Typical procedures involved vigorous stirring of surfactant (such as bis(2-ethylhexyl) sulfosuccinate) stabilized heptane/water mixtures to afford optically clear microemulsions. Injection of aqueous $Cd(ClO_4)_2$ followed by heptane solution of $(TMS)_2Se$ gave the desired nanocrystalline materials. This inverse micellar approach was used to tune quantum dot

size over the range of 1.7-4.5 nm by simply adjusting the micelle size as dictated by the water-to-surfactant ratio.[36,37]

Synthetic control over quantum dot size is of particular importance given their size-dependent optoelectronic properties. However, the materials produced in these early experiments were difficult to isolate, as irreversible aggregation occurred in the dried samples and the nanoscopic nature of the particles was lost. This aggregation problem was addressed by Henglein and coworkers by precipitation of the CdSe nanocrystals in the presence of polymeric hexametaphosphate, which provided an encapsulating shell to the nanocrystals, leading to improved solubility and a decreased tendency to aggregate.[38] In separate experiments, Brus and coworkers used an *in situ* modification of the nanocrystal surface, where the micellar-based synthesis described previously was followed by a second addition of $Cd(ClO_4)_2$, and finally the addition of Ph(TMS)Se. This "monofunctional" selenium reagent acts as an end-capper in the quantum dot growth procedure, and provides a phenyl periphery to the nanocrystal structure. The phenyl groups at the nanocrystal periphery prevent aggregation during isolation, and provides longer-term solubility to the nanocrystal relative to the uncapped samples. These key studies led to new perspectives in the nanocrystal chemistry that emphasized the importance of the peripheral chemistry. Such methods are critical for advancing quantum dot-based technologies. The extent to which the nanocrystal periphery can be tailored will dictate success or failure in many applications, and it is this "tailoring" that forms the main thrust of this thesis.

1.2.2 High Temperature Organometallic Syntheses

Critically important to quantum dot research is the development of preparative methods that afford quantum dots with high crystallinity and very narrow size dispersity. Early synthetic procedures were unsatisfactory, as relatively broad size distributions were typically obtained, due to unfavorable kinetics and size dispersity of the inverse micelles. While fractional precipitation significantly reduced size dispersity, this also reduces the yield, and does not improve the crystallinity of the materials.

Synthetic advances developed by Bawendi and coworkers directly addressed the problems of size distribution and crystallinity.[39] Key to this advance is the separation of the nucleation and growth steps. In their new methods nucleation occured in a fast burst by rapid injection of reactive organometallic precursors, *e.g.*, dimethyl cadmium and selenium/tri-*n*-octyl phosphine, in a hot coordinating solvent/surfactant, *i.e.* tri-*n*-octylphosphine oxide (TOPO). The nuclei grow at a uniform rate, resulting in a narrow size distribution in the product (ca. 5 - 10%). TOPO, by virtue of its surfactant nature, provides an inverse micellar environment for nanocrystal growth. TOPO also serves to stabilize the isolated nanocrystals by coordination to surface cadmium atoms. This surface passivation simultaneously prevents aggregation and provides solubility in organic media.

The high-temperature "TOPO"-based CdSe nanocrystal preparation remains in common use today though the choice of Cd source now varies considerably. A typical procedure involves the injection of a tri-*n*-octyl phosphine (TOP) solution of $Cd(CH_3)_2$ and $(TMS)_2Se$ (or Se(0) powder) into a rapidly stirred solution of TOPO at 300 °C under an inert atmosphere (Figure 1.5). This injection immediately results in rapid

nucleation, followed by uniform particle growth at a temperature-dependent rate. Nanocrystal growth is terminated at the desired size by removal of the heat source. The high temperatures employed in this synthesis are advantages for both the growth kinetics, and for the annealing of the nanocrystalline structures that occur at these temperatures, serving to reduce defects and give highly crystalline materials. Repeated precipitation and washing of the nanocrystals, *e.g.* with methanol, removes excess TOPO from the mixture to give soluble, highly crystalline quantum dots with narrow size distribution. Similar preparative methods are used for CdS and CdTe nanocrystals, by substitution of the appropriate organometallic precursor for $(TMS)_2Se$, *e.g.* $(TMS)_2Te$ and $(TMS)_2S$.

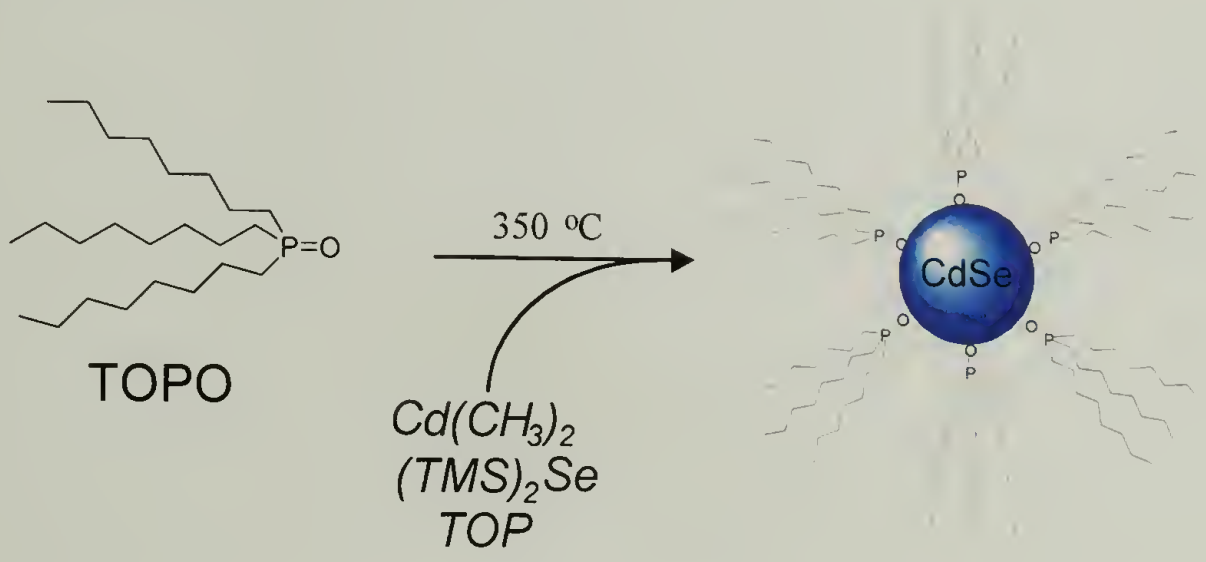

Figure 1.5: Synthesis of high quality CdSe nanocrystals developed by Bawendi and coworkers

High temperature syntheses give nanocrystals with narrow size distributions, high crystallinity, and few internal defects. However, these nanocrystals have relatively low quantum yields, typically in the range of 5 to 15%. This low quantum yield is attributed to surface defects, or "dangling bonds," (electron pairs with no coordinating group attached) that act as charge carrier traps and ultimately result in non-radiative

recombination of electrons and holes. The groups of Alivisatos and Bawendi have independently addressed these surface defects by developing inorganic passivation procedures.[40,41] For example, CdSe nanocrystals can be overcoated with an inorganic shell composed of a larger band gap semiconductor, such as ZnS or CdS (Figure 1.6). This core/shell architecture eliminates CdSe surface defects and protects the CdSe nanocrystal core from oxidation. It is important to note that the core is almost wholly responsible for the absorption and emission characteristics of these systems, and the shell acts only to passivate the surface.

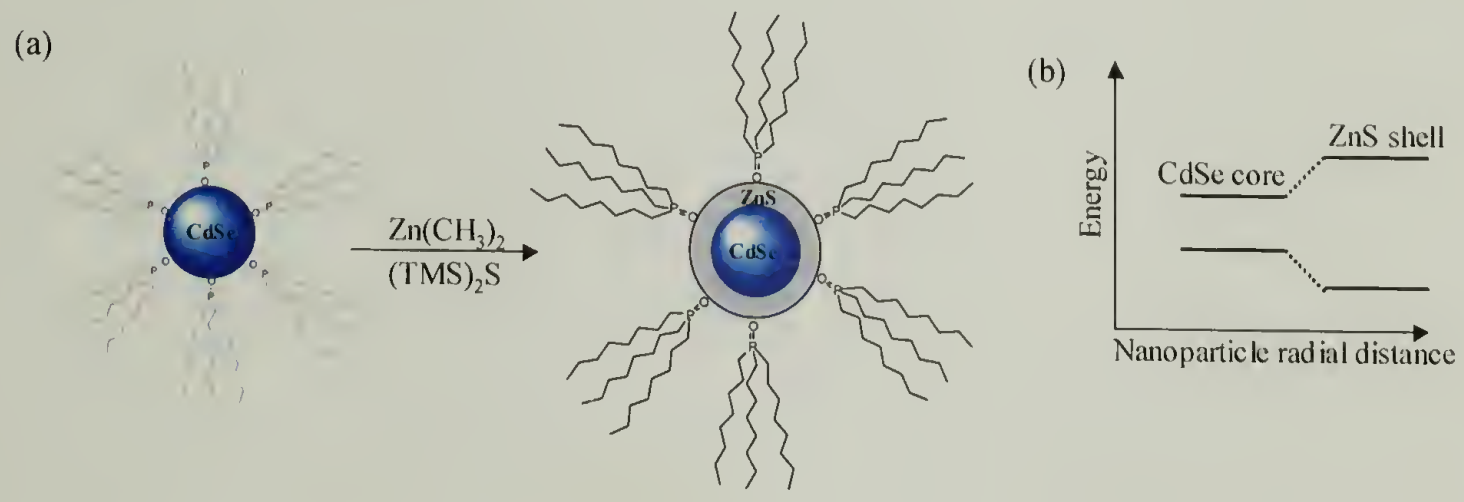

Figure 1.6: (a) Overcoating of CdSe nanocrystals core with a ZnS shell; (b) the larger bandgap ZnS shell provides a protective layer for the CdSe core

While the organometallic preparations described above produce high quality nanocrystals with high quantum yields, the pyrophoric and toxic nature of the precursors has, to some degree, limited their general accessibility and production on a large scale. Recent reports that employ less toxic and more stable cadmium precursors, such as CdO, $CdCO_3$, and $Cd(OAc)_2$, are quite valuable, especially as these methods are still able to provide high quality CdSe nanocrystals. While the use of these precursors requires high temperatures, the precursor chemicals are much easier to handle, and in

some cases these new procedures afford nanocrystals with quantum yields greater than 50%, even in the absence of an inorganic shell. These high quantum yields are attributed to a combination of factors, including the passivation of the nanocrystal surface by aliphatic amines used in the growth procedures, and control over the cadmium to selenium ratios (*i.e.,* the "emission bright point" increased as the Cd:Se ratio deviated from 1:1).[42-45]

1.3 Integration of Quantum Dots into Polymer Materials

Modification and manipulation of the organic ligand environment used to encapsulate and passivate quantum dots is clearly important for future developments in the field. The ligands establish the solution properties of the nanocrystals, enhance their luminescence by surface passivation, and maintain their nanoscopic integrity by preventing aggregation.[33,46-48] The integration of quantum dots into polymeric materials is one of the most interesting and challenging topics in organic-inorganic hybrid materials. The unique and varied properties of polymers, including their chemical structure, thermal behavior, processibility, and ability to assemble into ordered structures, offer the potential for compatibilizing nanocrystals, directing their assembly, and providing pathways for charge transport. The spatial distribution of nanocrystals within polymer matrices greatly depend on the interactions between the ligand periphery and the polymer environment, and has been a topic of extensive theoretical study by Balasz and coworkers.[49] In addition, polymer-nanocrystal composite materials, especially those using quantum dots, are already finding applications ranging from photovoltaics cells to biological sensors.[50-59] The following sections provide a

non-exhaustive review of some recent advances in the field of nanocrystal-polymer composites.

Four primary design strategies are used to integrate quantum dots into polymer matrices, including 1) the simple mixing or blending of quantum dots and polymers, 2) the synthesis of quantum dots within polymers, 3) the chain-end attachment of polymers to quantum dot surfaces, and 4) the growth of polymers directly from quantum dot surfaces. These four techniques share the common goal of dispersing quantum dots in polymer matrices, but differ in their level of effectiveness and sophistication. Each of these approaches has varying degrees of success and versatility, carrying certain advantages that best apply to particular targets.

1.3.1 Polymer-Quantum Dot Blends

The simplest method of incorporating quantum dots, or nanoparticles in general, into polymers is simply mixing the two components to give the blend or composite material. However, this technique is usually accompanied by significant nanocrystal aggregation. The disparate nature of polymers and nanocrystals precludes the production of a random, homogenous particle dispersion, as the entropic gain associated with such random dispersion is not sufficient to overcome the enthalpic penalty. Ultimately, phase separation in these composite materials destroys the nanoscopic integrity of the particles, and results in diminished properties of both the particles and polymer. Several methods have been considered to overcome, or at least control to some degree, the phase separation that occurs during this polymer-nanocrystal mixing process. For example, the incorporation of CdSe nanocrystals into poly(3-hexylthiophene) (P3HT) was explored by Alivisatos and coworkers.[55,56,60] In order to

avoid gross aggregation, the polymer and nanocrystals were dissolved together in a mixture of chloroform and pyridine, good solvents for the polymer and the nanocrystal, respectively. Thin films obtained by spin-casting these solutions afforded CdSe-based composites where gross aggregation was avoided, though uncontrolled segregation of the quantum dots in the polymer matrix were still observed (Figure 1.7(a)). As a potential solution to this nanocrystal segregation problem in quantum dot-polythiophene composites, efforts have been undertaken to end functionalize P3HT with an amine moiety.[61] In this chemical scheme, shown in Figure 1.8, a Stille coupling is used to

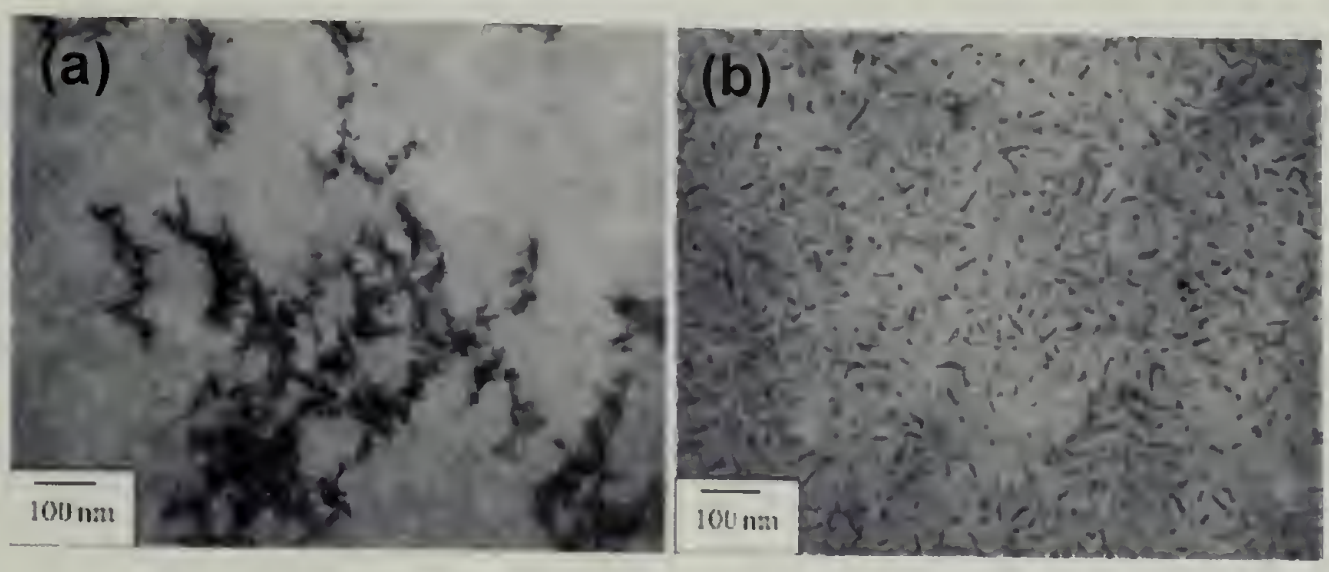

Figure 1.7: TEM micrograph of (a) CdSe nanocrystals/unfunctionalized poly(3-hexyl thiophene) blend cast from a binary solvent system,and (b) CdSe nanocrystals blended with amine functionalized poly(3-hexyl thiophene) Reprinted figure with permission from Huynh, W. U.; Dittmer, J. J.; Alivisatos, A. P. *Science* **2002**, *295*, 2425-2427. Copyright 2002 American Association for the Advancement of Science.

functionalize the chain-end of P3HT with a nitrile substituted thiophene. This nitrile group is subsequently reduced to a primary amine using lithium aluminum hydride.

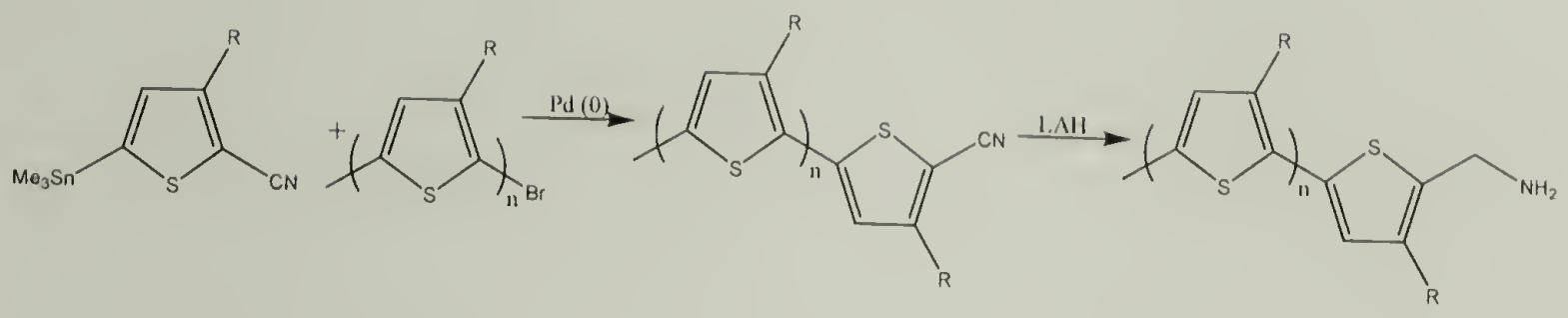

Figure 1.8: Synthesis of amine functionalized poly(3-hexyl thiophene)

Use of these chain-end functionalized polythiophenes minimizes quantum dot segregation within the polythiophene matrix (Figure 1.7b). Power conversion efficiency, the ratio of electrons generated to photons absorbed, in the dispersed case were found to be three times larger than that of the aggregated case. In the samples tested, it was found that a 40 wt% loading gave the highest power conversion efficiency, a result attributed to suppression of quantum dot aggregation, thereby allowing for a greater incorporation of polymer while still maintaining an interpenetrating network of nanocrystal and polymer.

Earlier efforts to combine polymers and nanocrystals used pendant functionalized polymers for nanocrystal passivation. For example, Schrock and coworkers prepared norbornene derivatives with pendant phosphines or phosphine oxides, and subsequently copolymerized these with methyltetracyclododecane by ring opening metathesis polymerization (ROMP) using a molybdenum alkylidene catalyst. This copolymerization gave a diblock copolymer with pendant functionality for nanocrystal passivation (Figure 1.9).[62] The polymer was then dissolved in THF with CdSe nanocrystals and cast into optically clear solutions and homogenous films. These functionalized norbornene monomers were also used in diblock copolymer syntheses,

with unfunctionalized norbornene as the second monomer. This gave a diblock with one functional and one non-functional block. Annealing and self-assembly of these diblock copolymers in the presence of nanocrystals resulted in nearly complete segregation of the nanocrystals into the functional block, as shown by TEM micrographs. This was a significant and early contribution to block copolymer-nanocrystal assemblies, as the authors showed control over nanocrystal patterning through phase-separation and self-assembly to generate a periodic array of nanocrystals. This contribution helped set the stage for future efforts focused on directing nanocrystals into higher order structures through the use of functional polymer materials, functional nanocrystals, and the principle of self-assembly.

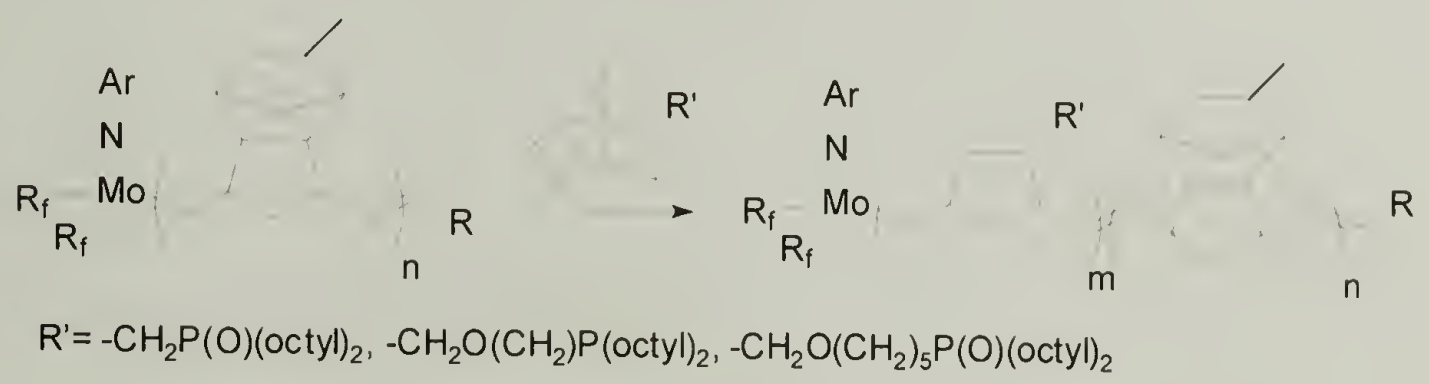

Figure 1.9: Diblock copolymer architecture containing quantum dot-coordinating phosphine or phosphine oxide moieties

In an alternate approach, Bawendi and coworkers adjusted the polymer structure to better match the alkyl periphery of conventional TOPO-covered CdSe nanocrystals. Specifically, poly(lauryl methacrylate) was blended with CdSe/ZnS core-shell nanocrystals encapsulated with TOP.[57] The aliphatic nature of the lauryl (dodecyl ester) side chains of this polymer serve to "solubilize" the quantum dots by favorable enthalpic interactions with their aliphatic (TOP) periphery. The benefit of this compatibilization is manifest in the optical clarity of the composites obtained upon

blending. Such optical clarity in these materials demonstrates the absence of large aggregates, though the degree of dispersion of the nanocrystals was not provided by TEM measurements. Reported solid-state quantum yields of these composites ranged from 22% to 44 %.

1.3.2 Growth of Quantum Dots in Polymers

The development of procedures whereby nanocrystals are grown in polymers to afford novel hybrid materials carries three potential advantages over simple blending techniques, including 1) the integration of nanocrystals in a polymer matrix in an unaggregated fashion, 2) the growth of nanocrystals in specific regions of the host polymer, and 3) the fabrication of nanocrystal gradients throughout a polymer matrix.

Polystyrene random ionomers with pendent carboxylic acids were used by Moffitt and coworkers to prepare CdS-polymer composites.[63] These random copolymers were cast as thin films in their ionized (carboxylate) form, then neutralized by soaking in a solution of cadmium acetate dihydrate allowing for penetration of Cd^{2+} ions into the polymer, after which the films were washed with a toluene/methanol mixture to remove excess salt. Treatment of these films with H_2S afforded CdS nanocrystals embedded in the random copolymer.

A more advanced system was developed by Douglas and coworkers to prepare CdS nanocrystals in salt-induced block copolymer micelles.[64] In this work, cadmium acetate was added to a THF solution of poly(styrene-*b*-2-vinylpyridine). The cadmium ions accumulated in the poly(2-vinylpyridine) block by complexation with the pyridine nitrogen, yielding a salt induced micelle. This micelle contains a Cd^{2+}/poly(2-vinylpyridine) core and a polystyrene corona, which upon addition of H_2S forms CdS in

the micelles. In a related approach "double hydrophilic" block copolymers have been explored as nanocrystal scaffolds by Antonietti and coworkers for the synthesis of CdS nanocrystals.[65] In this work, poly(ethylene glycol)-*b*-polyethyleneimine (PEG-b-PEI) copolymers were used, where the PEI block serves to stabilize the nanocrystals. In these methods, the block copolymer prevents aggregation and provide solubility to the particles, allowing this composite to be cast or processed as required.

While the methodologies described above are very useful for the preparation of polymer stabilized nanocrystals and higher order structures, the quality of the nanocrystals obtained by these methods is inferior to samples prepared through the high temperature organometallic routes described previously. Thus, for the preparation of hybrid materials of optimal quality, the nanocrystal growth and polymer functionalization steps should be separated. The challenges and opportunities inherent in this approach form the subject of much of this thesis.

1.3.3 Chain-End Attachment of Polymers to Quantum Dot Surfaces

The formation of self-assembled monolayers (SAMs) of small molecules and polymers on flat surfaces of many types has garnered much attention in the literature, and this concept has more recently been applied to nanocrystals.[60,66-72] Generally, SAMs are formed by surface deposition of end-functionalized organic molecules or polymers from solution. This approach has recently been successfully performed on the curved surfaces of quantum dots is a valuable and versatile technique for the modification of quantum dots surfaces allowing for tunable interactions between the quantum dot and its environment.

Prior to the beginning of this thesis work, there were very few examples of polymer chain-end tethering to quantum dots. One notable example was reported by Hedrick and coworkers on thiol-terminated polyesters for growth and stabilization of CdS nanocrystals.[73] More, recently Peng and coworkers employed thiol terminated dendrimers to encapsulate CdSe nanocrystals.[48] Photooxidation studies were performed to compare these dendritically encapsulated nanocrystals to those functionalized with short chain thiols. Significant differences were observed in the photochemical stability of the linear versus the dendritic system, as well as a substantial difference in the photochemical stability of CdSe nanocrystals coated with dendrimers of various generations. As expected, higher generation, *i.e.* higher molecular weight, dendrons provided better protective coatings, a finding attributed to the steric crowding of the dendritic ligand, which slows the penetration of oxygen and ions to the quantum dot surface.

An additional benefit of dendritic encapsulation is the multiplicity of chain-ends inherent in dendritic structures that are available for further chemical modification. In one example, Peng and coworkers used a dendritic ligand with a thiol focal point and multifunctional hydroxy group periphery (Figure 1.10). This dendritic periphery is amenable to chemical modification, and through simple functional group transformations, the hydroxyl groups were converted to esters, carboxylic acids, and amides using chemistry that did not adversely affect the nanocrystal itself. These functional group transformations can significantly effect solution properties, as well as the solid-state dispersion, of the nanocrystals. For instance, the dendritic capped, hydroxyl-terminated dendrimers were water soluble, while the ester terminated

dendrimers were only soluble in organic solvents. These studies reiterate the importance of the ligand structure, especially the chain-end moieties of the ligands, as these groups tend to dictate the physical properties of the quantum dots (Figure 1.10). Peng and coworkers later extended their studies to dendritic ligands containing an acyclic olefin periphery. These unsaturated chain-ends could be used in interdendrimer, and intraparticle, cross-linking to give a cross-linked shell of ligands about each nanocrystal. Subsequent acid-induced etching of the of the nanocrystal gave hollow "dendritic boxes."

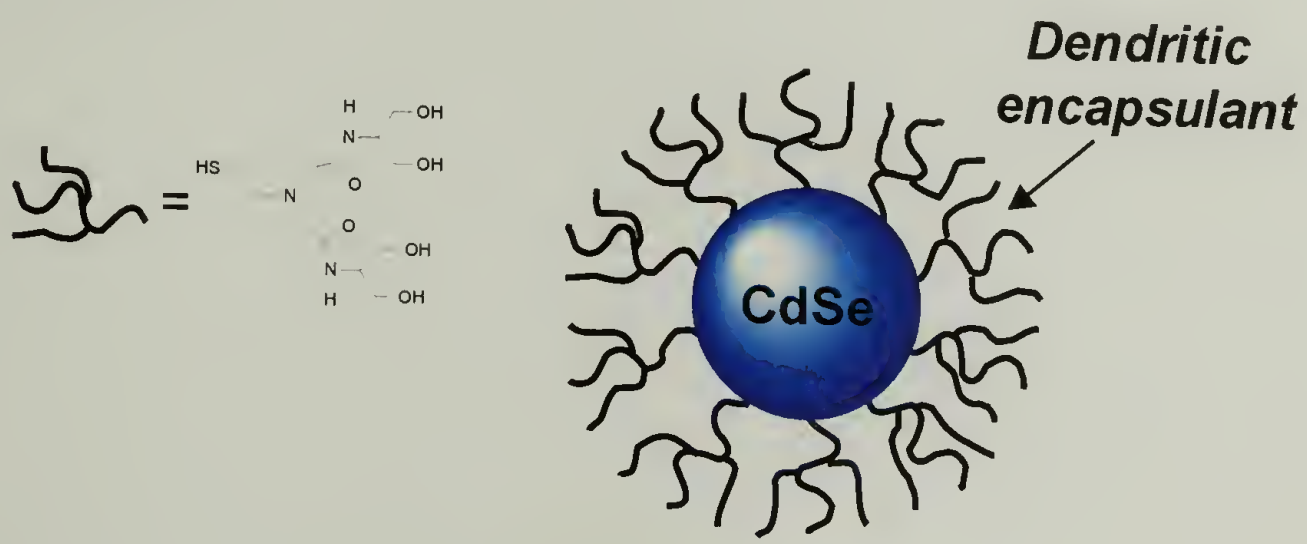

Figure 1.10: Dendrimer encapsulated CdSe nanocrystals with hydroxyl periphery

Very recently, Fréchet and coworkers synthesized phosphonic acid terminated oligothiophenes for quantum dot functionalization.[74] This synthesis allowed for effective control over the ligand's head group, the moiety responsible for attachment to the nanocrystal surface as well as the tail of the ligand. Control over the polythiophene chain length allows for control over electronic levels, allowing for alignment of the ligand and nanocrystal bandgaps. Control of the electronic levels and solubility can be controlled by adjustment of the polythiophene conjugation length and side groups, respectively. While this work represents an important advance in quantum

dot/eonjugated polymer hybrid materials, the complexity and tediousness of the polythiophene ligand synthesis will restriet its widespread use. Alternatively, work in this thesis (**Chapter 4**) foeuses on growing eonjugated polymers from the nanoerystal surfaee, whieh employs fewer synthetie steps and allows for greater versatility.

1.3.4 Radial Growth of Polymers From Quantum Dot Surfaces

The initiation of polymerization reaetions, espeeially eontrolled or "living" polymerizations, from the surfaee of semieonduetor nanoerystals is appealing as a versatile approaeh for the eompatibilization of nanoerystals with a very wide variety of solution and solid-state polymer environments. This approaeh requires funetionalized nanoerystals that eontain moieties eapable of initiating polymerization reaetions. One example of sueh a polymerization was reported by Patten and eoworkers for atom transfer radieal polymerization (ATRP) from the surfaee of CdS/SiO_2 eore/shell nanoerystal.[75] These eore/shell nanoerystals were funetionalized at the surfaee with 3-(2-bromopropionyloxy)-propyl dimethylethoxysilane (BIDS), then added to a solution of $NiBr(PPh_3)_2$ and methyl methaerylate (MMA), and heated to 100 °C for three hours. The poly(methyl methaerylate) grown from the nanoerystals was eleaved from the surfaee with hydrofluorie acid, and gel permeation ehromatography was used to determine the moleeular weights (ea. M_w=1.75 x 10^5 g/mol) and polydispersities (PDI ea. 1.3) of the eleaved ehains. This study showed that reasonably eontrolled free-radical polymerizations eould be performed from the nanoerystal surfaee, while preserving the nanoerystal properties due to the presenee of the proteetive SiO_2 shell. Methods to eliminate the need for this shell, but still maintain nanopartiele eompatibility with the polymerization eonditions, are deseribed in **Chapter 2** and **4**.

As mentioned earlier, water-soluble and highly luminescent nanocrystals are under investigation as luminescent tags for identification of biologically active molecules and diseases, *e.g.* cancer cells. In all, cases as synthesized quantum dots (TOPO-covered) must be further functionalized in order to impart water solubility and active recognition sites to the nanocrystals. For example, Thompson and coworkers functionalized CdSe/ZnS core/shell nanocrystals with dithiothreitol (DTT), and subsequently attached oligonucleotide to the nanocrystal periphery through a carbidiimide coupling performed directly on the nanocrystal surface.[59] Two oligonucleotide sequences were used for the fluorescence *in situ* hybridization (FISH) studies that followed. One sequence was a random and the other was "Y-specific", *i.e.* complimentary sequence present on the human Y chromosome. The FISH experiments showed that nanocrystals functionalized with the "Y-specific" sequence attached exclusively to the complimentary base sequence of the Y chromosome derived oligonucleotide, while the random sequence functionalized nanocrystals showed no such attachment. Further advances in the area of stable, water-soluble, functionalizable nanocrystals will be very useful in extending these studies towards multiple biological targets.

1.3.5 Self- and Directed-Assembly of Quantum Dots

Highly ordered nanoparticle arrays are of fundamental interest and technological importance. This is especially true for semiconductor nanocrystals, where high-density, ordered arrays are of interest for many applications including sensors, storage devices, and electro-optical devices. Ordered arrays of semiconductor nanocrystals have been obtained by careful crystallization from solution, or, as shown in part of this thesis

work, through the use of polymer templates. The use of polymers as the basis for quantum dot-polymer composites offers much potential for the directed and self-assembly capabilities of quantum dots in thin polymer films.

Diblock copolymer templates offer an appealing alternative to colloidal crystallization for nanocrystal templating, as they are easily processible and the inherent ability to self-assemble into ordered arrays. For example, Kotov and coworkers have used a layer-by layer (LBL) deposition to assemble CdTe nanocrystals of various sizes and emissions.[76] The CdTe nanocrystals were coated with thiogylcolic acid and a partner polyelectrolyte, poly(diallyldimethylammonium chloride). The LBL deposition of various size nanocrystals allows for the formation of graded semiconductor films which show promise as photodetectors, waveguides, and bipolar transistors. Wie and coworkers used hydroxyl functionalized CdS quantum dots to assemble in block copolymer films.[77] Here, the hydrophilic quantum dots were dissolved in DMF along with a polystyrene-*b*-poly(ethylene oxide) (PS-*b*-PEO) block copolymer. When the solution was spincast onto a flat surface, it was observed that the quantum dots selectively segregated into the PEO domains. TEM and SAXS confirmed the assembly which is surmised to occur because of the miscibility of the hydrophilic quantum dots in PEO. This work shows the possibility of quantum dot assemble in copolymers; more versatile synthetic approaches must be developed to fully explore all avenues.

1.4 Summary and Future Outlook

This chapter provided a brief overview of quantum dots, especially CdSe nanocrystals, from early synthetic work to more recent efforts in polymer functionalized hybrid materials and assemblies. Remarkable advances have been made in quantum dot

researeh in recent years, and the future is most promising. Semiconductor nanocrystals can now be synthesized routinely with high crystallinity and quantum yields that allow advantageous use of the unique properties associated with the nanoscale, such as tunable bandgaps, large surface-to-volume ratios, and improved proeessibility. The integration of these nanoerystals into polymer matrices and ultimately into devices is highly relevant for the new generation of photovoltaic cells, LED's, and tunable lasers, as well as biotags and diagnostie deviees. As synthetie methods become inereasingly routine and eommereialized, even greater foeus will be plaeed on nanocrystal applications.

This thesis is focused on developing synthetie techniques for the funetionalization and assembly of CdSe nanocrystals. The approaehes employed vary from eontrolled free radieal polymerization, to ring opening metathesis polymerization, to metal mediated polyeondensation teehniques. All of these methods have been optimized to give polymer funetionalized quantum dots that maintain an excellent dispersion within polymer matriees. In some eases, the surfaee modified nanoerystals are shown to have dramatically different solid-state and solution properties that are dietated by the interaetions between their polymer periphery and the surrounding environment.

The manipulation of nanoerystal surface has allowed for the assembly of CdSe nanoerystals in bloek eopolymers as well as at the liquid-liquid interface of oil and water. Through the judieious ehose of polymer eneapsulant, quantum dots have been assembled in speeifie domain of diblock eopolymers, to give higher order structures. The funetionalization of quantum dots with eross-linkable ligands enables the

generation of robust nanocrystal capsules at the oil-water interface. These capsule represent model systems for delivery and sensor applications and may eventually allow for the chemical modification of nanocrystals at the interface of two immiscible fluids. These synthetic techniques are employed to create novel composite materials while maintaining the unique electro-optical properties of the quantum dots.

CHAPTER 2

DISPERSION OF QUANTUM DOTS IN POLYMER MATERIALS – A GRAFTING FROM APPROACH

2.1 Introduction

Nanotechnology faces critical challenges associated with the ability to produce controlled and ordered structures on the nanoscale that achieve the desired applications. While the CdSe quantum dots introduced in **Chapter 1**, are promising candidates for use in the next generation electronic and biological applications, many of these applications will require a stable dispersion of quantum dots in polymer matrices, and a suppression of nanocrystal aggregation. Dispersed quantum dots will better maintain their unique inherent opto-electronic properties relative to aggregates of quantum dots within polymers. However, the high surface energy and inherent instability (*i.e.* tendency towards oxidation) of quantum dots, and of many nanoparticles in general, presents substantial challenges to these objectives.

An advancement of quantum dots from fundamental nanoscience to practical nanotechnology requires the development of versatile ligand-based functionalization methods that provide control over quantum dot physical properties and effective mediation of their interactions with their surroundings. Tailored ligand peripheries offer a variety of potential nanocrystal-based hybrid materials, ranging from simple particle dispersion in polymer matrices, to highly ordered structures formed by directed- or self-assembly. At the simplest level, the uniform dispersion of nanocrystals in a continuous phase is critical to maintaining homogeneous properties in the composite. Such dispersions maintain the nanoscale integrity of the quantum dots and thus their

unique properties. Versatile routes to nanocrystal functionalization allow for straightforward variation of this ligand environment, thereby allowing for their incorporation into polymeric materials, fluids, and interfaces.[78-82] The most common and reliable syntheses of high quality CdSe nanocrystals give an aliphatic ligand periphery composed primarily of tri-*n*-octylphosphine oxide (TOPO). This ligand periphery affords well-defined nanocrystals that are soluble in hydrophobic solvents, but does not provide for their uniform integration into most polymers. The development of effective chemistries that afford functional nanocrystal surfaces for use in subsequent polymerization, while simultaneously protecting the nanocrystals from oxidation and aggregation, are critical to the preparation of useful nanocrystal-based composite materials. In our approach to quantum dot functionalization, we expand considerably the chemistry of quantum dots to enable the synthesis of such composites. This is done by modifying the surface-bound ligands of CdSe nanocrystals to mimic the TOPO-coverage for surface passivation, while simultaneously providing surface functionality for subsequent polymerization.

2.2 Ring-Opening Metathesis Polymerization (ROMP) From CdSe Nanocrystals

ROMP methodology provides an appealing and potentially powerful technique for the functionalization of CdSe nanocrystals. In ROMP, transition metal catalysts (*e.g.*, Ru, Mo, and W) are used for the ring-opening polymerization of cyclic olefins.[83,84] In the case of the ruthenium benzylidene catalysts developed by Grubbs' and coworkers, a wide range of functionality is tolerated by the catalyst. It is this functional group tolerance that led us to investigate ROMP chemistry in the presence of,

and from the surface, of CdSe nanocrystals. Here, the effectiveness of ROMP for compatibilizing and dispersing CdSe nanocrystals in polyolefins is described. [85]

Ligand **1** was synthesized by the reaction of di-*n*-octyl phosphine oxide (DOPO)[86] with 4-vinylbenzylchloride under basic conditions (Figure 2.1), and purified by crystallization from hexanes. This ligand was synthesized using phase transfer

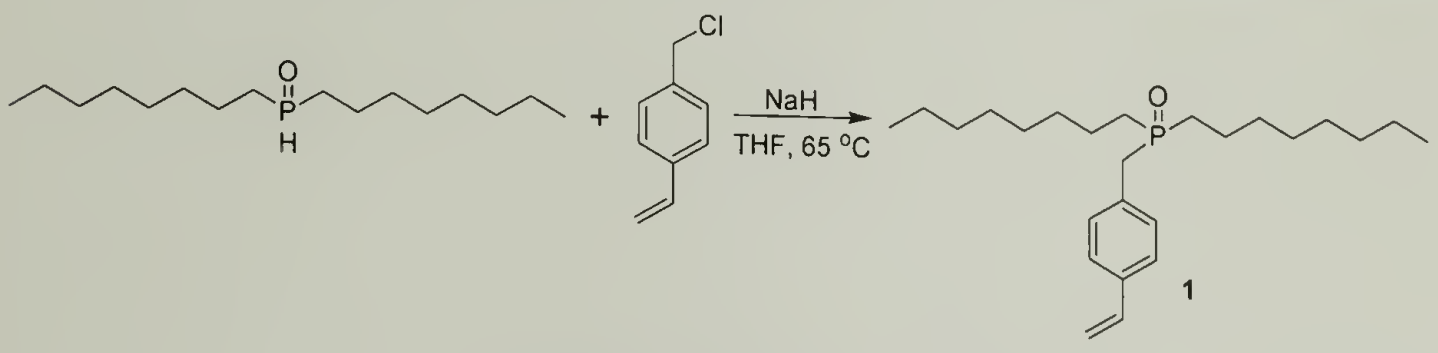

Figure 2.1: Synthesis of ligand **1**

conditions, or alternatively in a solution of tetrahydrofuran (THF) with sodium hydride. While both approaches were found effective greater yields were achieved using phase transfer conditions. The ^{1}H NMR spectrum of **1** confirms a new benzyl resonance at δ 3.1 ppm, and the ^{31}P spectrum consists of a single resonance at δ 47.3 ppm, characteristic of a trialkyl phosphine oxide (*e.g.*, the phosphorous of TOPO resonates at approximately δ 49 ppm). While compound **1** is capable of passivating the quantum dot surface, its instability at high temperatures precludes its use for growth of CdSe nanocrystals. Therefore, **1**-covered nanocrystals were prepared by ligand exchange chemistry. TOPO-covered CdSe nanocrystals of approximately spherical shape were prepared,[43] and TOPO was stripped from the surface by heating the nanocrystals in pyridine. Pyridine displaces the TOPO from the nanocrystal surface, and the newly stripped nanocrystals were stirred in a THF solution of **1** to give the newly functionalized CdSe nanocrystals. Surface coverage by the newly introduced phosphine

oxide was implied by the insolubility of the nanocrystals in methanol and verified by ^{1}H and ^{31}P NMR spectroscopy, where resonances of **1** were observed, and those of TOPO were not. The interparticle separation evident by transmission electron microscopy (TEM) images further confirmed successful surface coverage by ligand **1** (Figure 2.2). Confirmation of the ability of compound **1** to passivate the quantum dots in a manner that resembles coverage with TOPO was critical for proceeding with our polymerization studies.

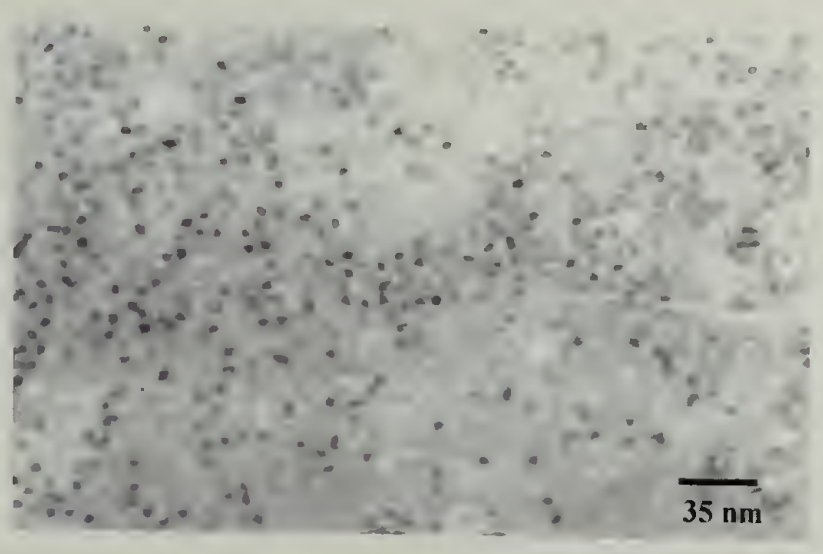

Figure 2.2: Transmission electron micrograph of **1**-covered CdSe nanocrystals.

Control polymerizations were performed in the absence of nanocrystals, by addition of **1** to a CH_2Cl_2 solution of bis(tricyclohexylphosphine) benzylideneruthenium dichloride (**2**) (Figure 2.3).[83] This metathesis exchange reaction gave an equilibrium

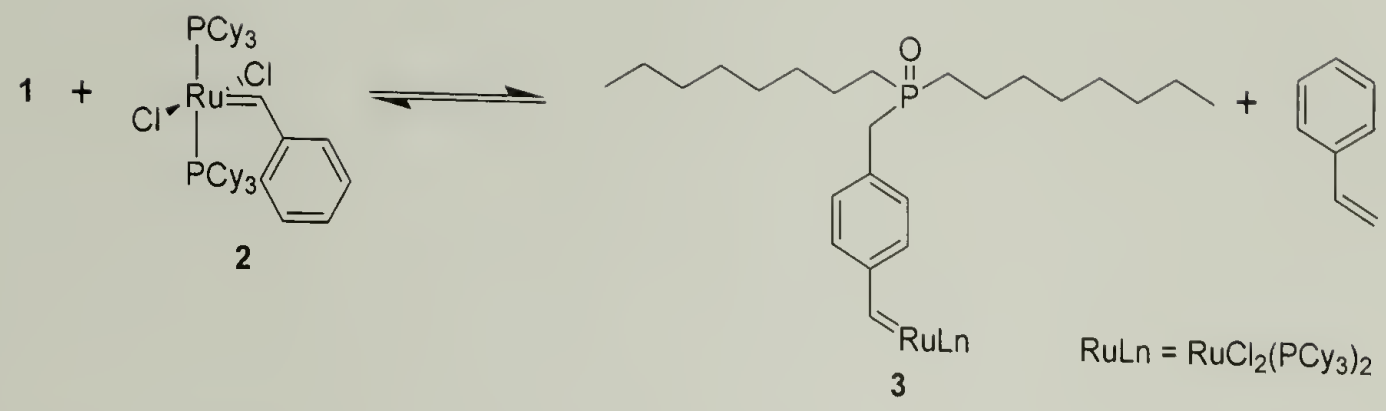

Figure 2.3: Functionalization of catalyst **2** by ligand exchange with compound **1**

mixture of **2** and a new phosphine oxide containing ruthenium benzylidene catalyst **3,** as evidenced by ^{1}H NMR spectroscopy that showed benzylidene resonances at δ 19.97 and 19.91 ppm for unreacted **2** and exchange product **3**, respectively. In addition, new resonances at δ 3.0 ppm were assigned to the benzyl methylene group (CH_2-P) of **3**. The relative amounts of **2** and **3** could be controlled based on the added amount of **1** used, such that **2** could be completely consumed if desired. The metathesis-active nature of compound **3** was noted by the disappearance of benzylidene signals from both **2** and **3** upon addition of cyclic olefins to this equilibrium mixture. These polymerizations were performed at room temperature to give polymers with GPC-estimated molecular weights from 10,000-50,000 g/mol, and the expected polydispersity (PDI) indices of approximately 2.

Addition of catalyst **2** to a solution of **1**-covered nanocrystals in CH_2Cl_2 resulted in a benzylidene exchange process that could be monitored by NMR spectroscopy in a similar fashion as for the control polymerization. Upon addition of cyclooctene to **3**-functionalized nanocrystals, successful ROMP was evident from the replacement of the original benzylidene singlet resonance with a triplet at δ 19.28 ppm, characteristic of the

chain-end ruthenium carbene (Figure 2.4). The polymerizations were performed at a variety of monomer and catalyst concentrations in CH_2Cl_2, typically at 0.2 M monomer and 0.4 mM catalyst. These conditions were found to be optimal, as more concentrated samples with higher catalyst loadings led to uncontrolled polymerization and cross-linking.

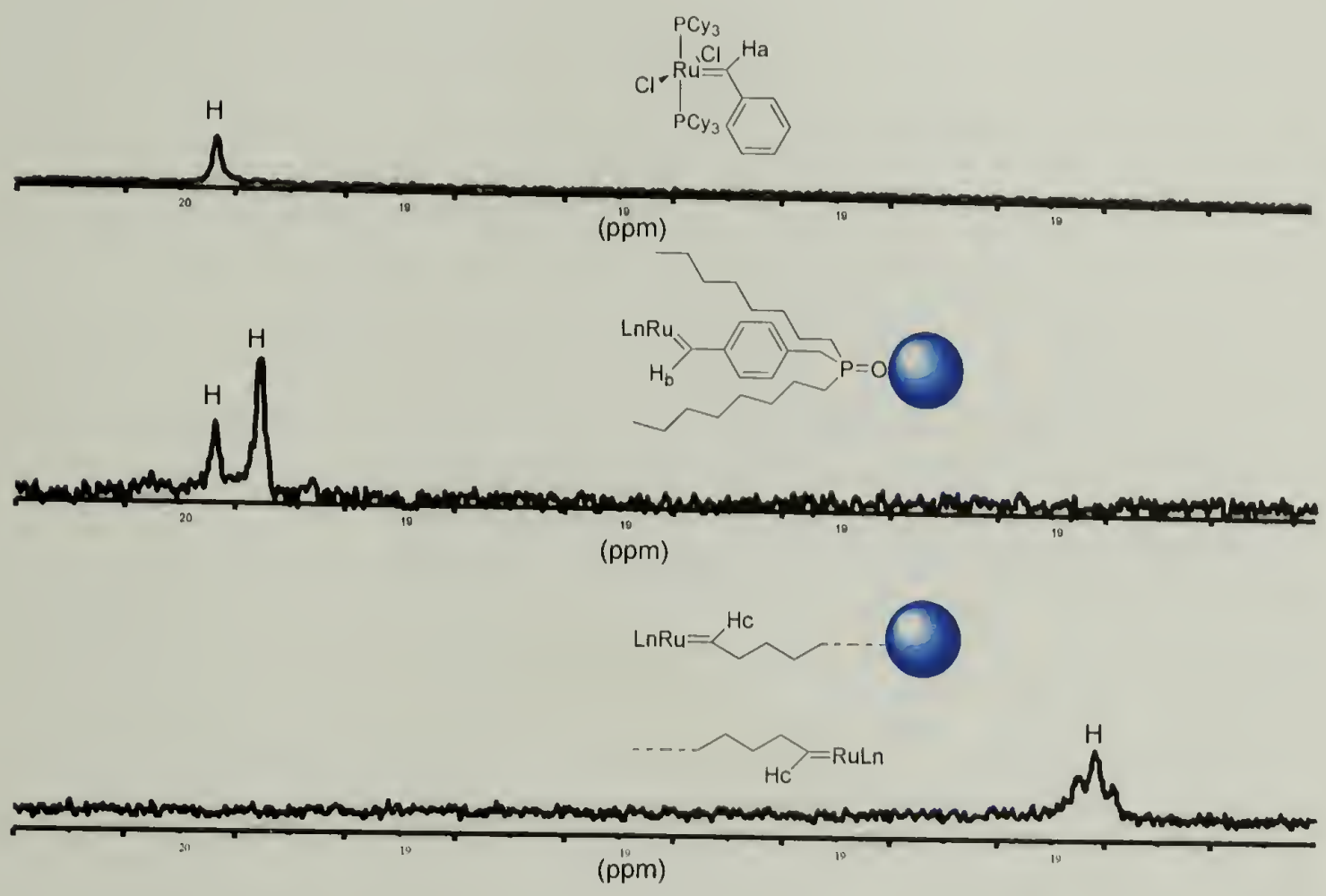

Figure 2.4: Selected region of ^{1}H NMR spectra showing the ruthenium benzylidene proton of compound **2** (top); **2** and metathesis exchange product (middle); and the CdSe-poly(cyclooctene) composite (bottom)

Polymer formation was noted spectroscopically by appearance of resonances at δ 5.4 ppm in the proton NMR spectrum, characteristic of polycyclooctene unsaturation, and by disappearance of the monomeric olefin resonances initially present at δ 5.6 ppm. The process as a whole is illustrated in Figure 2.5. Conventional TOPO-covered

nanocrystals were transformed to functional **1**-covered nanocrystals, followed by addition of ruthenium catalyst to give "macroinitiator" **5**, and finally polymerization (of cyclooctene in Figure 2.5) to give nanocrystal-polymer composite **6**. Our choice of

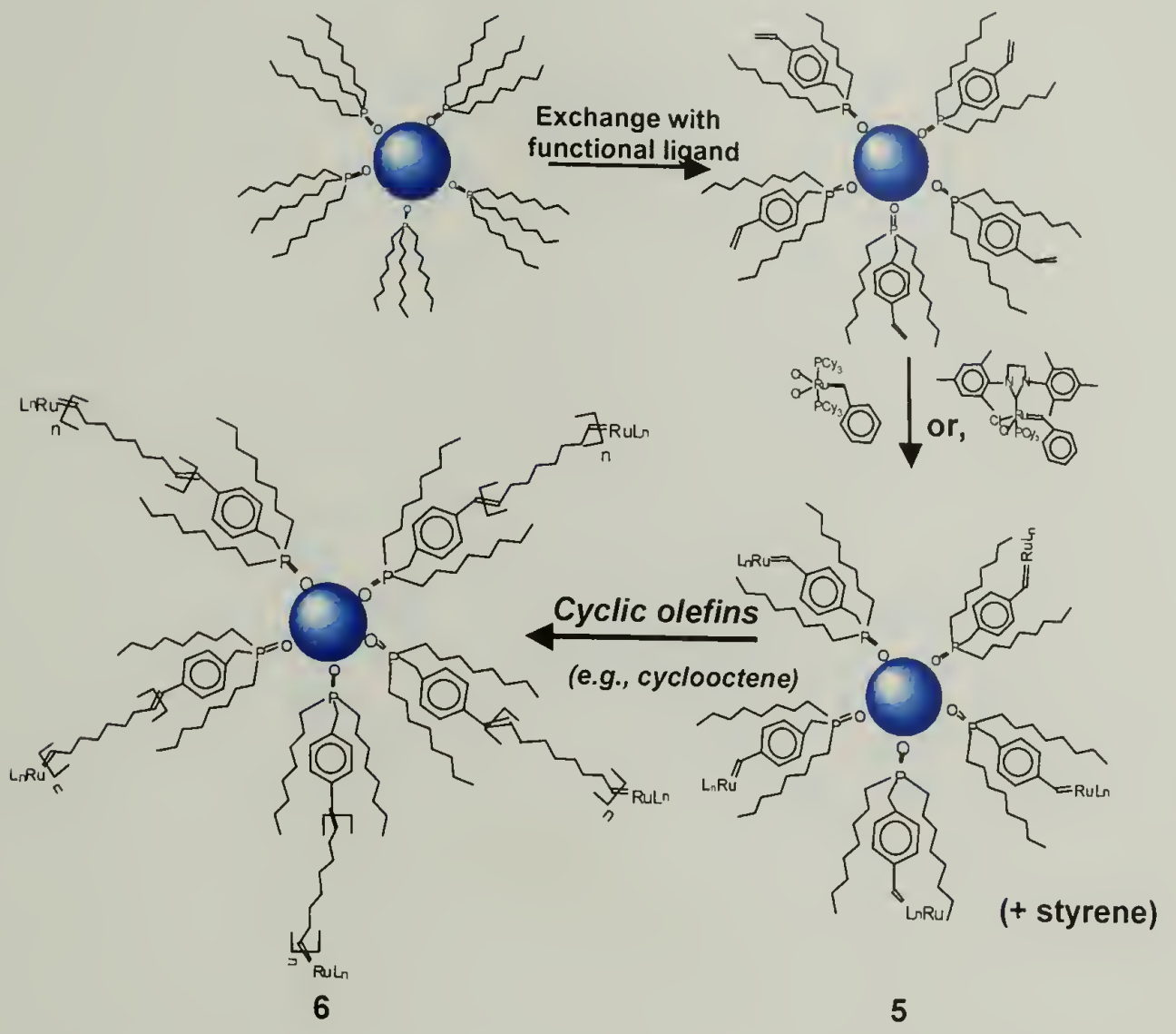

Figure 2.5: Initially, TOPO-covered CdSe nanocrystals are stripped of their aliphatic periphery and replaced with ligand **1**. Addition of Ru catalyst yield macrointiator **5** and subsequent monomer addition gives composite material **6**

catalyst **2** or **7**, (1,3-Bis-(2,4,6-trimethylphenyl)-2-imidazolidinylidene)dichloro(phenylmethylene)(tricyclohexylphosphine)ruthenium, allows for advantageous use of the chain transfer capabilities of the catalyst. The ruthenium center of **2** or **3** will react with unsaturated moieties in the system during the course of the polymerization, effectively chain transferring from one ligand to another. This convenient feature allows for the use of rather low catalyst loadings in this graft-

from chemistry. This appears to effectively provide surface coverage for the nanocrystals, as the ^{1}H NMR spectrum of nanocrystal-polymer composite **6** shows the decrease and eventual disappearance of vinylic signals representative of **1** at δ 6.7 ppm, and appearance of new resonances at δ 6.10-6.40 ppm, associated with the internal olefin protons attached to the aromatic ring in **6**. The very low amount of catalyst needed for these experiments makes its removal from the composite product feasible, or in some cases unnecessary.

Samples of **1**-covered CdSe nanocrystals could be used in polymerization of other cyclic olefin monomers from the nanocrystal surface. The process described above proved successful when cyclooctene was replaced with dicyclopentadiene, *exo*-7-oxanorbornene-2,3-dicarboxylic anhydride, or *exo*-*N*-ethyl-7-oxanorbornene-2,3-dicarboxylimide. In all three cases, ring-opening metathesis polymerization from **1**-covered nanocrystals proceeded effectively to give novel CdSe-polyolefin composites. In the case of dicyclopentadiene, a crosslinked network composite was obtained as a consequence of the difunctional nature of the monomer. Poly(*exo*-7-oxanorbornene-2,3-dicarboxylic anhydride) poly(*exo*-*N*-ethyl-7-oxanorbornene-2,3-dicarboxylimide) composite materials incorporate anhydride and imide functionalities, repectively, along the polymer backbone, and represent potential attachment sites for further functionalization. The ability to incorporate CdSe nanocrystals into a broad range of polymers (semicrystalline, network, and functional materials) demonstrates the generality of the approach and will expand the scope quantum dot-based technologies in the future.

The CdSe-polymer composites prepared by the graft-from ROMP technique gave optically clear solutions in organic solvents, with absorption and photoluminescent emission profiles similar to organic solutions of the starting nanocrystals (Figure 2.6). UV-visible spectra of toluene solutions of composite **6** immediately following their preparation showed a broad absorption between 250 and 450 nm, a result of absorption by both the nanocrystals and residual ruthenium catalyst. Quenching the polymerizations with ethyl vinyl ether,[87] followed by careful precipitation of the composite material in methanol, was successful in removing residual catalyst. Alternatively, the use of trace quantities (catalyst-to-monomer ratio ca. 1/5000) of the more active catalyst **7** gave similar polymer-nanocrystal composites that showed negligible absorption from the catalyst. The use of either catalyst successfully affords the desired composites, but the use of **7** does not require catalyst removal in order to clearly observe quantum dot absorbance and photoluminescence.

The CdSe-polycyclooctene composites were either solution or spin cast into thin films less than a hundred nanometers in thickness, and analyzed by TEM to reveal exeellent quantum dot dispersion in the polycyclooctene matrix (Figure 2.7). The observed dispersion of nanocrystals in these thin film composite materials was maintained even after hours of heating at 120 °C. This is a result of the effective surfaee coverage and polymer growth process initiated from the nanocrystal surface. The quantum dots in the composite materials have a mean interparticle separation that is significantly greater than that observed for **1**-covered nanocrystals. The value of ligand **1** as a functional phosphine oxide, capable of simultaneously coordinating to the nanocrystal and covalently attachment to polymers, was confirmed by control

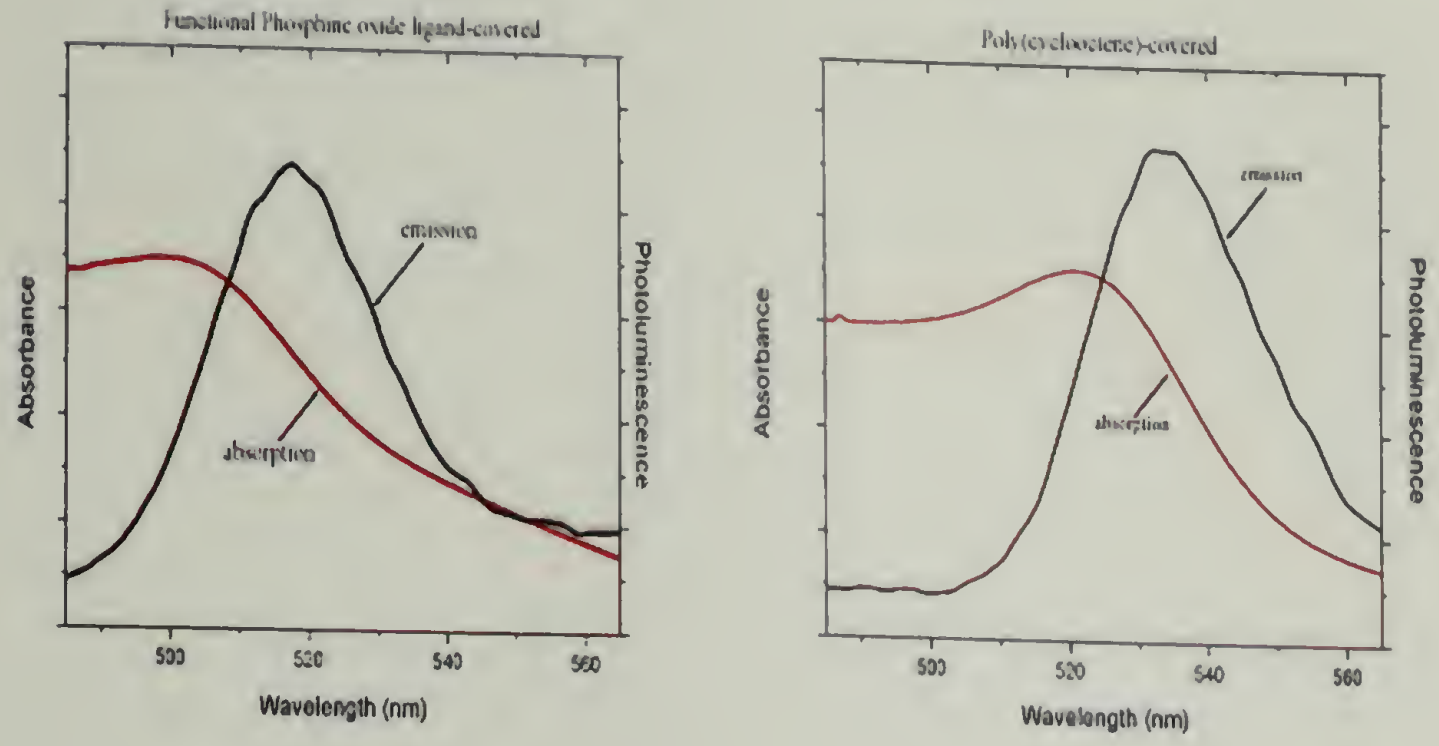

Figure 2.6: Absorbanee and photolumineseenee speetra of 1-funetionalized CdSe nanoerystals (left) and polyeyelooetene funetionalized CdSe nanoerystals (right)

experiments where ROMP was performed in the presenee of eonventional TOPO-covered nanoerystals. The eomposite materials obtained in these eontrol experiments showed substantial nanoerystal aggregation. This result is not surprising eonsidering the lack of ehemieal attaehment between the quantum dot and polymer, and the ineompatible nature of the TOPO surfaee eoverage with the polyeyelooeene matrix. Thus, it is elear that the growth method used in this study effeetively prohibits sueh nanoerystal aggregation for quantum dots in partieular, and would be expeeted to do so for nanoerystals in general.

To summarize, we have demonstrated the effeetive use of ring-opening metathesis polymerization from the surfaee of CdSe nanoerystals for the preparation of CdSe-polymer eomposite materials. This versatile growth method allows one to use both eommereially available and tailored monomers to prepare eomposite materials of dispersed nanoerystals in polymers. The simplieity and generality of this method will

allow for further development of a diverse collection of nanocrystal-polymer composites with a variety of solution and electronic properties. The uniform dispersion in these composite materials will enhance the optoelectric properties and mechanical properties of the composites relative to the aggregated cases, where such properties are significantly retarded.

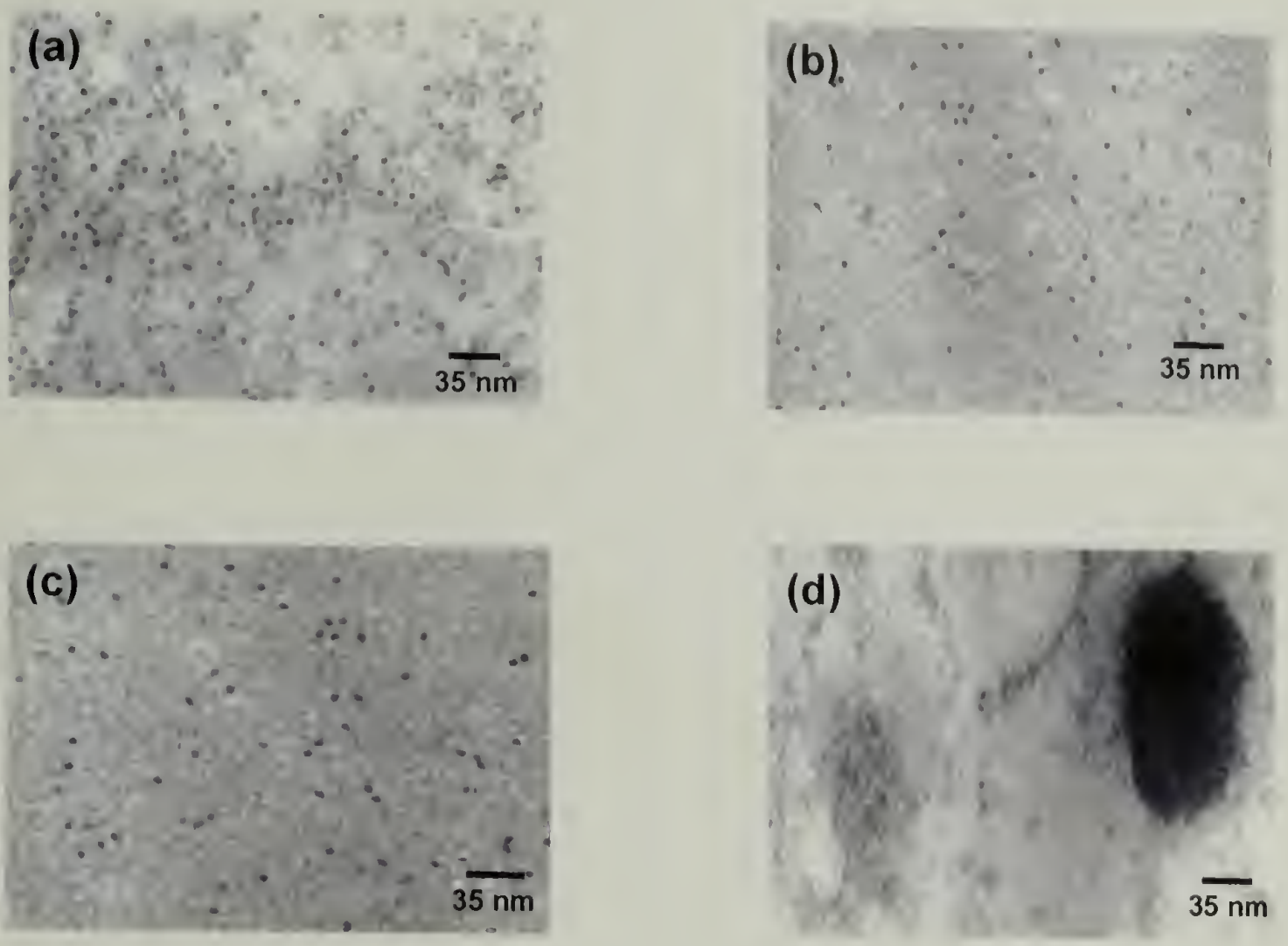

Figure 2.7: (a) **1**-functionalized CdSe nanocrystals, (b) polycyclooctene covered CdSe nanocrystal composite material, (c) nanocrystal-polycyclooctene composite material after annealing at 95 ^{o}C for 17 hrs, (d) TOPO-covered CdSe nanocrystals in a polycyclooctene matrix

2.3 Reversible Addition Fragmentation Chain Transfer (RAFT) Polymerization from CdSe Nanocrystals

The surface initiated ROMP chemistry described in the prior section represents a marked improvement over conventional blending methods. However, new methods must be developed for surface-grafting of the very wide variety of polymers not preparable by the ROMP technique. The approach described in this section is adaptable to many vinyl monomers, to give random but uniform dispersion of CdSe nanocrystals in polymer matrices. This straightforward and versatile method uses reversible addition fragmentation chain-transfer (RAFT)[88] polymerization as a controlled free radical method to grow polymers radially outward from the nanocrystal surface. RAFT was chosen for its ability to polymerize a wide range of monomers in a controlled fashion, without the need for transition metal catalysis.[89] The controlled free radical technique offers the possibility to graft polymers of low polydispersity to the nanocrystal surface. In addition, the low concentration of free radicals inherent to the RAFT technique offers advantages over conventional radical polymerization, such as for AIBN initiated polymerization where nanocrystal degradation is typically observed.

The successful application of the RAFT methodology to nanocrystal grafting requires appropriately tailored nanocrystals as precursors. For this we prepared compound **10**, for its two key features: 1) a phosphine oxide moiety capable of binding to the CdSe nanocrystal surface, much in the same was as TOPO passivates the nanocrystals and 2) a trithiocarbonate functionality capable of mediating RAFT polymerization. Most common RAFT initiators do not meet the requirements of this technique because they do not include a functional group that can be modified to

include a binding site for nanocrystal attachment. Addressing this requirement led to the synthesis of a hydroxy-*n*-propyl substituted phosphine oxide **8**, synthesized by hydrophosphorylation of allyl alcohol and DOPO using 2,2'-azobisisobutryonitrile (AIBN) as the radical source. Trithiocarbonate **9** was then prepared according to literature a procedure,[90] and used to prepare compound **10** by carbodiimidazole (CDI) mediated coupling with phosphine oxide **8** (Figure 2.8). The structure of **10** was confirmed by ^{1}H and ^{31}P NMR spectroscopy. The characteristic methylene resonance alfa to the ester was observed at δ 4.14 ppm in the ^{1}H NMR spectrum, and a single resonance at δ 49.1 ppm, characteristic of a trialkyl phosphine oxide, was observed in ^{31}P NMR spectrum. High resolution mass spectrometry of **10** (678.4333 a.m.u.) was found to be consistent with the calculated value (678.4303 a.m.u.).

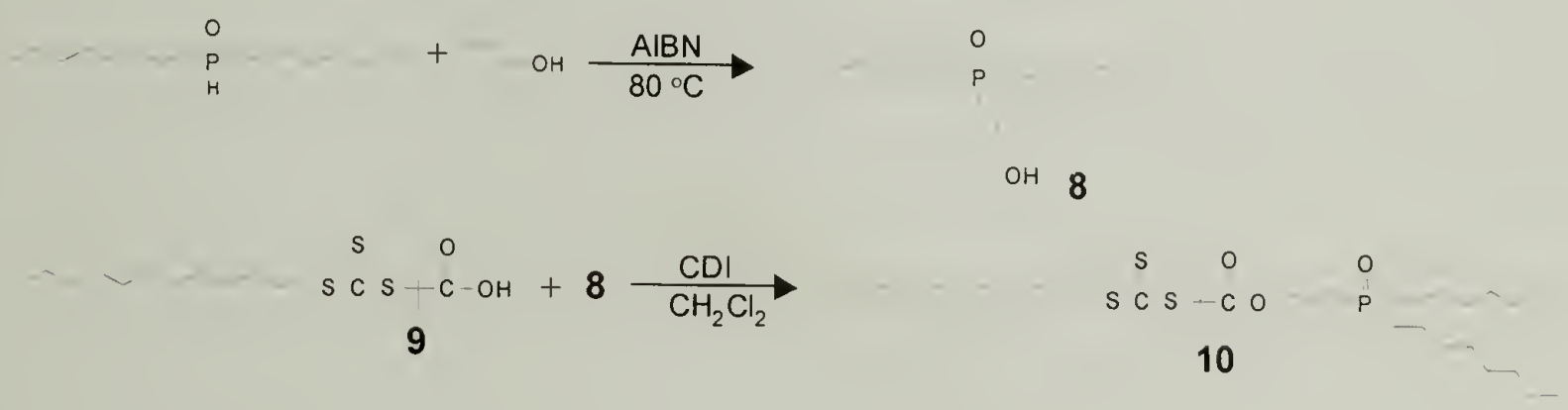

Figure 2.8: Procedure for the synthesis of ligand **10**. The first step depicts the hydrophosphorylation of DOPO to give **8**, and the second step depicts the CDI coupling of **8** and **9** to give ligand **10**

TOPO-covered CdSe nanocrystals were heated in pyridine, then stirred in a tetrahydrofuran solution of **10** at 50 °C for several hours to give **10**-functionalized CdSe nanocrystals. These trithiocarbonate functionalized nanocrystals were isolated by centrifuge filtration using a 50,000 MWC Pall centrifuge device,[30] and repeated dissolution and centrifugation (in a centrifuge filter device) was performed until no

excess ligand was present. Successful removal of unbound ligands was verified visually by a loss of the original yellow color, distinctive of trithiocarbonate **10**, in the supernatant. The new nanocrystal surface coverage was confirmed by recovery of an optically clear hexane solution of nanocrystals, and by ^{1}H and ^{31}P NMR spectroscopy where resonances characteristic of **10** were observed, and TOPO resonances were not.

Radial polymerization from the quantum dot surface was performed by addition of monomer(s) to a benzene or toluene solution of **10**-covered nanocrystals containing a free radical initiator. These nanocrystal/initiator solutions were subjected to three freeze-pump-thaw cycles, and the polymerizations were performed under a nitrogen atmosphere at 70 °C. Di-*t*-butyl peroxide was ultimately chosen as the free radical initiator, as the use of AIBN or benzoyl peroxide resulted in rapid nanocrystal degradation. This degradation was not surprising, as CdSe nanocrystals are known for their susceptiblity to free radical degradation.[91] The lower free-radical concentration produced by *t*-butylperoxide allows polymerization to proceed from the CdSe nanocrystal surface with a reduced concern for nanocrystal degradation. In addition, as the polymerization proceeds, the polymeric encapsulating shell that forms around the nanocrystal functions as a steric barrier to prevent radicals from reaching the nanocrystal surface. These factors, low free radical concentration and steric effects, help maintain the original high quality of the **10**-covered nanocrystals used for these grafting-from experiments.

Fuctionalization of CdSe nanocrystals with trithiocarbonate **10** allowed for successful graft-from polymerization of a wide variety of monomers, in homopolymerization, random copolymerization, and block copolymerization (Table 1).

Verification of polymer growth from the nanocrystal surface was confirmed by gel permeation chromatography (GPC) and NMR spectroscopy. GPC was performed on polymer stripped from the nanocrystal surface by stirring the polymer-functionalized nanocrystals in a THF solution of *n*-hexylphosphonic acid (HPA), and subsequent precipitation into hexanes. Homopolymers of polystyrene, poly(methyl acrylate), and poly(*n*-butyl acrylate) of significant molecular weights were grown successfully from the nanocrystal surface with low PDIs. Similarly, a number of random copolymers were grafted including poly(styrene-*r*-methyl acrylate), poly(styrene-*r*-acrylic acid), and poly(styrene-*r*-isoprene), with molecular weights ranging from 9,000 to 49,000 g/mol and PDI's from 1.2 to 1.3. Monomer incorporation into random copolymers grown from the nanocrystal surface was generally found to be tunable and reflective of feed ratios. One exception was found in the case of acrylic acid, where homopolymerization was not possible. However, copolymerization of acrylic acid and styrene could be performed when acrylic acid feed ratios were kept under 30 mol%. Table 1 shows the range of controlled free-radical polymerization from the CdSe nanocrystal surface obtained during this study.

Table 1: Polymers successfully grown from the quantum dot surface

Polymer	Mn (g/mol)	PDI
polystyrene	27000	1.17
poly(methyl acrylate)	31000	1.17
poly(butyl acrylate)	42000	1.32
poly(styrene-*r*-methyl acrylate)	49000	1.29
poly(styrene-*r*-acrylic acid)*	37000	1.19
poly(styrene-*r*-isoprene)	9000	1.30
poly(styrene-*b*-methyl acrylate)*	21000	1.18
poly(styrene-*b*-butyl acrylate)*	38000	1.32

* Degradation of the nanoparticle was observed in the form of a blue shift in the fluorescence emission and UV-Visible absorption spectra

The preparation of surface grafted poly(styrene-*b*-methyl acrylate) was accomplished in two steps. In the first step, a block of polystyrene was grown from the nanocrystal surface, and the polystyrene-grafted nanocrystal sample was precipitated into methanol. In the second step, a toluene solution of polystyrene-functionalized nanocrystals and methylacrylate was heated to 70 °C with *t*-butyl peroxide for 22 hrs. The polystyrene-poly(methyl acrylate) diblock copolymer-CdSe nanocrystal composite prepared in this fashion was isolated by precipitation into methanol. Block copolymer formation was confirmed by an increase in molecular weight as observed by GPC from the original polystyrene homopolymer. In addition, ^{1}H NMR spectroscopy showed resonances of both polystyrene and poly(methyl acrylate) in the samples isolated from the composite material. The polydispersity indices were narrow (PDI < 1.3), in accord with the RAFT polymerization technique, for all polymer architectures including block copolymers. The slow initiation kinetics inherent to *t*-butyl peroxide required longer reaction times relative to convention free radical polymerizations initiated by AIBN or BPO, typically polymerizations required 24 hours; but in the cases of butyl acrylate and block copolymers, longer reaction times were required (ca. 32 - 48 hrs).

A key result of this study is the retention of the unique optical properties of the CdSe nanocrystals following polymerization. This is clearly observed in the photoluminescence and UV-visible spectra of Figure 2.9. The band-edge absorption maximum of the CdSe nanocrystals, characteristic of the nanocrystal size, is found at 525 nm in both the **10**-covered nanocrystals and the polystyrene and poly(methyl acrylate)-nanocrystal composites. From the fluorescence spectra, it is also evident that the nanocrystal integrity remains intact, with emission maxima centered around 545 nm both before and after polymerization.

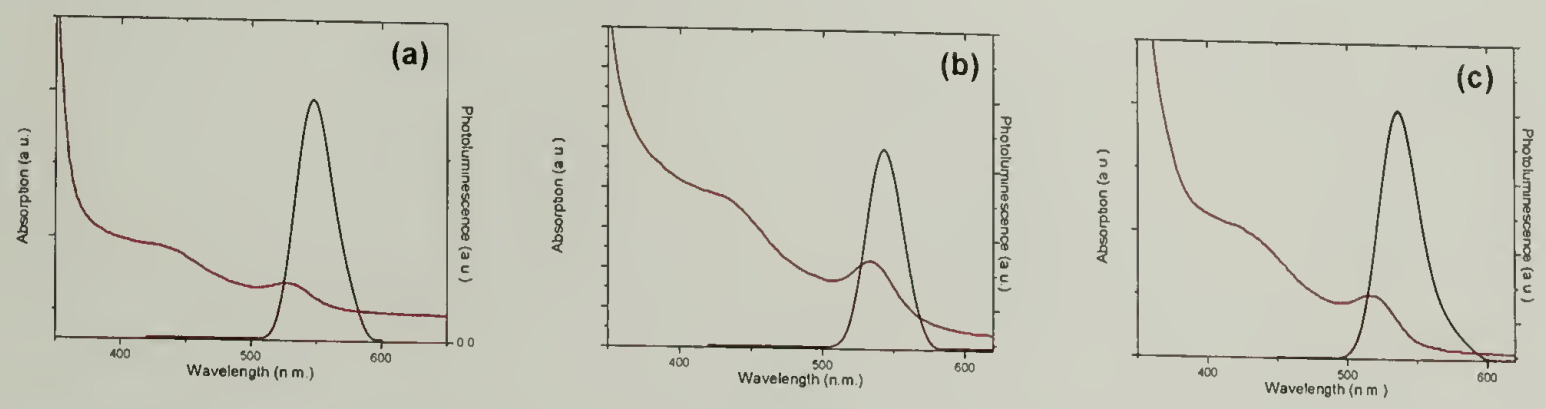

Figure 2.9: Absorption and fluorescence spectra of **(a) 10**-covered CdSe nanocrystals, **(b)** poly(methyl acrylate)-covered CdSe nanocrystals, and **(3)** poly(styrene)-covered CdSe nanocrystals in toluene

The combination of optical characterization along with transmission electron microscopy confirms that the nanocrystal integrity is maintained throughout the polymerization process. This is in direct contrast to the use of conventional free-radical initiators with quantum dots, where the optical properties are lost irreversibly. In addition, the method does not require the use of an inorganic overcoating of the original quantum dots, thus providing a simple approach to these composite materials.

Solution or spin casting of toluene solutions of CdSe-polymer composite materials gave optically clear thin films. Transmission electron micrographs reveal the

uniform nature of the thin film composites, as the nanocrystals are dispersed throughout the matrix in an unaggregated fashion. Figure 2.10a shows an image of a polystyrene-encapsulated nanocrystal film prepared by the RAFT process, while Figure 2.10b shows the case where styrene was polymerized in the presence of TOPO-covered CdSe nanocrystals. In the latter case the micrographs illustrate aggregation of the nanocrystals in the polymer matrix. Thus, growth of the matrix material radially outward from the nanocrystal surface compatibilizes the two disparate materials into a uniform composite.

Figure 2.10: Transmission electron micrographs of **(a)** poly(styrene)-covered CdSe nanocrystals prepared by the RAFT technique in poly(styrene), and **(b)** TOPO-covered CdSe nanocrystals in poly(styrene) prepared by RAFT

In summary, we have adapted the RAFT-method to polymerize vinyl monomers from the surface of CdSe nanocrystals. The synthesis of trithiocarbonate ligands, and their ability to cover CdSe nanocrystals, was key to this approach. The RAFT technique proved to be a versatile and general for tailoring CdSe nanocrystals with a variety of polymers, while maintaining the unique structural and optical properties of the nanocrystals. The controlled free-radical nature of RAFT allowed for the chemistry

to be performed in the absence of a protective inorganic shell on the nanocrystal. Through the use of these trithiocarbonate tailored nanocrystals, several nanocrystal-polymer composite materials were prepared, and the choice of materials into which nanocrystals could be dispersed is now expanded considerably to include polystyrene, polymethylacrylate, and derivatives of each. This, in turn, opens new possibilities for self- and directed-assembly studies on quantum dots. Finally, the retention of photophysical properties of the quantum dots following polymerization is both impressive and critically important for using these composite materials in nanocrystal-based applications.

CHAPTER 3

WATER SOLUBLE CADMIUM SELENIDE NANOCRYSTALS PREPARED BY FUNCTIONALIZATION WITH PEG-SUBSTITUTED PYRIDINE

3.1 Introduction

Colloidal nanocrystals, especially those with active electronic and luminescent properties, have attracted a great deal of interest in exploratory biotechnology research as fluorescent tags.[92-95] Fluorescent labeling of biological compounds allows for the study of their transport and the identification of their location within the cellular or extracellular environment. The ability to monitor and identify these compounds allows scientists to garner a greater understanding of their function. Quantum dots offer significant advantages over conventional organic fluorophores for their narrow photoluminescence emission profiles (c.a. 20-30 nm fwhm), resistance to photobleaching (hundreds of times greater than organic dyes), and continuous absorption above the bandgap (Figure 3.1).[96] These unique properties allow quantum dots to be used as individual biological tags or in multiplexing applications, where nanocrystals of various emission wavelengths can be excited simultaneously and for extended periods of time by a single light source.[97] The use of nanocrystals in multiplexing experiments, where multiple compounds are fluorescently tagged with different emissions and monitored simultaneously, is deemed critical in the study of complex biological systems, as this would allow for the simultaneous monitoring of multiple parameters.

The work in this thesis centers on the ligand encapsulating environment of nanocrystals, which strongly dictates their solubility and miscibility properties. The

ligand periphery can be tuned in a variety of ways, including hydrophobic, hydrophilic, neutral, charged, or conductive. Conventional CdSe nanocrystals covered with tri-*n*-octylphosphine oxide (TOPO) ligands are hydrophobic,[98,99] and ligand exchange processes are typically used to obtain hydrophilic, water-soluble samples. This is often done by exchange of TOPO for α,ω-thiocarboxylic acid ligands, where the thiol group coordinates to the quantum dot surface and the carboxylic acid endgroup imparts water-solubility.[100,101] While these thiol functionalized nanocrystals are water-soluble, they are prone to photooxidation resulting in precipitation of the nanocrystals and loss of fluorescence.[91] Photooxidation is a consequence of extended exposure of these thiol-covered nanocrystals to UV irradiation, resulting in the oxidation of the thiols to form disulfides, which do not have a strong affinity for the nanocrystal surface. As a result of this photooxidation, the nanocrystals are left with little bound ligand to impart solubility, resulting in their aggregation and irreversible precipitation. This photo-instability has lead to the need for alternate water solubilization techniques. One example uses CdSe nanocrystals coated with a ZnS shell that are then overcoated with silica. This approach appear to be an effective for producing water-soluble CdSe nanocrystals with better stability than α,ω-thiocarboxylic acid covered samples but it is quite intricate synthetically, and probably not practical for the routine synthesis nor commercialization.[102]

The discovery of new procedures that offer simple, effective, and stable aqueous solubilization of quantum dots continues to present an important challenge in the field. The encapsulation of nanocrystals with poly(ethylene glycol) (PEG) would significantly diversify properties and potential applications of quantum dots, as a PEG ligand

coverage can satisfy multiple requirements, including organic solubility, water solubility, and biocompatibility.[103] PEG itself (i.e., HO-(CH_2CH_2O)n-OH) does not solubilize CdSe nanocrystals, as the hydroxyl chain-ends do not coordinate to the CdSe surface. Thus, we set out to provide a rapid route to photo-stable, amphiphilic PEG functionalized CdSe nanocrystals, using a new set of encapsulating ligand molecules. As described below, pyridine was chosen as the ligand moiety, in a scheme that covalently attaches PEG to the pyridine group. Such "PEGylated pyridines" had not been reported prior to this work, thus we set out to synthesize these novel molecules and test them as ligands for CdSe nanocrystals.[104]

3.2 Amphiphilic CdSe Nanocrystals

Pyridine terminated PEG compounds **11** and **12** were synthesized by Mitsunobu couplings of 4-hydroxypyridine with hexaethylene glycol and hexadecylethylene glycol monomethylether, respectively. These reactions were performed at room temperature in tetrahydrofuran, using diisopropylazodicarboxylate (DIAD) as the coupling agent, as illustrated in Figure 3.1. Compounds **11** and **12** are not discrete molecules, but rather possess an average number of ethylene glycol repeat units dictated by the inherent (albeit low) polydispersity of the commercial poly(ethylene glycol) samples employed.

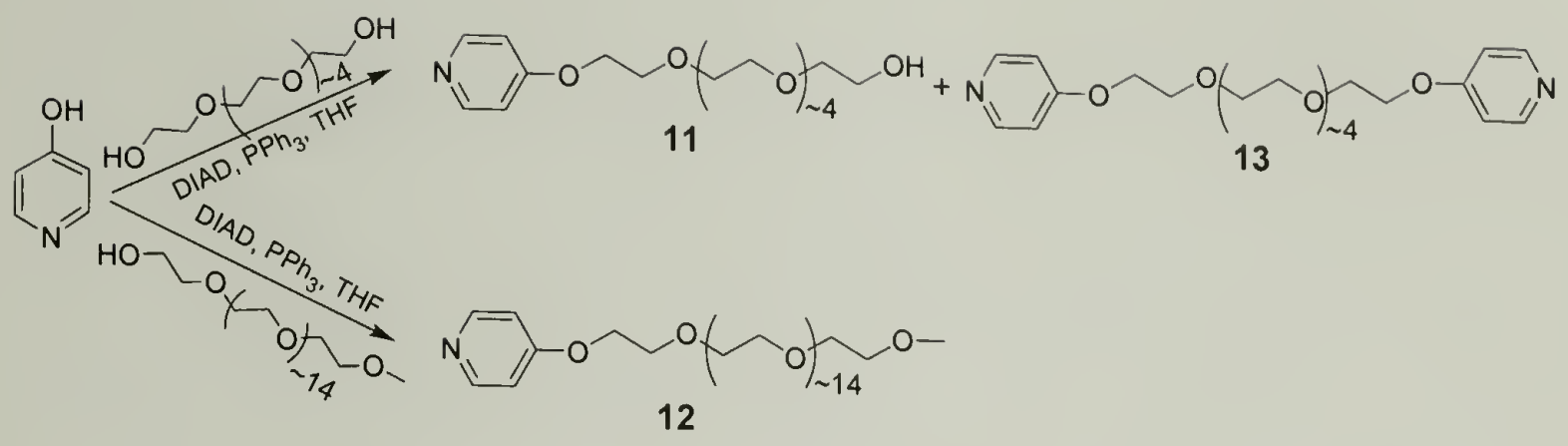

Figure 3.1: Mitsunobu coupling of PEG and 4-hydroxy pyridine to yield of ligands **11** and **12**

The synthesis of mono-substituted hexaethylene glycol **11** was performed with a three times excess of PEG-diol to minimize the formation of the α,ω-dipyridine side product **13**. When the percentage of the dipyridine compound formed in the coupling reaction was kept to a minimum, it was easily removed from the crude product mixture by column chromatography on silica gel. Compounds **11** and **12** are amenable to scale-up and were prepared in multigram quantities in yields of 50% and 80% yield, respectively, after purification. ^{1}H NMR spectroscopic characterization of **11** and **12** showed triplets at δ 4.1 and δ 3.8 ppm, assigned to the two PEG methylene groups nearest the aromatic ring. These diagnostic resonances are shifted downfield from the terminal methylene groups of the unsubstituted PEG starting materials. The ^{13}C NMR spectra of **11** and **12** showed the expected aromatic and aliphatic resonances, while the spectrum of **11** includes a resonance at δ 61.4 ppm for the $\underline{C}H_2OH$ chain-end. This particular resonance is absent in the carbon spectrum of monomethyl ether **12**, and indicative of complete hydroxyl end-group substitution in the purified product.

We first observed the affinity of electron-rich, *para*-substituted pyridines for CdSe nanocrystals when introducing 4-(dimethylamino)pyridine (DMAP) in the presence of TOPO-covered CdSe nanocrystals. This gave complete displacement of TOPO by DMAP (as judged by solubility changes, as well as ^{1}H and ^{31}P NMR spectroscopies). Such a rapid TOPO-for-DMAP exchange is not seen in the case of unsubstituted pyridine, rather, a large excess of refluxing pyridine is required to achieve near complete displacement of TOPO from the nanocrystal surface. We attribute the observed affinity of DMAP for the CdSe surface to its enhanced basicity relative to pyridine. The pK_a values of the conjugate acids of DMAP and pyridine are approximately 9.0 and 5.2, respectively. The dialkylamine species in the *para* position increases the basicity of the nitrogen, which leads to strong coordination between the ligand and the nanocrystal surface. As 4-alkoxy-substituted pyridines exhibit basicity on the order of DMAP, our finding should be extendable to a number of pyridine derivatives containing electron-donating substituents in the *para* position.

Ligands **11** and **12**, containing *para*-ether substituents, can be utilized effectively in a number of ligand exchange scenarios for attachment to the CdSe surface. Two of these scenarios are depicted in Figure 3.2. For example, displacement of TOPO by conventional pyridine stripping, followed by adsorption of **11** or **12** to the nanocrystals in THF, provided an effective exchange method. Alternatively, the exchange process could be performed directly in water by addition of aqueous solutions of **11** or **12** to a suspension of pyridine-covered CdSe nanocrystals, whereupon the suspension became homogenous instantly. An even more convenient ligand exchange and aqueous solubilization was accomplished by simply adding **11** or **12** to a solution of

TOPO-covered nanocrystals in THF and allowing the mixture to stir at room temperature overnight. The observed changes in solubility of the product relative to the starting material, in conjunction with NMR spectroscopic measurements, confirmed the success of these ligand exchange strategies. The exchange process directly transforming the nanocrystal TOPO coverage to **11** or **12** in THF was found to be the most successful and reproducible of the methods tried.

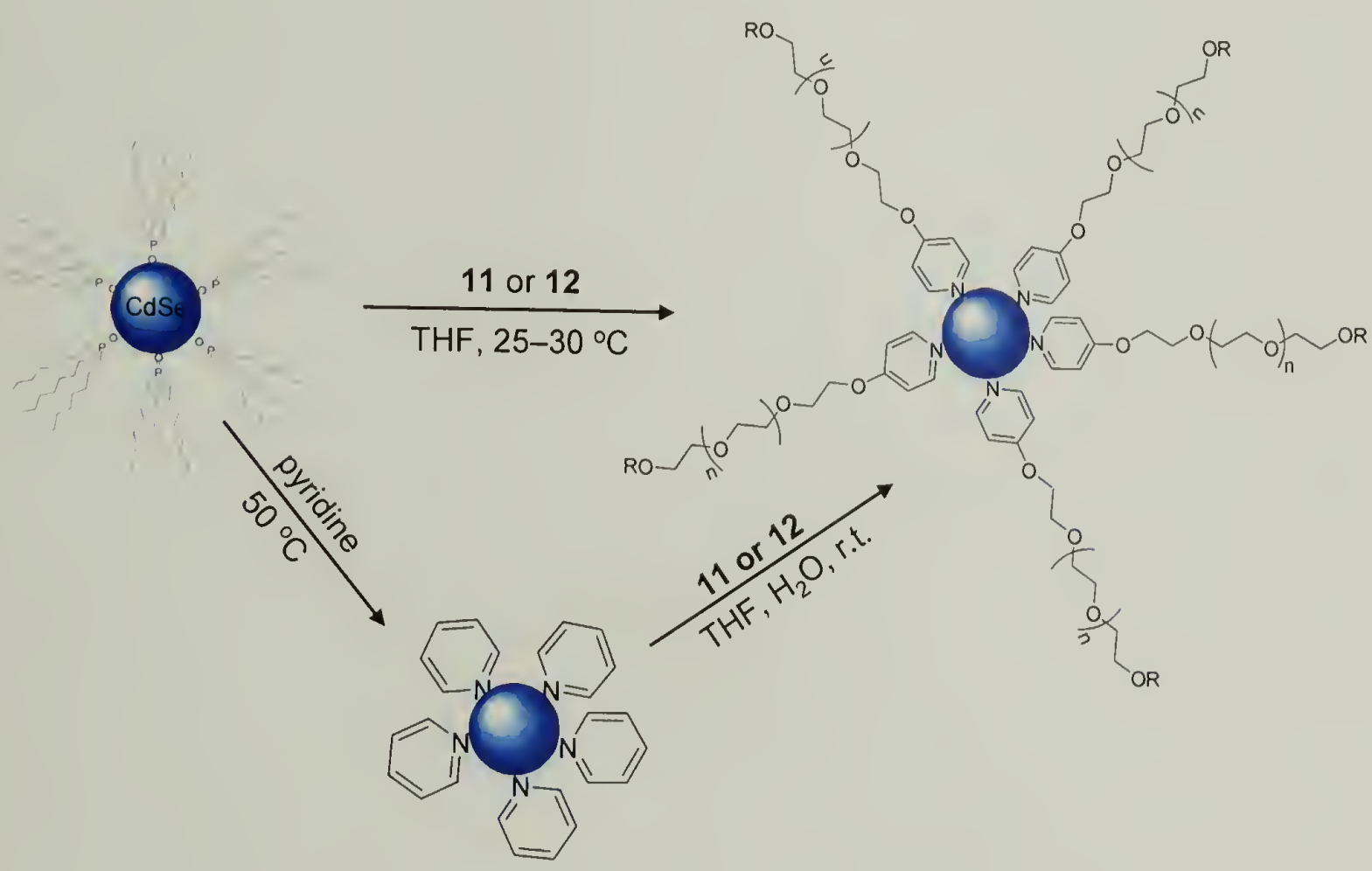

Figure 3.2: Schematic representation of two different ligand exchange chemistries used to convert TOPO-covered CdSe nanocrystals to PEG-pyridine covered CdSe nanocrystals

Dissolution of **11**- and **12**-covered CdSe nanocrystals in either organic (with the exception of hexane and ethyl ether) or aqueous (pH 7) media afforded optically clear solutions, with similar absorption and emission maxima in either solvent environment. Figure 3.3 shows an example of 3 nm CdSe nanocrystals covered with ligand **11**, where

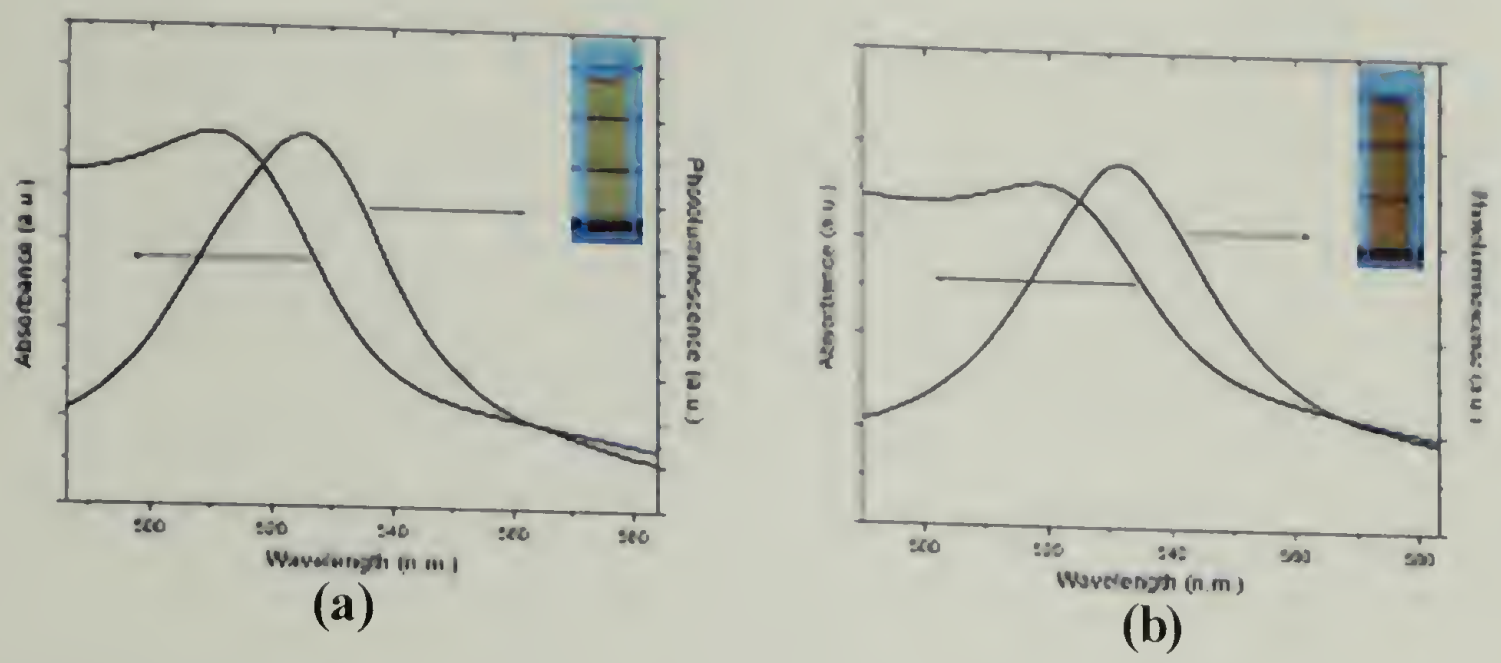

Figure 3.3: Absorbance and photoluminescence spectra of **11**-functionalized CdSe nanocrystals in (a) CH_2Cl_2 and (b) water

the first exciton absorption peak (*i.e.*, band edge absortion) is located at approximately 515 nm, and the photoluminescence emission maximum is found at approximately 525 nm. The emission maximum of **12**-functionalized nanocrystals is similar to the original TOPO-covered nanocrystals, demonstrating that the optical properties of the quantum dots are maintained in either solvent environment. A small blue shift (~ 5-10 nm) was observed in the emission spectrum of this sample, and in some cases the blue shift continued to grow over a period of months, indicating some degradation of the nanocrystal surface. Most of these PEG-functionalized nanocrystals have shown excellent stability with no sign of precipitation when stored in organic solvents, under ambient conditions, for over one year. Furthermore, the stability of nanocrystals solubilized by ligands **11** and **12** proved superior to 3-mercatopropionic acid in aqueous media, under ambient conditions, as well as under conditions of ultraviolet irradiation (254 nm wavelength), while the thiol-covered nanocrystals were found to precipitate quickly (Figure 3.4). The stability of these nanocrystals under UV irradiation was

performed on dilute solutions of PEG-pyridine covered and thiol-covered nanocrystals. The samples were irradiated side-by-side by a 150 Watt lamp exposed to air. Under these conditions, the thiol-covered partieles eompletely precipitated within 1-2 hours, while slight precipitation of the PEG-pyridine covered particles was observed after 5-6 days, and substantial precipitation after 9-10 days.

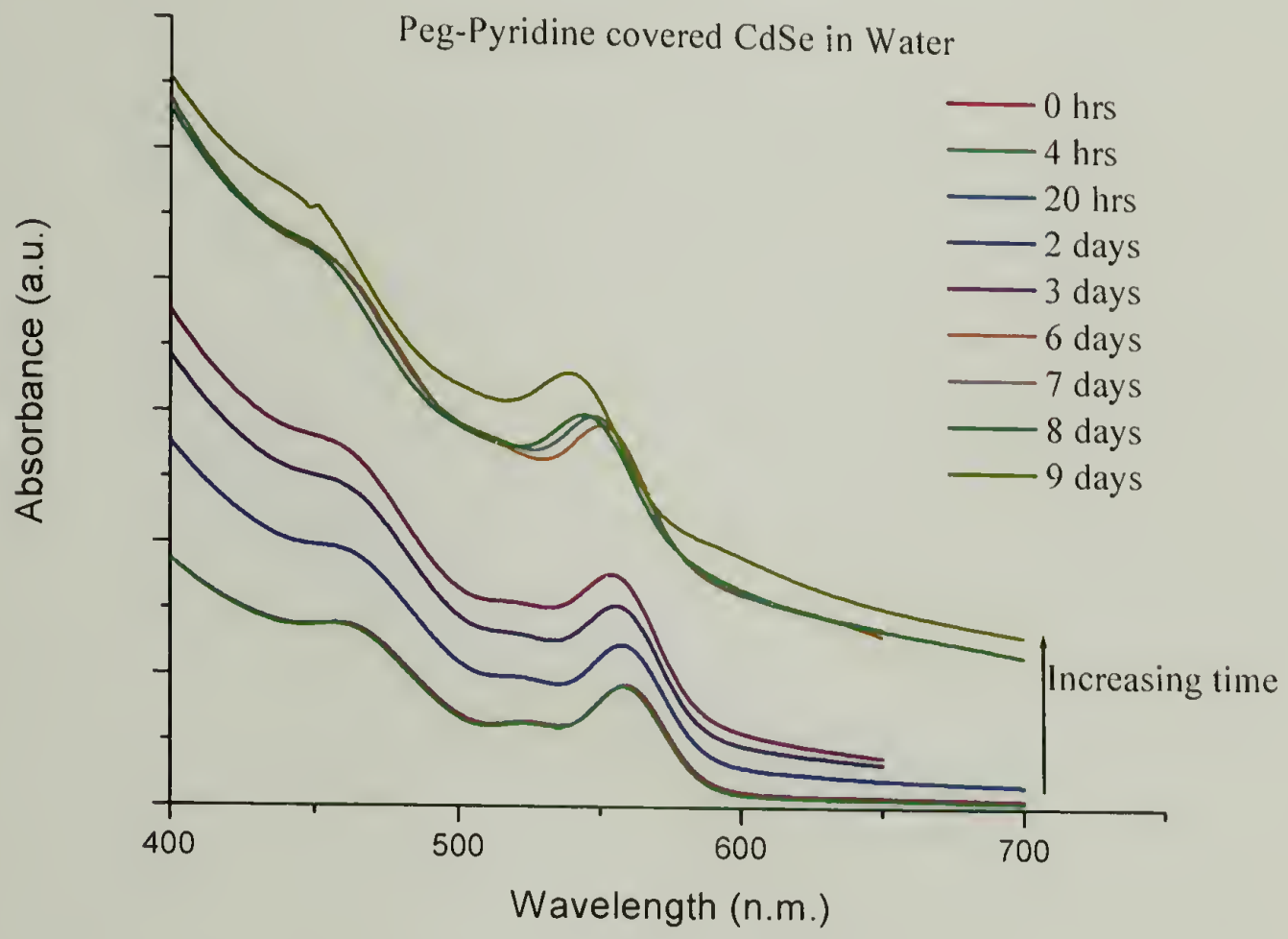

Figure 3.4: Absorbance profiles of PEG-pyridine eovered CdSe nanoerystals in water, showing little ehange in the first exeiton absorbance over several days of irradiation. The speetra are not normalized; solvent evaporation results in the observed inerease in absolute absorption

The enhaneed photostability of the PEG-pyridine eovered CdSe nanoerystals is attributed to the faet that this system does not suffer from the disulfide formation that occurs in samples of thiol-functionalized nanoerystals. In addition, aqueous samples of these PEG-eovered nanoerystals, when stored in the dark and under nitrogen, eontinue

showed good solubility, similar to that of the thiol-covered particles.[105] Transmission electron micrographs of **11**- and **12**-covered nanocrystals show excellent dispersion whether cast from organic or aqueous solution.

This PEG-pyridine ligand coverage has been applied further to CdSe/ZnS core/shell nanocrystals. These systems showed similar stability to the CdSe nanocrystals discussed above, but exhibit photoluminescent quantum yields that are an order of magnitude greater than the CdSe core nanocrytals. The successful functionalization of both CdSe nanocrystals and CdSe/ZnS core/shell nanocrystals demonstrates the versatility of this approach, and is promising for a range of future studies.

It should be noted that this work represents the first use of *para*-substituted pyridines for nanocrystal passivation, and we expect such methodology to grow in its usefulness due to the availability of 4-alkoxypyridine and 4-aminopyridine moieties, and the diverse range of substituents that can be conceivably attached at the 4-position. While there have been other reports that utilize PEG as a component of the CdSe nanocrystal passivation method,[106] this is the first extension to long PEG chains, and the first report where PEG is used as the sole ligand moiety to provide amphiphilic nanocrystals. This new ligand architecture gives rapid access to both water and organic soluble CdSe nanocrystals. Importantly, this method requires neither ionization nor the use of thiols to impart water solubility to the nanocrystals. We believe the simplicity of this technique, as well as future extensions of it, will further stimulate the integration of nanocrystals into both materials science and biological applications.

3.3 Future Work

An important aspect of these PEG-functionalized CdSe nanocrystals is the free hydroxyl groups at the PEG chain ends, to which subsequent chemical modification remains to be explored. Hydroxyl chain ends will allow for chemical attachment of a variety of moieties, including recognition units, fluorescent compounds, and chemical sensors. Appropriate attachment of biological targeting units will allow the study of fluorescent tagging of specific cells, genetic material, proteins, and organelles. After successful targeting of individual biological species, multiplexing studies can be explored allowing for the extended, simultaneous study of various quantum dot tagged species and their interactions with one another. These types of studies are valuable for elucidating the function of biological compounds in their cellular environment. Similar to the hydroxy chain end of this ligand, the pyridine moiety can also be modified. An interesting area for future work on this project would be to change the pyridine coordinating group for a terpyridine group. The inclusion of this terpyridine functionality may improve the coordination between the nanocrystal surface and the ligand because terpyridine has three possible coordination sites. Improved ligand coordination is always welcome as it improves the stability of the nanocrystals.

The topic of toxicity is consistently raised in discussions of quantum dots intended for biological applications. Cadmium is particularly concerning due to its highly toxic nature, and quantum dots are now undergoing *in vitro* and *in vivo* studies to further understand their impact on natural and living systems. The unique encapsulating environment of PEG found in **11** and **12**-functionalized nanocrystals offers the potential of decreasing the cytotoxic effect that the nanocrystals may

otherwise elicit. The PEG periphery may act as a shield between the nanocrystals and the biological environment. This can serve to reduce protein adsorption that often accompanies the introduction of foreign matter into the body. In addition, the PEG-periphery may reduce the toxic nature of the nanocrystals. Thus, the potential impact of this work is far reaching in nature, as this particular CdSe nanocrystal encapsulating system may serve as the basis for a number of applications in biological and material science, **Chapter 5** will describe the use of these materials in the self-assembly of quantum dots in block copolymers.

CHAPTER 4

CONJUGATED POLYMER-QUANTUM DOT COMPOSITES

4.1 Introduction

The unique optoelectronic properties of quantum dots described in previous chapters lead to their potential use as platforms in novel hybrid materials and devices, such as photovoltaic cells[107-109] and light emitting diodes.[110-112] However, the evolution of quantum dots from the laboratory demonstration stage to the device fabrication stage requires a number of key factors to be addressed, perhaps the most prominent of which is an appropriate compatibilization of the quantum dots within the host material or environment. This compatibilization, in turn, requires a tailoring of the ligand periphery at the quantum dot surface. Prior to the work to be presented in this chapter, ligand exchange chemistries were required for such surface tailoring.[85,100,102] While ligand exchange is currently standard practice for modification of the nanocrystal surface, such procedures often results in surface oxidation, changes in quantum dot size and size-distribution, and diminished photoluminescence intensity or quantum yields. This chapter presents two key advances in quantum dot synthesis and functionalization chemistry, including 1) the growth of highly photoluminescent CdSe nanocrystals directly in an environment of functional ligands, and 2) the subsequent use of these functionalized quantum dots for the preparation of poly(phenylene vinylene) (PPV)-CdSe composite materials that possess properties which are unobtainable by conventional polymer-nanocrystal blending techniques.[113]

Studies on the fabrication of nanocrystal-based composites with conducting polymers have led to numerous advances in optoelectric properties, but also revealed

numerous difficulties associated with incorporating nanocrystals into conducting polymer matrices. The major obstacle in constructing such composite materials is centered at the polymer-quantum dot interface. The insulating nature of the nanocrystal TOPO-periphery limits charge transport between the quantum dot and the surrounding matrix, an important criteria in many devices. Further exacerbating the fabrication of these systems is the incompatibility between the TOPO or pyridine ligand periphery and the surrounding polymer matrix. This incompatibility leads to nanocrystal aggregation within the polymer matrix, severely limiting the interfacial interactions in the system. A few reports have described techniques to address these aggregation problems, ranging from simple cosolvent casting[107,108] to more sophisticated techniques related to tuning the ligand or polymer environment for better compatibilization.[110,114,115] While these techniques mark important advances in the fabrication of nanocrystal-conducting polymer composites, they suffer from either insufficient nanocrystal dispersion, or multi-step polymer syntheses.

In this chapter we describe a straightforward method for directly synthesizing functional CdSe nanocrystals, and their subsequent modification with poly(*para*-phenylene vinylene) (PPV) by the "growth-from" approach. The example of PPV-quantum dot composites is used, where an intimate connection between the polymer matrix and the quantum dot surface reveals the profound effect on the photophysics of composites *vs.* simple blends. These results are of fundamental importance for future research and development of quantum dot based solar cells and LEDs.

4.2 CdSe Nanocrystals Tailored with Poly(phenylene vinylene)

The effective dispersion of CdSe quantum dots into thin films of PPV required two steps: 1) growth of the quantum dots in a phenyl bromide functionalized phosphine oxide ligand, shown as compound **13** in Figure 4.1, and 2) subsequent copolymerization of 1,4-divinylbenzene and 1,4-dibromobenzene derivatives in the presence of **13**-covered quantum dots for the surface-grafting of PPV. This nanocrystal growth method phenyl bromide functionalized nanocrystals with high quantum yield, and the absence of ligand exchange chemistry allowed for the inherent photoluminescence properties of

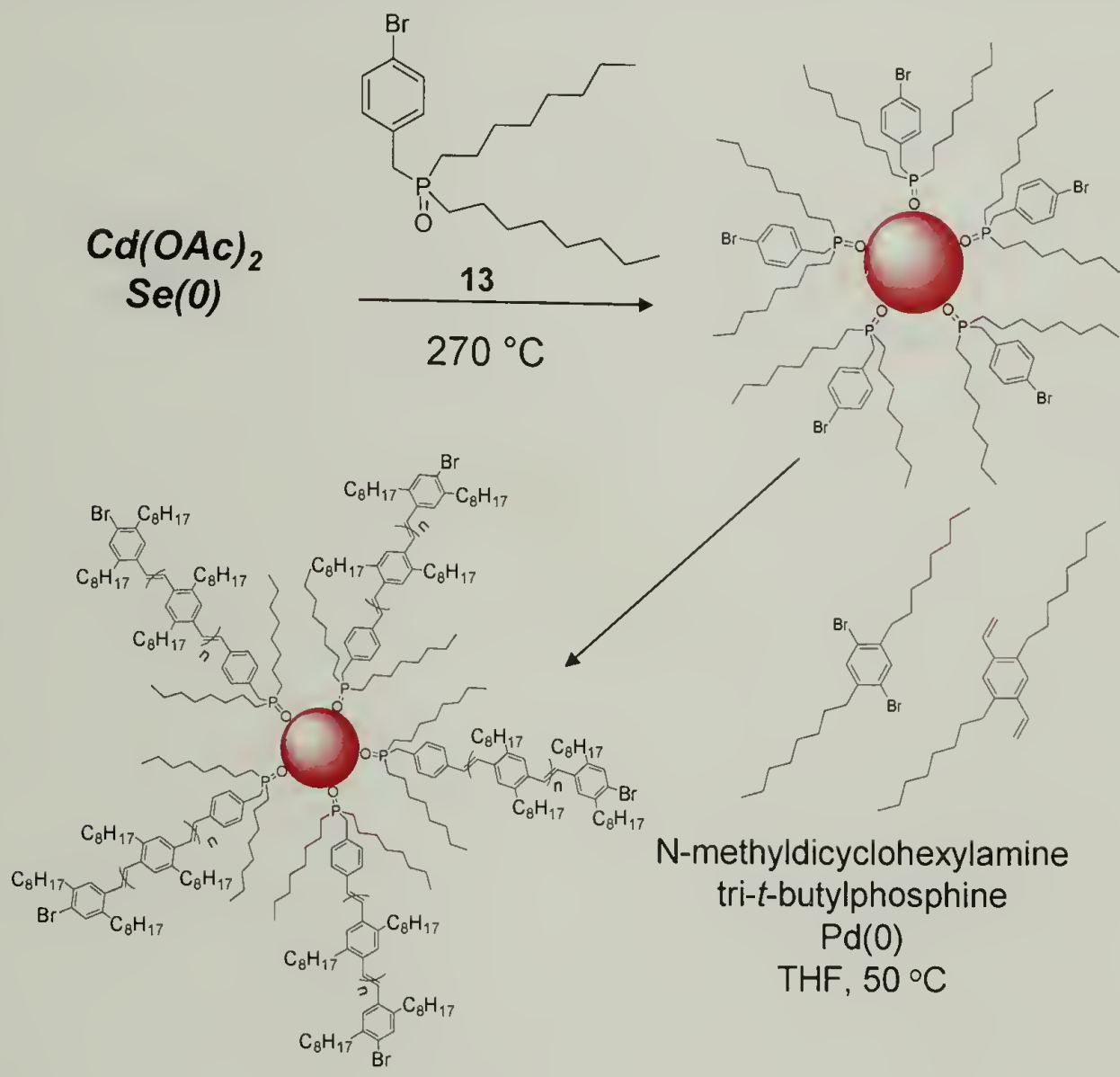

Figure 4.1: Synthesis of **13**-covered CdSe nanocrystals and their subsequent functionalization with PPV

the quantum dots to be maintained. Furthermore, grafting polymers from these functional quantum dots eliminates the difficulties associated with suppressing particle aggregation during blending of quantum dots and polymeric materials such as PPV.

Ligand **13** contains a phosphine oxide group similar to that of TOPO, as well as a phenyl bromide substituent necessary for subsequent phenylene vinylene polymerization chemistry. This novel phosphine oxide was prepared in 85% yield by nucleophilic substitution of di-*n*-octylphosphine oxide[86] on 4-bromobenzylchloride under phase transfer conditions, using tetra-*n*-butylammonium hydrogen sulfate (Bu_4NHSO_4) as the phase-transfer catalyst in a solvent mixture of toluene and $NaOH_{(aq)}$. A unique and valuable feature of compound **13** is its excellent thermal stability up to the temperature range of 250-275 °C, a critical feature for growth of high quality nanocrystals with narrow size dispersion. The use of compound **13** in place of TOPO in the quantum dot synthesis gave high quality, spherical nanocrystals containing a phenyl bromide periphery. A high resolution transmission electron microscope (TEM) image of a typical sample of **13**-covered quantum dots, shown in Figure 4.2, reveals the highly crystalline nature of the nanocrystals prepared in compound **13**. Electron diffraction further revealed the crystalline nature of these functionalized quantum dots, showing higher order reflections characteristic of the hexagonal packing of the wurtzite crystal structure. The presence of a band edge peak in the UV-Visible absorbance spectrum of **13**-covered nanocrystals, shown in Figure 4.3a, confirmed their quantum confined nature. Photoluminescence measurements on hexane solutions of **13**-covered nanocrystals showed their considerable quantum yield (65%) and narrow emission spectrum, as shown in Figure 4.3b. This data confirms the successful preparation of

high quality, functional quantum dots in ligand **13**, where ligand exchange chemistry was not necessary to achieve the desired functionalization of the nanocrystal periphery.

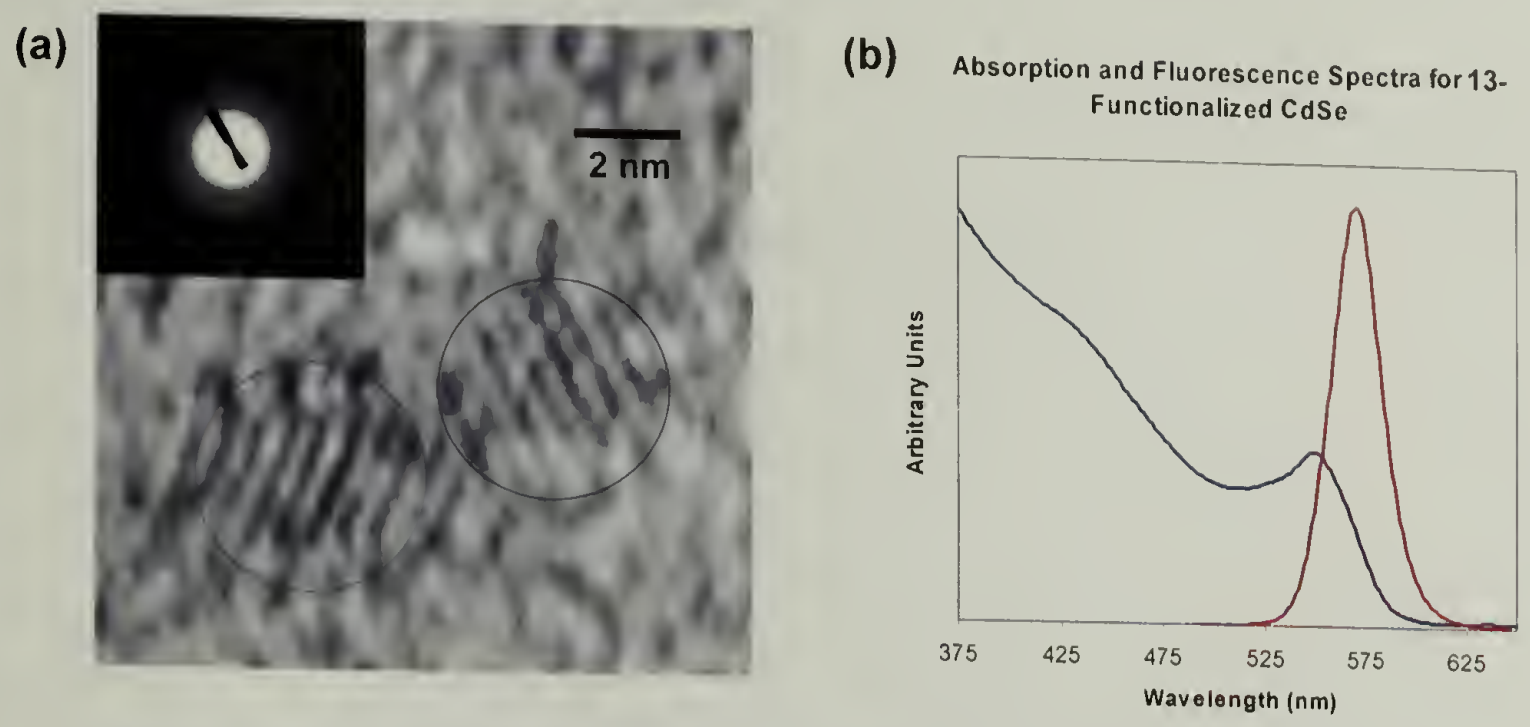

Figure 4.2: a) Transmission electron micrograph of **13**-functionalized CdSe nanocrystals at 650 K magnification. The lattice structure observed, as well as the electron diffraction pattern (inset) illustrates the crystalline nature of the quantum dots; b) UV-Vis (blue curve, band-edge absorption at 550 nm) and photoluminescence spectra (red curve, emission maximum at 570 nm; FWHM 30 nm) of **13**-covered quantum dots

Divinyl benzene derivates were polymerized from the surface of the **13**-covered quantum dots using the mild, palladium catalyzed Heck-type coupling conditions reported recently by Fu and coworkers.[116] The mildness of Fu's coupling conditions were important in our ability to functionalize the quantum dots with PPV while maintaining their nanoscopic integrity. For adaptation of this chemistry to quantum dots, a stirred tetrahydrofuran solution of **13**-covered quantum dots and $Pd_2(DBA)_3$ was heated at 50 °C for 24 hours in the presence of the 1,4-di-*n*-octyl-2,5-divinylbenzene and 1,4-dibromo-2,5-di-*n*-octylbenzene monomers.[117] The PPV-quantum dot composite product was isolated from the Pd catalyst and unbound PPV oligomers by repeated precipitation into methanol and subsequently redissolved in common organic solvents

(*e.g.*, hexanes, CH_2Cl_2, THF, etc.). Evidence of successful polymerization was supported by nuclear magnetic resonance (NMR) spectroscopy on $CDCl_3$ solutions of the composite material, where singlet resonances at δ 7.33 and 7.23 ppm were observed, corresponding to aromatic and vinylic resonances, respectively, in the polymer backbone. Further evidence of successful polymerization was obtained from matrix-assisted laser desorption ionization-time of flight (MALDI-TOF) mass spectrometry measurements performed on this quantum dot-PPV composite material. MALDI-TOF revealed the oligomeric PPV as primarily trimers and tetramers. This grafting-from approach is a polycondensation technique, and thus it affects a mixture of PPV bound to the quantum dots and "free" or unbound PPV. The unbound PPV acts as the host matrix in the composite material. It should be emphasized that the observed compatibility of the quantum dots with the polymerization conditions was key to the success of this study, as catalyst-induced quantum dot degradation was not observed by any of the analytical methods used (*e.g.*, TEM, UV-Vis and fluorescence).

Figure 4.3 illustrates striking differences in the transmission electron micrographs and photoluminescence spectra of the composite material prepared by these new methods, relative to PPV-CdSe blends prepared by simple mixing of the two components. TEM micrographs clearly show the aggregated morphology obtained by blending **13**- and pyridine-functionalized quantum dots (Figures 4.3a and 4.3b, respectively). One the other hand, the quantum dots are observed to be well-dispersed throughout the PPV matrix in the case of the composite material prepared by the graft-from approach (Figure 4.3c). The PPV-quantum dot composites were also found to possess unique optical properties not found in the blends (also illustrated in Figure 4.3).

PPV oligomers dominate the solution-state photoluminescence emission spectra (emission maxima approximately 440 nm) of both blends and composites (blue curves of Figure 4.3); only an extremely weak fluorescence contribution from the quantum dots is seen in the solution-state spectrum of the composite material. In the solid state, PPV dominates the photoluminescence of the blends (red curves of Figure 4.3a and 4.3b). However, in striking contrast to all other spectra, the quantum dot emission dominates the solid-state photoluminescence spectrum of the composite (red curve, Figure 4.3c, emission maximum approximately 570 nm), with almost complete quenching of the PPV emission. The emergence of a strong quantum dot emission, and loss of PPV fluorescence in the solid-state, is observed even in cases of very low quantum dot loading (2-5 wt.%). This result is particularly interesting when compared to the high nanocrystal loadings (50% or greater) typically needed to observe quantum dot emission in quantum dot-conducting polymer blends.

Insight into the importance of nanocrystal dispersion and effective surface tailoring is shown in Figure 4.3. While self-quenching events are expected to diminish the quantum yield of PPV when transitioning from solution to the solid state, this alone is not sufficient to explain the photoluminescence spectra of Figure 4.3c. We believe the increased intensity of the quantum dot emission relative to the PPV emission in the composite material is a result of increased contact between polymer and quantum dots in the solid state relative to the more extended conformation of PPV around the quantum dots in solution. Such an increased contact facilitates energy transfer, such that holes generated in the PPV, during excitation, are transferred to the quantum dots. Subsequently, these holes recombine with electrons in the quantum dot core, resulting

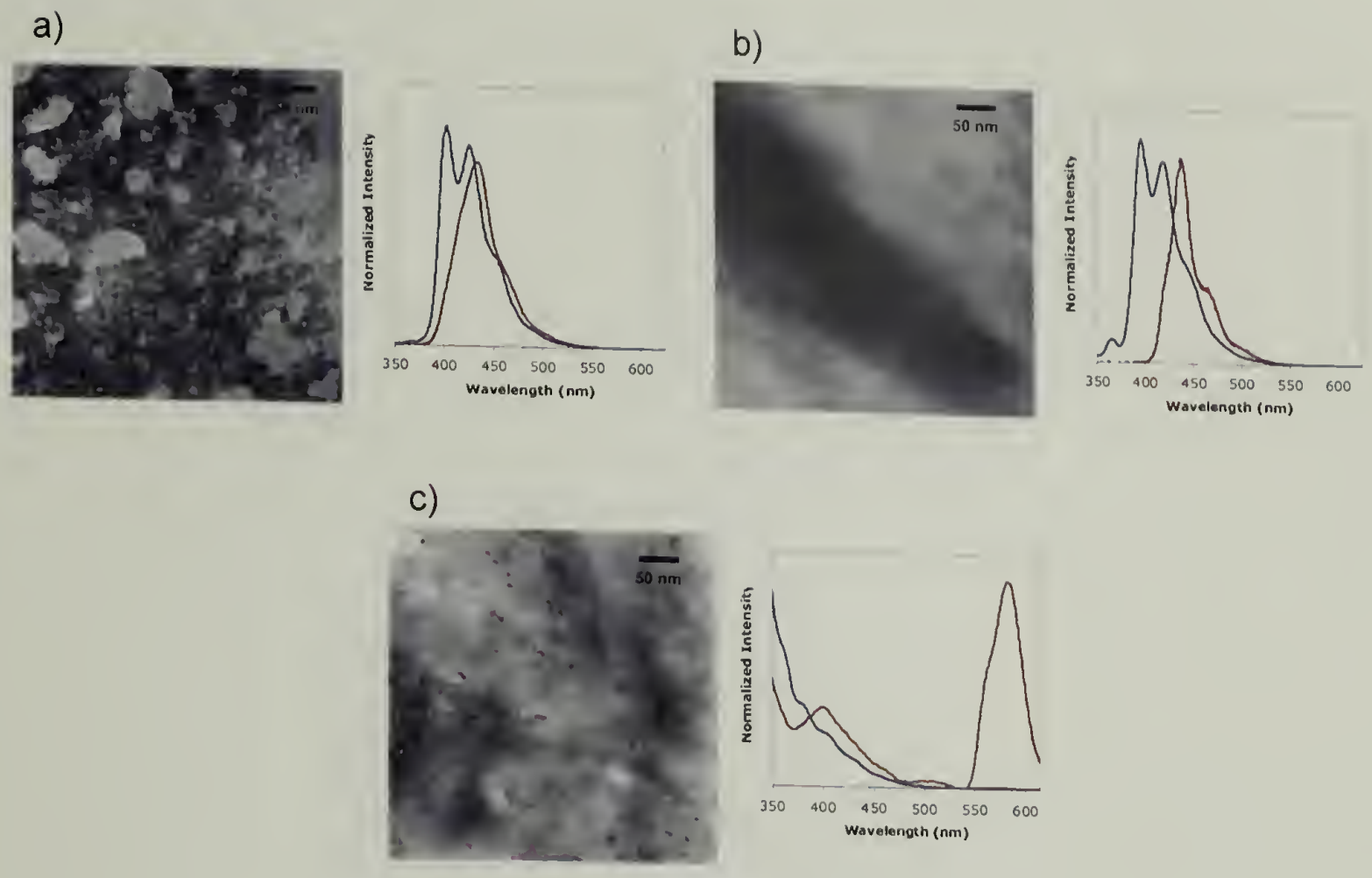

Figure 4.3: TEM micrographs and fluorescence spectra (excitation 330 nm; blue curve represents solution state fluorescence and red curve represents solid state fluorescence) of PPV-quantum dot hybrid materials. a) Pyridine-covered CdSe nanocrystals blended with PPV, b) **13**-functionalized CdSe nanocrystals blended with PPV, and c) composite CdSe nanocrystal-PPV, where PPV was grown from the nanocrystal surface. Each sample contained approximately 5 wt. % nanocrystal

in photoluminescence. Photoluminescence emission from the quantum dots in the solid state is by far more intense in the composite materials as prepared by this polymerization method relative to that of the blends. In the blends, very high weight percent loadings of quantum dots are required to observe photoluminescence emission. Figure 4.4 shows the examples of 10, 30, and 50 wt. % quantum dots blended with PPV. These blends possess substantial nanocrystal aggregation, as demonstrated by TEM images, that limits interfacial contact between the polymers and quantum dots. This reduction in interfacial contact, in turn, limits energy transfer pathways, and leads

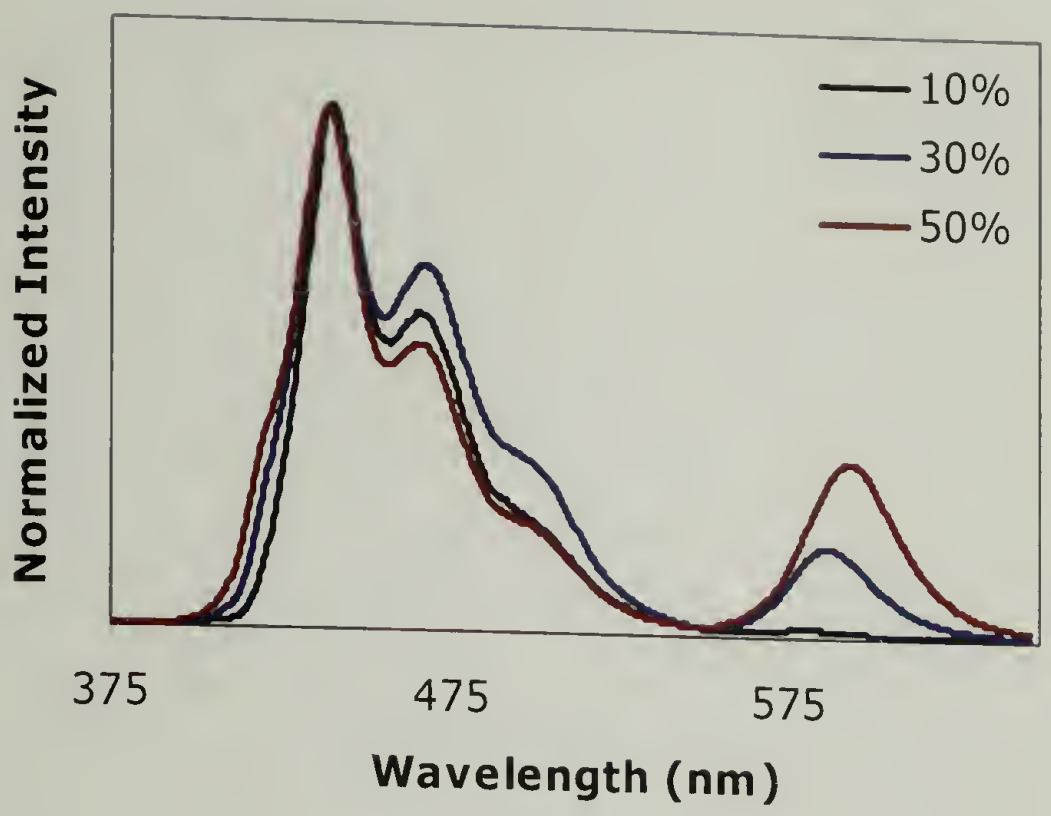

Figure 4.4: The effect of **13**-functionalized CdSe nanocrystal loading (wt %) on the solid state fluorescence emission spectra of CdSe-PPV oligomer blends

to self-quenching of nanocrystal fluorescence. Even at quantum dot loadings as high as 50 wt. %, emission from PPV dominates the photoluminescence profile. The low quantum dot loadings utilized effectively in the composite materials described here carry important fundamental and practical implications for future advances in quantum dot based materials, assemblies, and devices, where high nanocrystal loadings would disrupt the intended assemblies or make device fabrication impractical. This will also open opportunities for the use of quantum dots in conjunction with a range of polymers, where the effective use of reasonably low quantities of quantum dots will allow the intrinsic structural, morphological, and self-assembly properties of polymers to be exploited, rather than overwhelmed by large excesses of quantum dots.

In conjunction with Drs. Steven Switalski and John Pochan at Eastman Kodak Company (Rochester, N.Y.), an extensive analysis of the photoluminescence properties of PPV-quantum dot composites has been performed. Through these studies unique optical properties have been observed; for example, as the excitation wavelength used to excite the quantum dot-PPV composite is shifted to longer wavelengths (*e.g.* excitation wavelengths of 350 nm and greater), unexpected results are observed. The photoluminescence emission spectrum of the nanocrystal is bimodal, with maxima at 555 nm and 600 nm, as shown in Figure 4.5. This apparent splitting of the nanocrystal photoluminescence is more dramatic as the excitation wavelength was shifted more towards the red.

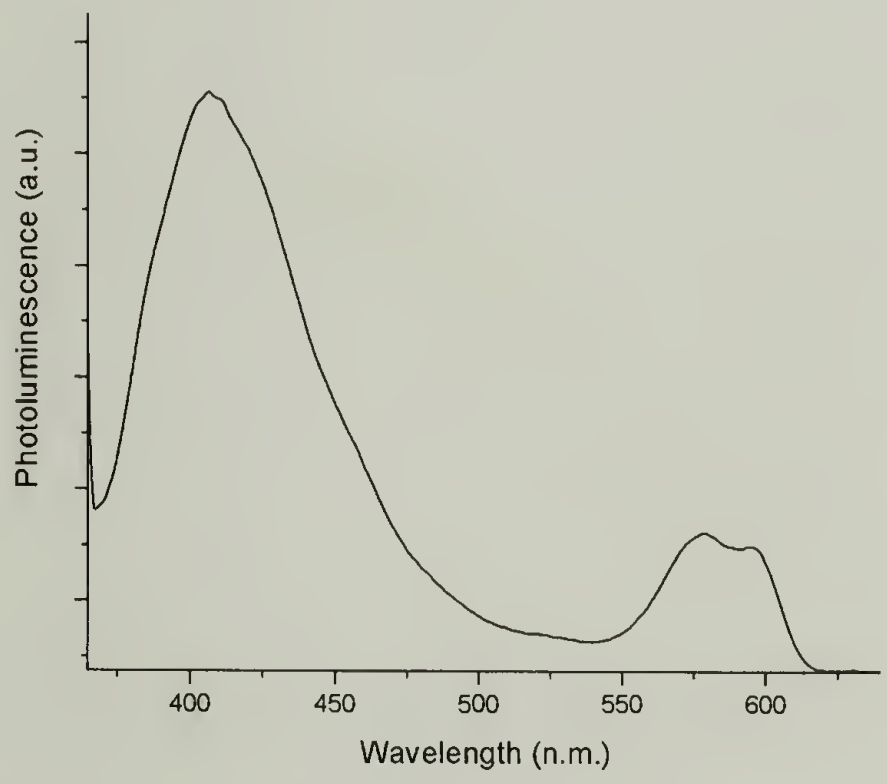

Figure 4.5: Photoluminescence spectrum of PPV-CdSe nanocrystal composite material excited at 350 nm. Emission of the quantum dot observed at 555 and 600 nm and shows two emission maxima

This unusual observation has not been reported for either nanocrystals or nanocrystal-polymer composite materials, and will be the subject of further study in the Emrick research group.

It was also observed that as the excitation wavelength was shifted further towards the red a second peak was observed in the deep red region (Figure 4.6a). This second peak is broader than the primary nanocrystal fluorescence peak, but careful examination of the excitation spectrum revealed a band edge absorption peak (Figure 4.6b). The observation of this distinctive peak has lead us to believe that the second peak is due to quantum dot emission. This second emission peak has also not been reported for quantum dots, and we hypothesize that this unique result is a direct result of strong interfacial contact between the nanocrystal and PPV. Both PPV and quantum dots have wave functions that extend out past their physical boundaries (*i.e.*, the wave functions extend out into their immediate environment), as a result of the close proximity of the PPV and the quantum dots, the wave functions may begin to overlap. This overlap would in effect create a new hybrid wave function which extends out further than either of the original wave functions. This increase in the extension of the wave function further delocalizes the electrons and reduces the bandgap of the nanocrystals. In other words, the extension of the nanocrystal wave function makes the nanocrystal core seem "larger" as illustrated by their red shifted optical behavior. This discussion is purely speculation, and many further experiments will be required to understand the behavior of these unusual composites.

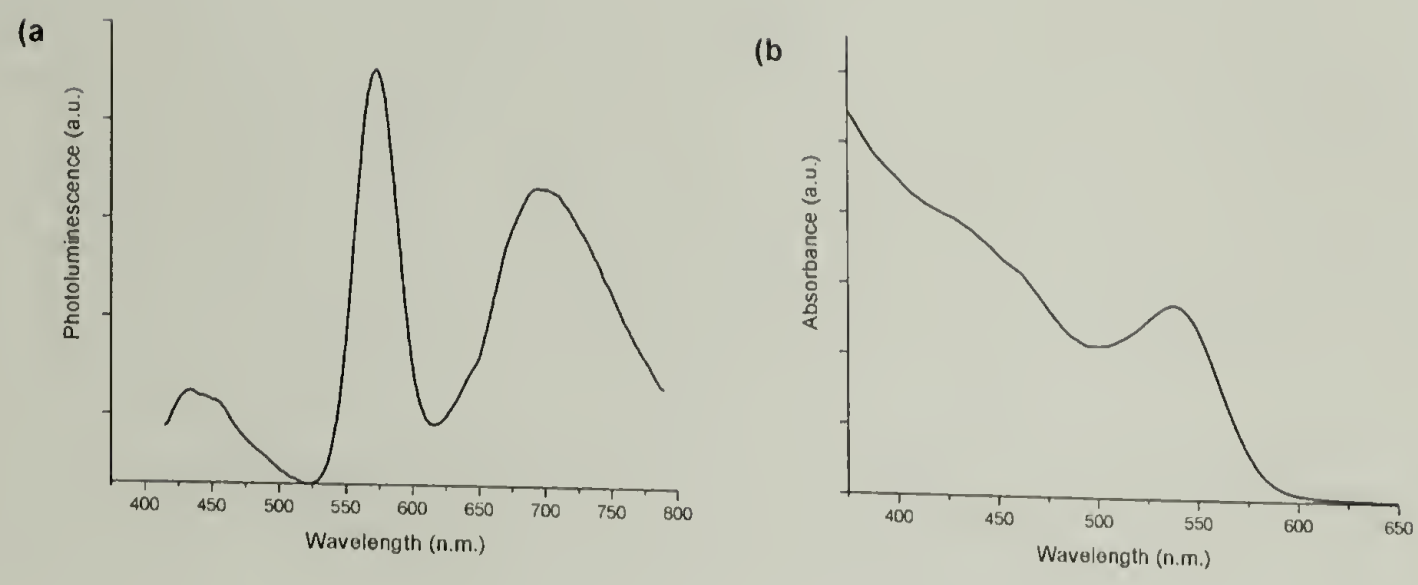

Figure 4.6: (a) Photoluminescence (excitation at 400 nm) and (b) excitation (emission at 700 nm) spectra of PPV functionalized CdSe nanocrystals

In summary, this section has described a preparation of PPV-quantum dot composite materials by novel methods that allow for the direct connection of the polymer and quantum dot components. The excellent dispersion of the quantum dots in PPV thin films obtained by this method dramatically impacts the photophysical properties of these composites relative to conventional blends. While PPV coverage is emphasized here, the novel quantum dot growth methods, and the general polymerization methodology, carries the potential for broad applicability that will enable new physical studies and device fabrication using polymer-quantum dot composite materials.

4.3 Summary and Future Outlook

Despite the tremendous progress in quantum dot-electronic polymers described in this chapter much remains to be studied on the topic. One area of further study will involve the unusual nanocrystal emission profiles in these composites that leads to the emergence of an additional emission peak as the excitation wavelength is shifted to the

red. These observations will not only have a major impact on the fundamental understanding of these systems, but may also lead to new approaches to light emitting devices by allowing more complex emission profiles.

Further study of various PPV derivatives will also solidify the versatility of this approach, as well as allow for a probing of the effects of PPV derivatives on the properties of composite materials. Substitution of electron donating and withdrawing substituents on the PPV backbone, *e.g.* through the addition of alkoxy and nitrile groups which donate and withdraw electron density, respectively, allows the bandgap of the PPV to be tuned and adjusted as desired (Figure 4.7). Such bandgap engineering will allow for tuning the absorption and emission spectra of the PPV relative to the quantum dot. By varying the PPV composition attached to the quantum dot surface, it may be possible to amplify the unique optical properties observed in the initial system, and allow for a more in depth understanding of these phenomena.

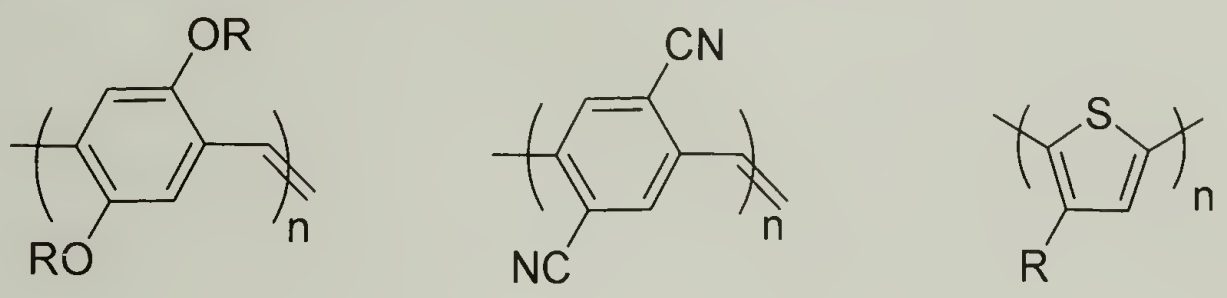

Figure 4.7: Proposed conjugated polymers that can be grown from the quantum dot surface

The polymerization of other conjugated polymers, *e.g.* polythiophene, from the nanocrystal surface is also interesting to further expand the versatility of this functionalization scheme. A unique attribute of **13**-functionalized nanocrystals is that their subsequent functionalization is not only limited to Heck couplings, but can include Sonogashira and Stille coupling for the polymerization of conjugated polymers. This

versatility may permit the growth of a variety of conjugated polymers from the nanocrystal surface, and also allow for further probing of optical and electronic properties.

CHAPTER 5

DIRECTED AND SELF-ASSEMBLY OF CdSe NANOCRYSTALS

Self-assembly processes offer many advantages over conventional "top-down" processing techniques, such as lithography and milling, as highly ordered features on the nanometer size scale can be obtained in the absence of any substantial externally applied force. Furthermore, self-assembly allows for the fabrication of complex devices based on nanoscopic materials that, due to their very small size features and/or other complexities, would be difficult and in some cases impossible to obtain using other processing techniques. The exceptional complexity of advanced devices places extraordinary demands on the properties of their components, and hybrid materials that integrate the properties of disparate materials will be required to address these demands as they allow for the creation of materials that combine the desired properties of the components while minimizing their short-comings.

As discussed in earlier chapters, quantum dots hold much promise as component of devices such as lasers, photovoltaic cells, memory storage, and light emitting diodes.[107,108,118-121] However, for many of these quantum dot-based devices, a predictable and regular spatial arrangement, and in some cases an exact placement, of the quantum dots is required. A beautiful example of CdSe nanocrystal assemblies was described by Murray *et. al.*[122] This involved a colloidal crystallization of CdSe nanocrystals into "superlattices." While much interest remains in such colloidal superlattices assemblies, the technique is rather difficult to perform, and is not likely practical for commercial application. Sita and co-workers[123,124] have described a technique that allowed for the directed self-assembly of metal nanoparticles with alkyl

periphery. These hydrophobic nanoparticles were found to preferentially adsorbed to the polystyrene (PS) domain of a P(S-*b*-MMA) diblock copolymer. Theoretical models developed by Balazs and co-workers[125] are providing insight regarding equilibrium or metastable phases of diblock copolymer/spherical nanoparticle composites. Some models predict the formation of ordered phases of diblock copolymers and nanoparticles, where the nanoparticle location is dictated by the minimization of its free energy.

The combination of inorganic nanoparticles and polymers represents one such case where the unique properties of each material, can be used advantageously to give a hybrid material with properties of each component. In **Chapter 2**, we showed that the dispersion and lateral distribution of nanocrystals within a polymer media affects their properties, and, thus, their ultimate utility. Polymer materials, unlike metal and other inorganic nanocrystals, have very desirable processing characteristics, such as adjustable viscosities, meltablity, solubility, controlled morphology, and elasticity. As a result of these favorable properties, significant efforts have begun in recent years to combine polymers and nanocrystals, where the dispersion and spatial arrangement of the nanocrystals can be controlled by the intrinsic morphology of the polymer.[126-129]

The unique assembly and morphological properties of block copolymers has been extensively studied. Russell and coworkers have shown that asymmetric diblock copolymers of polystyrene and poly(methyl methacrylate), denoted P(S-*b*-MMA), containing 30 volume percent PMMA, self-assemble into close-packed hexagonal arrays of PMMA cylindrical microdomains within a PS matrix.[130] Control over the interfacial interactions results in cylindrical microdomains oriented normal to the film

surface. The dimensions of the cylindrical microdomains can be controlled from 10-50 nm simply by varying the molecular weight of the copolymer.[131] As discussed in **Chapter 1**, various methods have been reported for the ordered incorporation of nanocrystals in block copolymer, but these techniques are difficult to produce or can only be used in conjunction with low-quality nanocrystals, *i.e.,* nanocrystals with low crystallinity and weak photoluminescence.

An exquisite example of nanoparticle-polymer self-assembly is found in the report of Böker *et.al.*[132] This work was based on discoveries associated with nanoparticle assembly at the oil-water interface, which forms the basis of this chapter. In this work, quantum dots were assembled into ordered arrays using polymer "breath figures" as templates. Breath figures are formed upon casting polymer solutions from volatile solvents, where the evaporation of the solvent cools the polymer film.[133-135] In this procedure, the breath figure array was generated by the evaporation of chloroform from a 7 weight percent solution of polystyrene containing 1 weight percent TOPO-covered nanocrystals (core diameter: 4nm) at a relative humidity of 80%. Chloroform evaporation causes the air-liquid interfacial temperature to drop below the dew point of water, resulting in condensation of water droplets on the surface. This condensation is followed by a condensation-limited growth of the droplets, *i.e.,* the rate of condensation controls the droplet growth rate, which gives in a narrow size distribution of the droplets. The droplets form a hexagonal lattice, and serve as templates for the nanocrystal assemblies. Prior to the polymer film reaching a critical viscosity, the TOPO-covered CdSe nanocrystals segregate at the interface, forming a uniform layer as depicted in Figure 5.1. Loss of solvent by evaporation solidifies the structure and gives

the nanocrystal decorated polymer film. This film can be visualized by fluorescence confocal microscopy, as shown in 5.1C, respectively. The high fluorescence intensity at the edge of the cavity provides evidence of nanocrystal assembly at the polymer-air interface. The assembly of quantum dots in this polymer template at the rim of the 3 to 5 μm indentations is shown in Figure 5.1C. The creation of assemblies that can be modified is an appealing prospect for forming stable, tailorable assemblies for sensing, controlled release, and catalysis and will be the focus of **Section 5.3**.

The remainder of this chapter will focus on the development of improved methods for the assembly of CdSe nanocrystals, where regularity of packing and spacing between the nanocrystals can be controlled precisely. Section **5.2** described two methods for the assembly of nanocrystals in block copolymer templates which was performed in collaboration with Matt Misner, Choon Soo, and Professor Tom Russell. The first involves the directed-assembly of nanocrystals by their deposition into polymer templates previously prepared from block copolymers.[136] The second allows for the simultaneous self-assembly of functionalized nanocrystals in a block copolymer. Section **5.3** describes the assembly and cross-linking of nanocrystals at the interface of two immiscible fluids. Key to the cross-linking of these nanocrystal fluid-fluid assemblies is the assembly of nanocrystals with functionalized ligands. The nature of the assembly, specifically at the planar or curved interface, leads to cross-linked nanocrystal sheets or capsules, respectively. As will be described, assemblies and materials made from precise nanoscopic building blocks offer extraordinary potential for new methods and materials for encapsulation and controlled release.

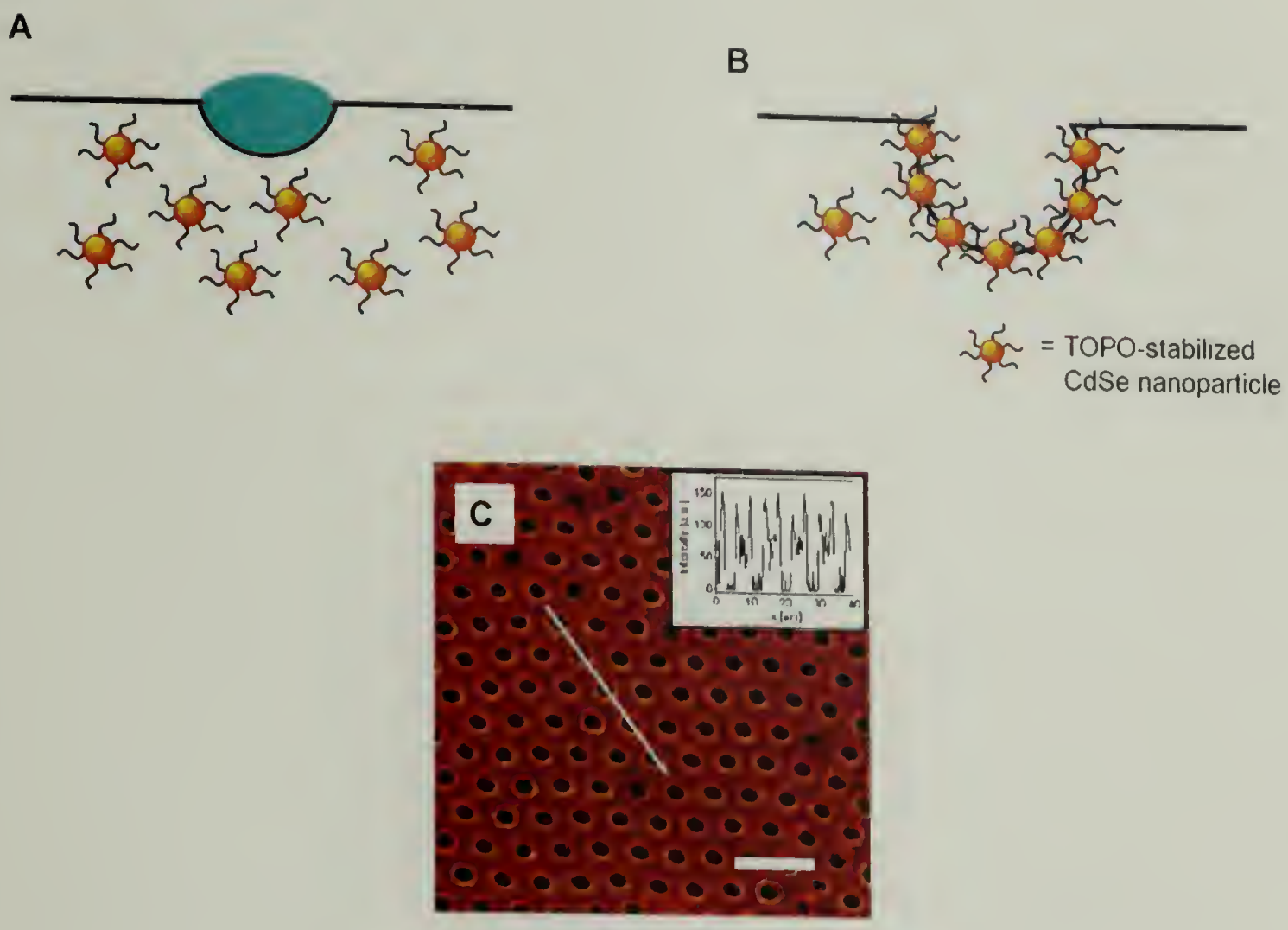

Figure 5.1: A schematic representation of CdSe nanocrystal assembly at a water droplet-solution interface during formation of a "breath figure." (A) Initially a small droplet of water condenses on the nanocrystal/polystyrene solution and (B) Subsequent segregation of the nanocrystals to the interface and evaporation of the solvent traps the nanocrystal at the polymer-air interface, thereby functionalizing only the surface of the holes. (C) confocal fluorescence microscope images of a sample obtained from solvent casting a chloroform solution of 7 wt.% PS (76 k) and 1 wt.% 4 nm TOPO-covered CdSe nanocrystals at 80% relative humidity. Scale bars: 16μm. The inset in C shows a fluorescence intensity scan along the line indicated

5.1 Assembly of CdSe Nanocrystals in Polymer Templates

The regular arrays achievable in diblock copolymer templates offer much promise for the assembly of nanocrystals over large length scales. Such templates would provide a means by which the nanocrystal dispersion in polymer materials, described in **Chapter 2,** can be improved on. While Xia and coworkers have shown that capillary forces can be used successfully to assemble micron size polystyrene

colloidal particles in an inorganic template, such studies had not been tried on the nanoscale.[137] Using this technique for the directed-assembly of nanocrystals in polymer templates represents a significant advance in directing the spatial distribution of nanocrystals in thin films, and provides a unique route to manipulate the lateral optical or electronic properties of films in a straightforward manner. In this case the increased surface area-to-volume ratio of the nanocrystals and templates adds increased surface interactions, that must be taken into account. Ideally, the self-assembly of both the nanocrystals and block copolymer would occur simultaneously. If performed correctly, this technique will allow for the segregation, and thus assembly of nanocrystals into specific regions of the block copolymer simply by casting the binary solution. The sections below describe techniques we have developed to achieve these types of morphologies.

5.1.1 Directed-Assembly of CdSe Nanocrystals Using Diblock Copolymer templates

Diblock copolymer templates, containing cylindrical domains of PMMA oriented normal to a silicon substrate were obtained by self-assembly of P(S-*b*-MMA) on a random copolymer of 58% polystyrene and 42% poly(methyl methacrylate). Exposure of the film to UV radiation selectively cross-links the PS domains, and simultaneously degrades the PMMA domains. Washing the films with acetic acid gave an array of 17 nm cylinders in a crosslinked PS matrix, where the cylinders had an aspect ratio of 1.7. These nanoporous templates were dipped into dilute heptane solutions of TOPO-covered nanocrystals (<500 μg/mL), then withdrawn normal to the

air-solution interface. As the film is withdrawn, capillary forces acting on the nanocrystal solution sequester the nanocrystals into the nanopores of the template. The nanocrystal deposition was found to be dependant on four parameters: 1) the concentration of nanocrystals in the solution, 2) the rate of removal of the porous template from the nanocrystal solution, 3) the solvent evaporation rate, and 4) the interaction of the solvent with the template. Solvent choice proved critical to the success of these experiments. In the ideal case, the solvent should wet the template, yet not swell the cross-linked polystyrene matrix. When toluene solutions of nanocrystals were used, no nanocrystal deposition was observed, probably a consequence of PS swelling in toluene that closes the nanopores and prevents nanocrystal deposition. A schematic of the deposition process is illustrated in Figure 5.2A. This Figure illustrates that as the substrate is withdrawn from solution, the meniscus of the nanocrystal solution extends above the solution surface across the nanoporous template. This results in the highest nanocrystal concentration at the edge of the receding front. As this solvent front moves across the template, capillary force traps the nanocrystal solution within the nanopores. The capillary force is defined by the interfacial energy between polystyrene matrix and heptane solution, as well as the dimensions of the pores. Upon complete removal of the polymer template from the heptane solution the solvent trapped in the nanopores evaporates, leaving behind the nanocrystals in the pores. These newly sequestered nanocrystals retain their photoluminescence, Figure 5.2B. In addition, the increased photoluminescence intensity observed from templates dipped in higher concentration suggests a greater density of nanocrystals residing in the templates.

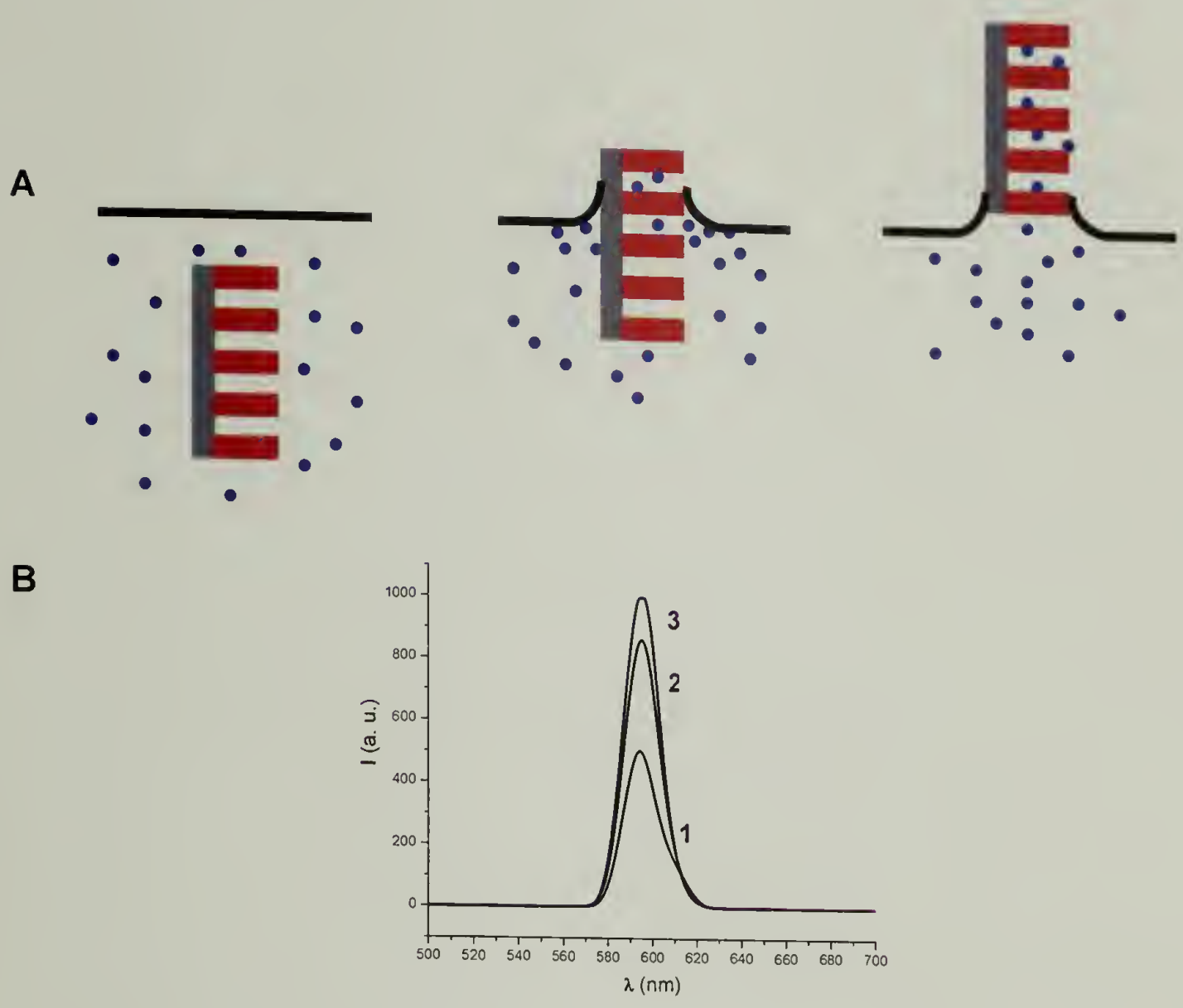

Figure 5.2: (A) Procedure for the deposition of nanocrystals into nanoporous block copolymer template by withdrawal from a heptane solution of TOPO-covered CdSe nanocrystals. (B) The photoluminescence spectra of the CdSe nanocrystal filled templates demonstrating that higher solution concentration in the dipping process gave templates with stronger emission signals. Solutions 1, 2, and 3 are 65, 130, and 240 μg/ml, respectively

To test the affect of nanocrystal solution concentration on the deposition into the template transmission electron microscopy was employed. Figures 5.4A-C show transmission electron micrographs of the polymer templates filled with 5 nm CdSe nanocrystals, deposited from solution with nanocrystal concentration varying from 65 to 240 μg/mL. Evident from these images is the increase in the average number of nanocrystals per nanopore with increasing concentration. Close inspection of the

templates reveals the average number of nanocrystals per pore is ~ 1.3, 2.5, and 3.3 for concentrations of 65, 130, and 240 μg/mL, respectively.

The effect of the template withdrawal rates was studied by varying the withdrawal rate from ~2 to 1200 cm/min. TEM images obtained using a 130 mg/mL solution where the withdrawal rates were 1200 cm/min and 2 cm/min, respectively showed a greater number of nanocrystals localized in the nanopores as the withdrawal rate is decreased, suggesting that the rate at which nanocrystals diffuse to the receding front limits the filling of the pores.[136] Consequently, the efficiency of packing increases with decreasing withdrawal rate.

The relative difference in size of the nanocrystals and the nanopores was found to have a dramatic effect on the nanocrystal deposition. Obviously, if the particle diameter is larger than the pore diameter, it is simply not possible for the particles to enter; however, if the nanocrystal diameter is much smaller than the pore diameter, then multiple particles will be deposited within each pore. Consequently, there is an optimal size ratio where the deposition of only one nanocrystal per pore is most favorable. Figure 5.3D shows TEM images of a template with 17 nm diameter pores where the nanocrystal diameter was 10 nm. Although not all the pores are filled, most of the pores are filled with only one particle. This is in dramatic contrast to the results shown in Figure 5.3A-C where the nanocrystal diameter was only 5 nm. In the case of 10 nm particles, the size of the nanocrystals is only increased by a factor of 2, but the deposition of multiple nanocrystals in the nanopores was completely suppressed.

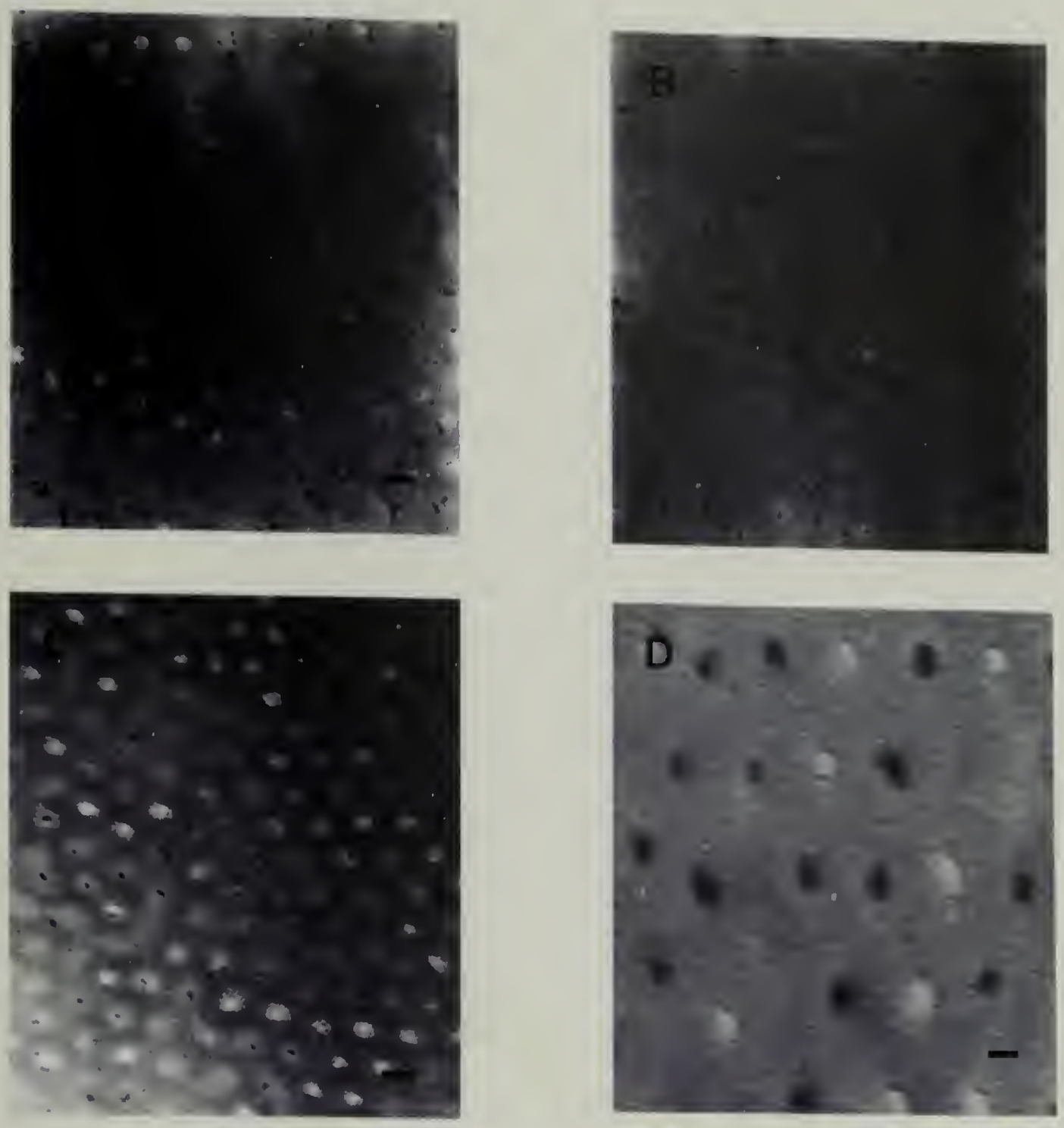

Figure 5.3: TEM micrographs showing the effects of solution concentration and withdrawal rate are shown above. The deposition of 5 nm particles solutions of (A) 240 μg/ml, (B) 130 μg/ml, and (C) 65 μg/ml (at ca. 20 cm/s). (D) 10 nm nanocrystals deposited into the polymer template illustrating the possibility of placing one particle per pore. The scale bar represents 20 nm

In this section, we have demonstrated a versatile technique for the deposition of CdSe nanocrystals in nanoporous polymer templates formed from block copolymers. The ordered structure of the template imparts a higher order structure to the nanocrystal

assembly, while maintaining the inherent photoluminescence of the nanocrystals. In addition, this technique can be extended to polymer templates having lamellar, as opposed to cylindrical, morphologies resulting in nanoscopic channels of nanocrystals. While this technique offers a direct approach to the formation of nanocrystal assemblies, multiple steps are required for their fabrication. Ideally, a technique that allows for the simultaneous assembly of both the nanocrystals and the polymer should be developed, as will be discussed in **Section 5.2.2**.

5.1.2 Simultaneous Self-Assembly of CdSe Nanocrystals and Block Copolymers

The two step process for making nanocrystal arrays described in the previous section might be simplified to a one step self-assembly process. One possible route to this assembly is to integrate the nanocrystals into the diblock copolymer assembly *during* the assembly process. A properly functionalize nanocrystal would be attracted to one of the blocks by means of enthalpic interactions. Thus, this represents a case where the surface ligand chemistry as well as the nanoscopic features are key to the assembly process.

As a control experiment, the PEG-covered nanocrystals (**Chapter 3**) were examined for their miscibility in PMMA. A 10 wt % solution (relative to PMMA) of **12**-covered CdSe nanocrystals and PMMA in toluene was spun cast onto a P(S-*r*-MMA)-coated silicon wafer. The cast films were allowed to dry under vacuum overnight. Performing TEM on these films revealed well dispersed quantum dots in the PMMA matrix as shown in Figure 5.4. This result indicates that PEG-covered nanocrystals were miscible with PMMA and the low surface tension between the PEG-

covered nanocrystals and the PMMA precludes nanocrystal aggregation. This observed miscibility is in agreement with studies showing PEG homopolymer to be miscible with PMMA between 10 and 30 wt%. In contrast, PEG-covered nanocrystals were found to

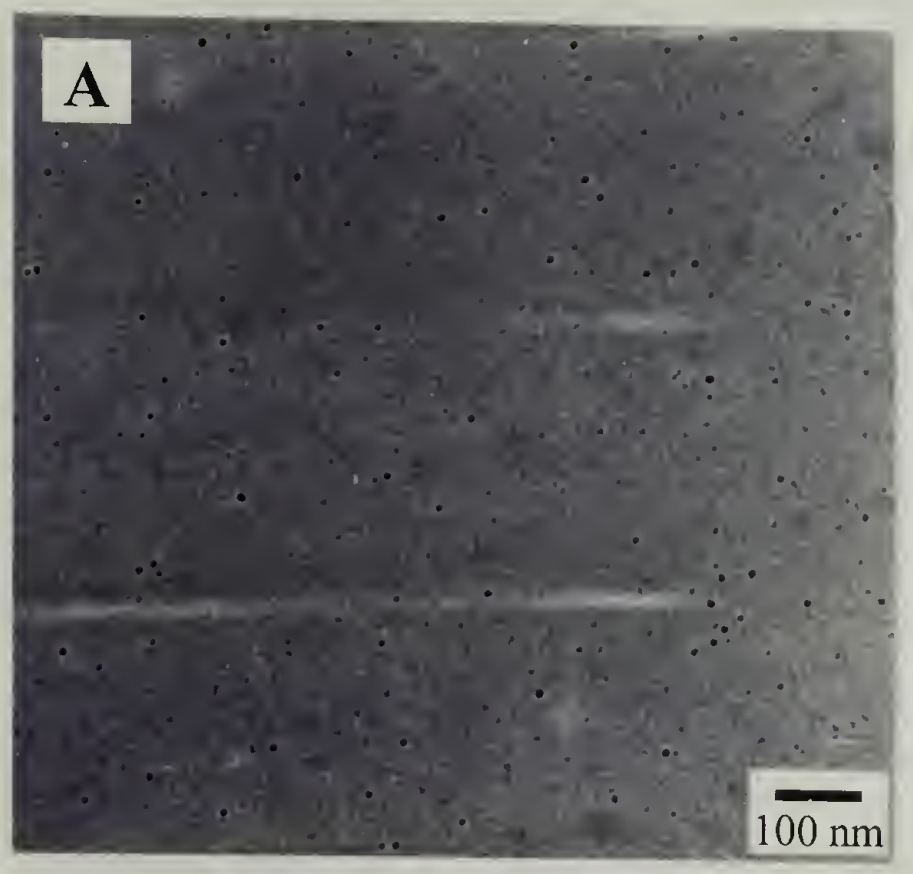

Figure 5.4: TEM image of **12**-covered CdSe nanocrystals dispersed in a PMMA matrix

aggregate when incorporated into PS films, due to unfavorable interactions between the PEG-covered CdSe nanocrystals and PS matrix. The nanocrystal dispersion in the PMMA was maintained after annealing the composite film at 170 °C for 24 hours, in contrast, annealing the nanocrystal/PS composite resulted in the film becoming turbid, suggesting further aggregation of nanocrystals on the micron scale.

While the dispersion of quantum dots in PMMA is of interest, the goal of this project is the assembly of nanocrystals in a block copolymer film. To accomplish this, **11**- or **12**-covered CdSe nanocrystals were dissolved in toluene with P(S-*b*-MMA) and spun cast onto a silicon substrate covered with P(S-*r*-MMA). The TEM image of

Figure 5.5 shows P(S-*b*-MMA) thin films containing nanocrystals that are ordered in a P(S-*r*-MMA) substrate upon annealing. The CdSe nanocrystals, assembled within the diblock copolymer thin film, with nanocrystals only occupying the PMMA domain. In a number of these samples, the nanocrystals appear to be placed more predominately at the interface of the two polymer domains. While this is an interesting result further studies need to be performed, Figure 5.5A. However, **12**-covered nanocrystals were predominately sequestered in the center of PMMA domain (Figure 5.5A). This result

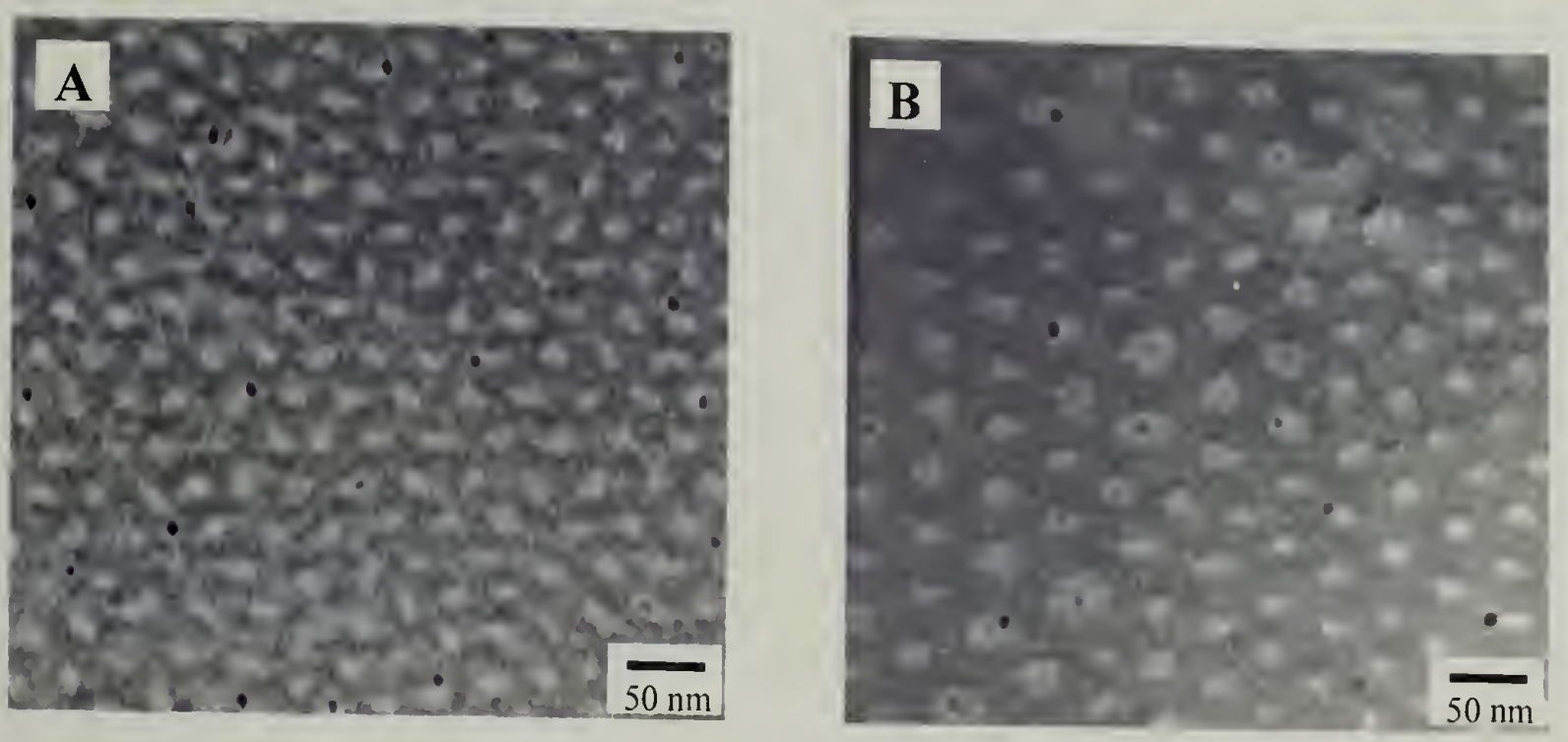

Figure 5.5: (A) **12**-covered and (B) **11**-covered CdSe nanocrystals assembled in a P(S-*b*-PMMA) copolymer template

may be due to the hydroxyl end groups of ligand **12**, which is expected to interact more favorably with PMMA than the methyl terminated ligand of **11**. Attempts to incorporate greater than 10 wt% nanocrystal into the composite material precluded block copolymer assembly into ordered arrays. This is not surprising, as incorporating high weight percentages of PEG in the diblock copolymer, and specifically into the PMMA phase, would significantly disrupt the diblock copolymer phase diagram.

In summary, this section has demonstrated the possibility of fabricating highly organized, thermodynamically stable nanocrystal-diblock copolymer composites by mixing and annealing. Nanocrystals compatible with one of the diblock copolymer can be prepared by ligands with strong affinity for a block component, and results in their self-assembly into a specific domain.

5.2 Interfacial Assembly of Nanocrystals in Immiscible Fluids

The interface between two immiscible fluids offers a unique platform for the assembly and subsequent modification of colloidal particles.[138-142] These interfaces have already been shown to be ideal for the assembly of elastic, semi-permeable capsules composed of micron-sized colloidal particles.[141] For nanoparticles, however, thermal energy, which causes spatial fluctuations of the particles, is comparable to the interfacial energy. This energy balance results in a weak interfacial segregation of the nanoparticles. Nanoscale particles, unlike micron sized particles, form assemblies were the particles are weakly confined to the liquid-liquid interface. The weak confinement of these particles allows for more complex architectures, *e.g.* in the form of 2-D phase separation of different size nanoparticle (an morphology not possible with micron sized particles).[142] The rapid diffusion of nanoparticles and reagents from either fluid also leads to very efficient interfacial chemistry. Surfaces of dispersed droplets offer a substantially greater interfacial area than a planar interface. Moreover, the size and shape of droplets can be controlled from microscopic to macroscopic dimensions by use of an external force. The fluid environment of the assembly allows for post-assembly chemical modification from either side, allowing flexible routes for modification and

cross-linking of these assemblies. Ligand encapsulated nanoparticles are well suited for hierarchical self-assembly, as the nanoparticle core dictates optical, electronic, or magnetic properties, and the surface-bound ligands define the particle's interactions with its surroundings. Highly ordered composite materials described in this chapter can be used as next-generation catalysts, electronics, or photonic devices.

The assembly of nanoparticles at the oil-water interface offers unique opportunities not present in polymer-nanoparticle assemblies. The rapid diffusion and high mobility of nanoparticles allows for the rapid achievement of equilibrium. Second, the fluid interface on either side of the assembly allows for diffusion of chemical reagents to and from each side, such diffusion could be useful for the subsequent chemical modification of these assemblies.

The assembly of CdSe nanocrystals at the liquid-liquid interface first attracted our attention when, in collaboration with Professors Thomas Russell (UMASS, PSE) and Anthony Dismore (UMASS, Physics) the formation of stable water droplets was observed upon vigorously shaking a toluene solution of TOPO-covered nanocrystals and water, as shown in Figure 5.6.[78] In this procedure, a drop of water was added to a solution of nanocrystals and shaken vigorously, resulting in nanocrystal-coated water droplets with diameters from 10 to 100 μm. To demonstrate the encapsulation of a water droplet by nanocrystals, the inset of Figure 5.6A shows a fluorescence image of a nanocrystal assembly containing the water soluble dye sulforhodamine-B. By independently monitoring the fluorescent emission of the CdSe nanocrystals and sulforhodamine-B, at 525 and 585 nm, respectively; we found the nanocrystals

segregated to the toluene-water interface, and the sulforhodamine-B, completely localized within the interior of the water droplet.

Atomic force, electron, and interface contrast microscopy on these samples showed these assemblies to be composed of a single monolayer.[78] The nanocrystals in these assemblies were found to be close-packed but liquid-like, from X-ray scattering and TEM studies, showing no long range order and an average particle-particle separation distance commensurate with the diameter of the nanocrystals plus twice the length of the stabilizing ligand. Fluorescence photobleaching studies on these liquid-like assemblies illustrate the highly mobile nature of these nanocrystals on and off the droplet as well as laterally around the droplet.

The interfacial assembly of nanocrystals at the oil-water interface is dictated by a minimization of the Helmholtz free energy. Calculations by Lin and Russell determined that placement of one nanocrystal at the oil-water interface decreases the entropy by about k_B (the Boltzmann constant). Consequently, the energy change, ΔE, must be negative to reduce the total free energy. The interfacial energy equation below shows three contributions to the interfacial energy including the particle-oil interface ($\gamma_{P/O}$), the particle-water interface ($\gamma_{P/W}$), and the oil-water interface ($\gamma_{O/W}$).

$$\Delta E = -\frac{\Pi R^2}{\gamma_{O/W}} \times [\gamma_{O/W} - (\gamma_{P/W} - \gamma_{P/O})]^2$$

R is the effective radius of the nanoparticle. Inserting values for $\gamma_{O/W}$, $\gamma_{P/O}$, and $\gamma_{P/W}$, ΔE is about -5 $k_B T$ for 2.8-nm-diameter nanoparticles, where T is absolute temperature. Because ΔE depends on R^2, the energy gain is smaller and the assembly is less stable for

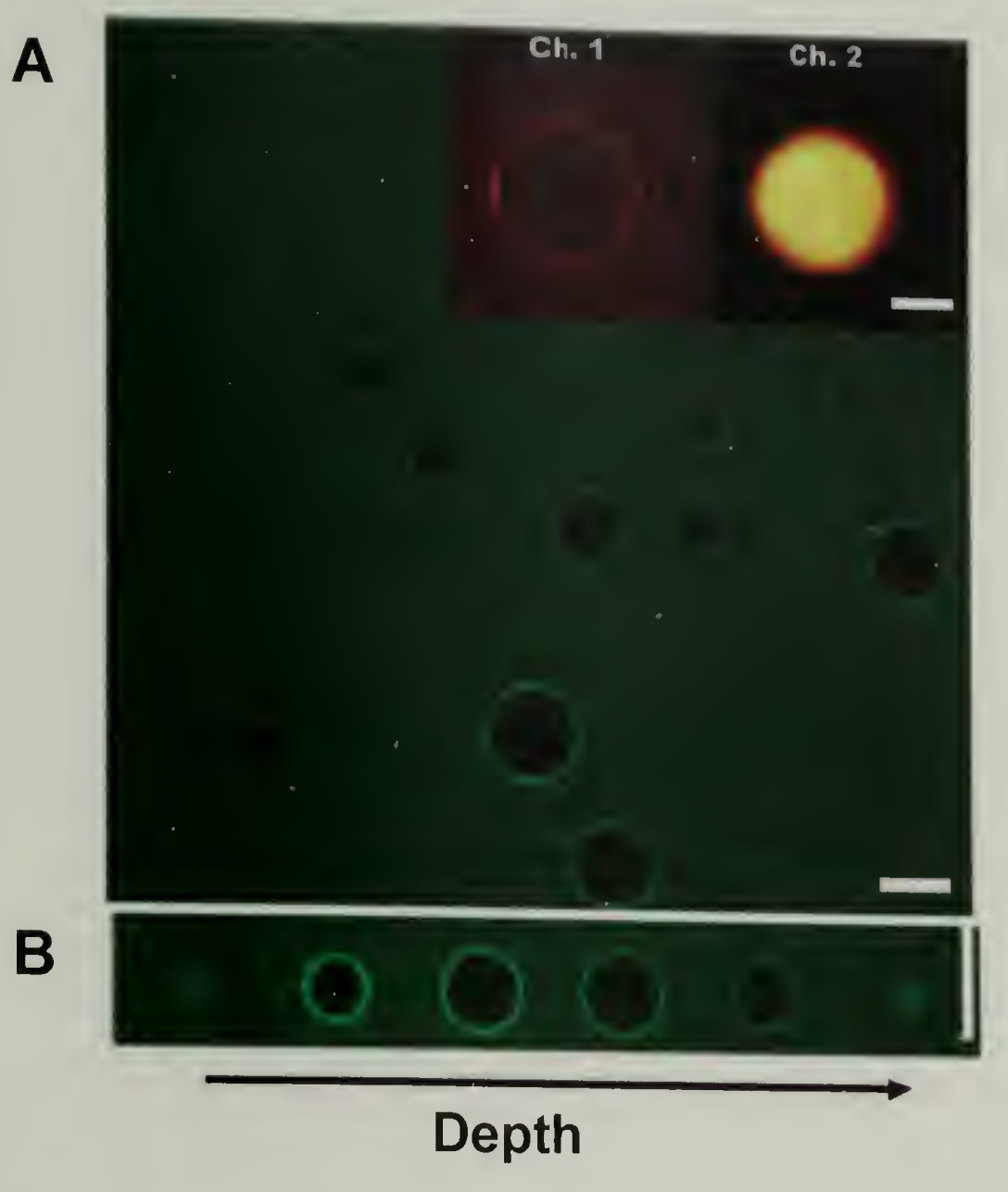

Figure 5.6: Confocal microscope image of TOPO-covered CdSe nanocrystal assembled at the interface of oil and water. (A) Confocal image of different size droplets, (inset) fluorescence image of nanocrystals assembled on a water droplet of sulforhodamine-B dye. Channel 1 represents fluorescence from the nanocrystals and channel 2 represents fluorescence from the dye. (B) Confocal cross-sectioning of a an individual droplet illustrating its spherical nature

smaller nanocrystals than for larger ones. Consequently, thermal energy is sufficient to induce a displacement of these nanoparticles from the interface. In fact, no droplet stabilization was observed when nanoparticles with diameters less than ~1.6 nm (not including the ligand) were used.

The weak energy associated with nanoparticle assembly at the liquid-liquid interface gives rise to instabilities in the system due to a thermally activated escape from the interface. As the nanoparticle size increases, its stability at the interface

increases, resulting in a longer interfacial residence time of the particles. Micrometer-sized particles are strongly held at the interface and once assembled resist displacement from the interface. In contrast, nanometer-size particles can be preferentially displaced at the interface by larger particles. Figure 5.7 shows the result of introducing a toluene solution of 4.6-nm particles to a preformed interfacial assembly of 2.8 nm particles. The 2.8 nm particles, with characteristic emission at 525 nm, are shown as green, while the 4.6 nm particles, with characteristic emission at 610 nm, are red. The red patch present on the spherical assembly indicates that the 4.6 nm particles displaced the smaller 2.8-nm particle. Furthermore, in keeping with the calculations of Yao Lin, the inverse case,

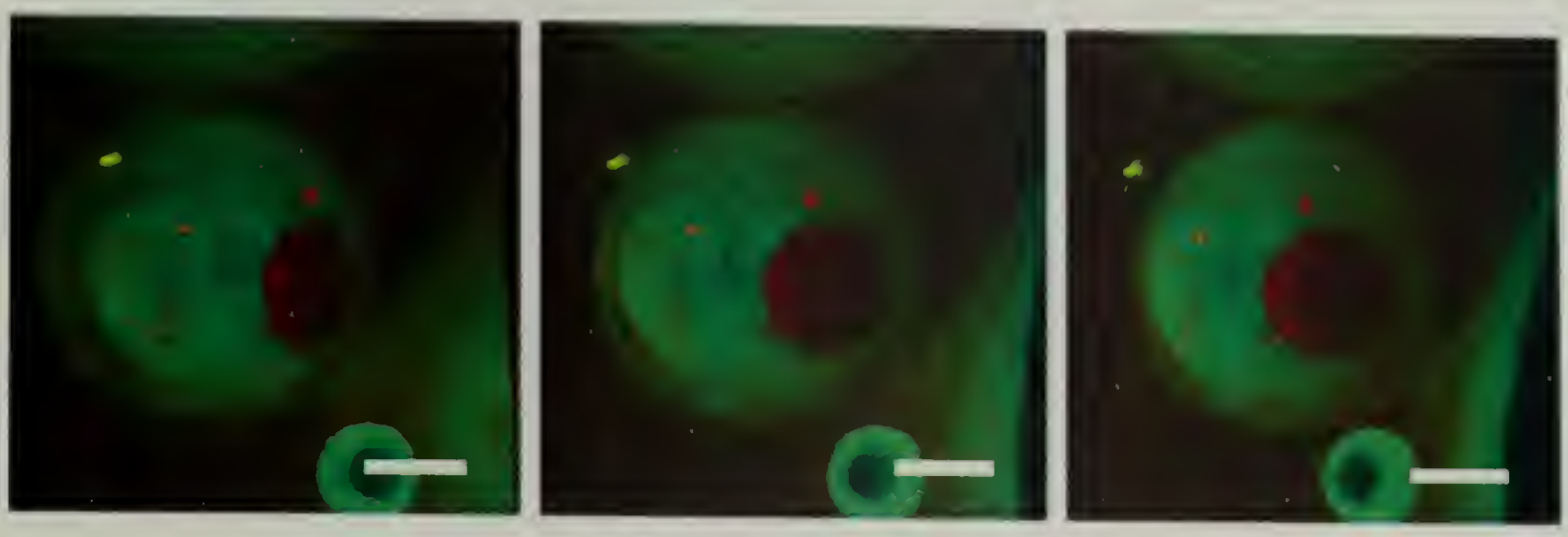

Figure 5.7: Three-dimensional reconstruction of confocal microscope image of 2-D phase separation of 2.8 nm particles (green) and 4.6 nm particles (red) assembled at the interface of oil and water. The scale bar, 16 μm

displacement of larger nanocrystals with smaller nanocrystals, did not occur. This observed displacement process is unique to nanometer size particles, as assemblies of microparticles could be used in a smilar fashion. While the weak assembly of these nanocrystals at the liquid-liquid interface offers unique possibilities and opportunities for fundamental assembly studies, an important target for this thesis is the preparation of stable and robust materials from these assemblies. Two techniques are described in

the following sections for the chemical cross-linking of the assemblies. Both methods utilize functionalized ligands as the key precursor to the assemblies and the cross-linked materials from these assemblies.

5.2.1 Cross-linked Nanocrystal Sheets by Radical Polymerization of the Fluid-Fluid Interfacial Assemblies

CdSe nanocrystals covered with vinylbenzene ligand **1**, and a core diameter of 2.9 nm were prepared as described in **Section 2.2**.[79] A toluene solution of these functional nanocrystals was added to an eppendorf tube containing an aqueous solution of 2,2'-azobis(2-(2-imidazolin-2-yl)propane) dihydrochloride (Wako VA-044), and the nanocrystal segregated to the planar oil-water interface. The eppendorf tube was then sealed under nitrogen, and heated to 60 °C for 6 hours. Under these conditions, radical initation and reaction across the ligands gave cross-linked membrane of nanocrystals at the toluene-water interface. The membrane was gently removed from the interface by pipette and suspended in toluene.

Three-dimensional confocal fluorescence microscope images of the sheets suspended in toluene (rotated to view at three different angles), are shown in Figure 5.8. The film has surface area of approximately 1 cm^2. The crumpled morphology is most likely a result of shear stresses encountered during manipulation by the micropipette. The fluorescence emission at 540 nm arises from the nanocrystals and remains unchanged before and after the assembly and cross-linking. The observation of a structurally intact elastic membrane floating freely in toluene verifies successful cross-linking of the nanocrystal assembly. It should be noted that while this membrane is

clearly observable by photoluminescence; it is not visible in a transmission optical microscope due to its ultrathin nature (approximately 5 nm in thickness if it is composed of a monolayer of nanocrystals).

Figure 5.8: Confocal microscope image of a sheet of cross-linked **1**-functionalized nanocrystals. The scale bar is 16 μm

Insight into the elastic nature of these films is provided by the crumpled morphology of the sample. The pronounced ridges observed are similar to those in macroscopic crumpled sheets such as paper or aluminum foil.[143] Russell and coworkers used elasticity theory to characterize this sheet by an area-expansion modulus G and a bending modulus κ. They assumed the membrane is composed of an

$$C_o \approx \left(\frac{1}{L}\right)\left(\frac{L}{(\kappa / G)^{1/2}}\right)^{1/3}$$

isotropic material, which resulted in a $(\kappa/G)^{1/2}$ being approximately equal to the film thickness. These calculations resulted in a $(\kappa/G)^{1/2}$ value of between 2 to 7 nm,

comparable to the expected membrane thickness of ~5 nm for a monolayer of nanoparticles.

Ultrathin sheets such as these presented here are of fundamental interest for their potential mechanical and barrier properties, as well as for possible applications in separations and catalysis. To evaluate the permeability of these cross-linked membranes, a droplet of an aqueous solution of sulforhodamine-B was suspended on the membrane in an eppendorf tube, and the diffusion of the dye was monitored, as shown in Figure 5.9. The curvature of the membrane arises from its contact with the side-walls of the tube and the energies of the toluene/water, toluene/wall and water/wall interfaces. To remove any toluene trapped between the dye and the membrane, additional dye solution was then added (Figure 5.9B) and the tube was tapped vigorously. The formation of an intimate contact of the dye solution across the entire membrane resulted in a decreased curvature of the membrane (Figure 5.9C), but no convective transport of the dye across the membrane was observed. Approximately twelve minutes after the introduction of the dye, it is seen to diffuse across the nanocrystal membrane and into the aqueous layer (Figure 5.9D).

A key result of this experiment was the observation of a sharp diffusion front shown in Figure 5.9D, indicating an absence of a convection current in the water phase. Control experiments performed on noncross-linked assemblies of CdSe nanocrystals resulted in rapid penetration of the dye through the nanoparticle assembly immediately dispersing the sulforhodamine-B in the water phase at the base of the tube. This control experiment confirms the robust barrier properties of the nanocrystal-membrane, and their ability to prevent convective mixing, while being permeable to small molecules.

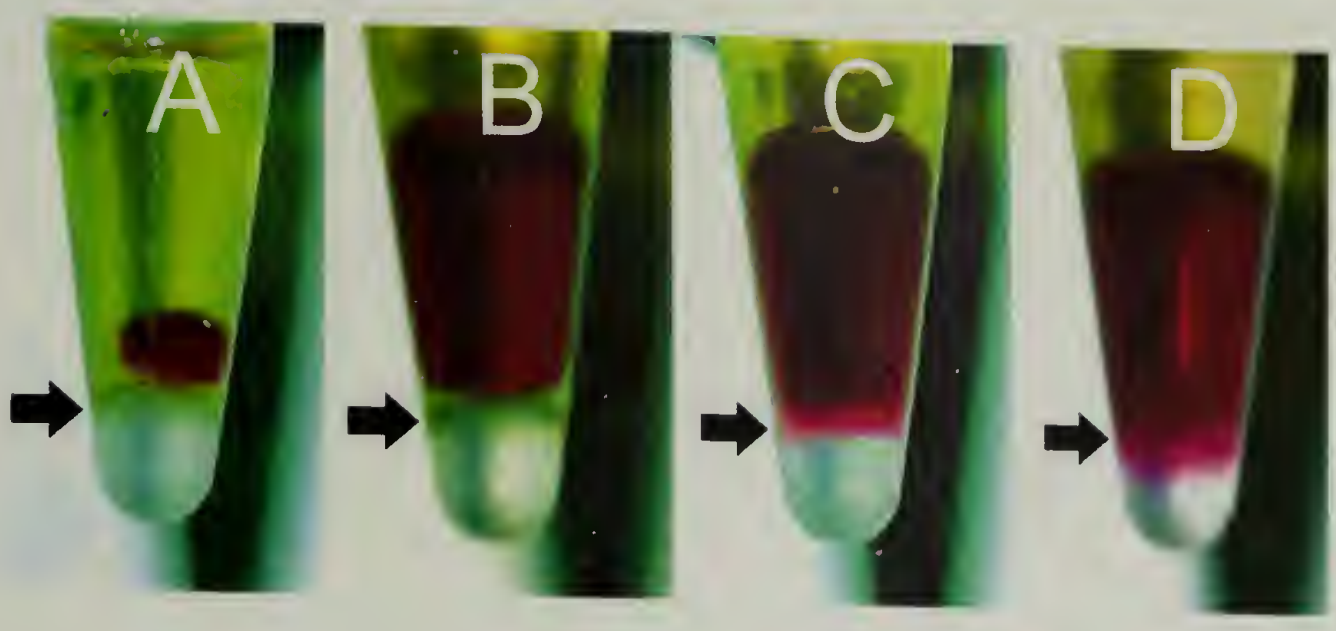

Figure 5.9: Digital photographs of organic dye (red solution) (A) placed on top of a cross-linked interfacial assembly of CdSe nanocrystals, (B) additional dye is added, (C-D) diffusion of the dye through the membrane in a nonconvective fashion

Extension of this technique to the cross-linking of nanocrystal assemblies at the interface of a droplet proved more difficult than for the planar assemblies. For example, consider the cross-linked capsule shown in Figure 5.10. The large capsule shown in tis confocal image contains apparent ruptures that are substantially larger than the nanoscale particles used to prepare the assemblies. The main difficulty in the capsule case arises from the nature of the free radical cross-linking chemistry, which requires heating the system to 60 °C. As discussed previously, nanoparticle diffusion from the interface increases with increasing temperature due to the differing thermal expansion coefficients of the two fluids and the thermally activated displacement of nanocrystals from the liquid-liquid interface. Thus, new chemistries will be needed to cleanly obtain cross-linked capsules from spherical nanoparticle assemblies. In light of the result shown in Figure 5.10, the new chemistries targeted used ligands on the nanoparticles that could be cross-linked at room temperature.

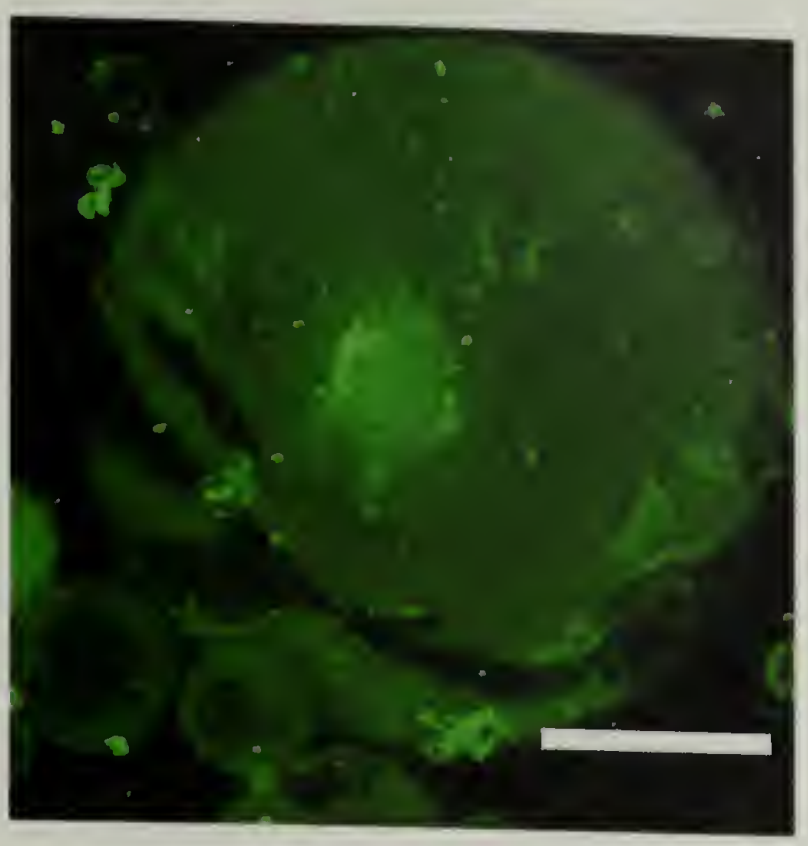

Figure 5.10: Confocal microscope image of **1**-covered nanocrystals cross-linked at the water-oil interface. The scale bar is 40 μm

5.2.2 Cross-linking of CdSe Nanocrystals on Water Droplets to Give Robust Capsules

As described in **Section 5.3.1**, free-radical cross-linking of interfacially segregated nanocrystals has been performed successfully at a planar interface. However, the thermal activation of the free radical initiator (at ~ 60 °C) disrupts the assembly and precludes a successful cross-linking in the case of capsules. To address this challenge, a procedure was developed whereby the cross-linking chemistry could be performed at room temperature. This involved the synthesis of norbornene functionalized CdSe/ZnS core/shell nanocrystals.[144] Norbornene was chosen for its ability to react by ring-opening metathesis polymerization at room temperature, requiring only the addition of an appropriate ruthenium benzylidene catalyst.

The synthesis of compound **14** employed a carbodiimide coupling of 5-norbornene-2-carboxylic acid and 11-thioacetate undecanol.[145] Subsequent deprotection of the thioacetate moiety with hydrazine acetate gave compound **15** in 86% overall yield, as shown in Figure 5.11. Compound **15** was characterized by NMR spectroscopy, where ^{1}H resonances of 6.1 and 4.0 ppm corresponding to the olefin protons and protons alfa to the ester, respectively, were observed. In the ^{13}C NMR

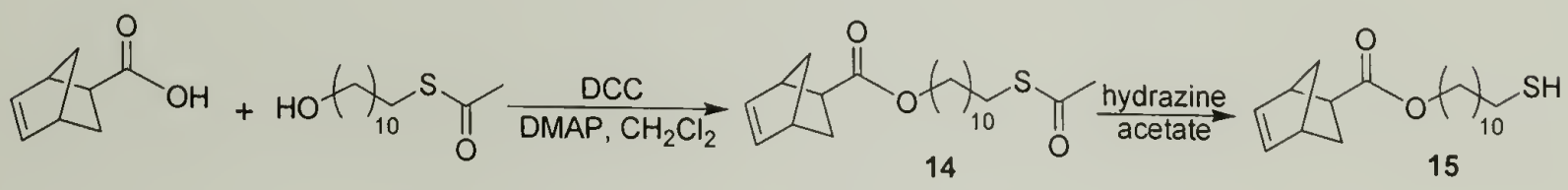

Figure 5.11: Synthesis of norbornene ligand **15**

spectrum, resonances at 175 and 26 ppm, corresponding the carbonyl group and the methylene carbon adjacent to the thiol, respectively, were found. Following a procedure developed by Rosenzwieg and coworkers, CdSe/ZnS core-shell nanocrystals of approximately 3.5 nm were prepared.[144] Then, the TOPO ligand periphery was removed by refluxing in pyridine. The "TOPO" free nanocrystals were then stirred for several hours in a THF solution of ligand **15** at 50 ^{o}C to give norbornene functionalized core/shell nanocrystals. Excess ligand was removed by precipitation into methanol, and the nanocrystal precipitate was redissolved in toluene. These norbornene-functionalized core/shell nanocrystals were found to assemble at the oil-water interface, in a similar fashion as described previously for the TOPO-covered nanocrystals.

A successful interfacial cross-linking strategy required the synthesis of a water-soluble ring-opening metathesis polymerization catalyst. Previous syntheses of such catalysts required an acidic environment for water solubilization, which would be

inappropriate in the presence of CdSe nanocrystals. The advantage of a water-soluble catalyst is that the cross-linking would occur from the aqueous side of the interface, precluding intercapsule coupling. While conventional, organic soluble, ring-opening metathesis catalysts were used to cross-link these assemblies, the results were less than desirable. In this case interparticle cross-linking was prevalent and precluded the formation of individual cross-linked capsules.

The synthesis of a water-soluble ring-opening metathesis catalyst was developed recently in the Emrick group by modification of the commercially available 2nd generation Grubbs' ruthenium benzylidene catalyst with pyridine terminated oligoethylene glycol ligands to give water-soluble metathesis catalyst **16**, shown in Figure 5.12.[146] Ph.D. student K. Breitenkamp has shown the effectiveness of this catalyst for ring-opening metathesis of water-soluble cyclic olefins in water. The ability of catalyst **16** to cross-link these interfacial nanoparticle assemblies, while not adversely affecting the inherent fluorescent properties of the nanocrystals, was a key result of this study, as described below.

Cross-linking of the nanocrystal assemblies was performed by the addition of 25 μL of an aqueous solution of catalyst **16** (1 mg/ml) to 300 μL of a toluene solution of **15**-functionalized CdSe/ZnS core/shell nanocrystals and 25 μL of ethyl vinyl ether. Ethyl vinyl ether was used to control the polymerization, and prevent the catalyst from reacting with nanocrystals not assembled at the interface. While catalyst **16** is water-soluble and added as an aqueous solution, it is amphiphilic, due to the nature of the PEG and may cross the liquid-liquid interface resulting in polymerization of nanocrystals and intercapsule coupling. The mixture was vigorously shaken until assembly of the

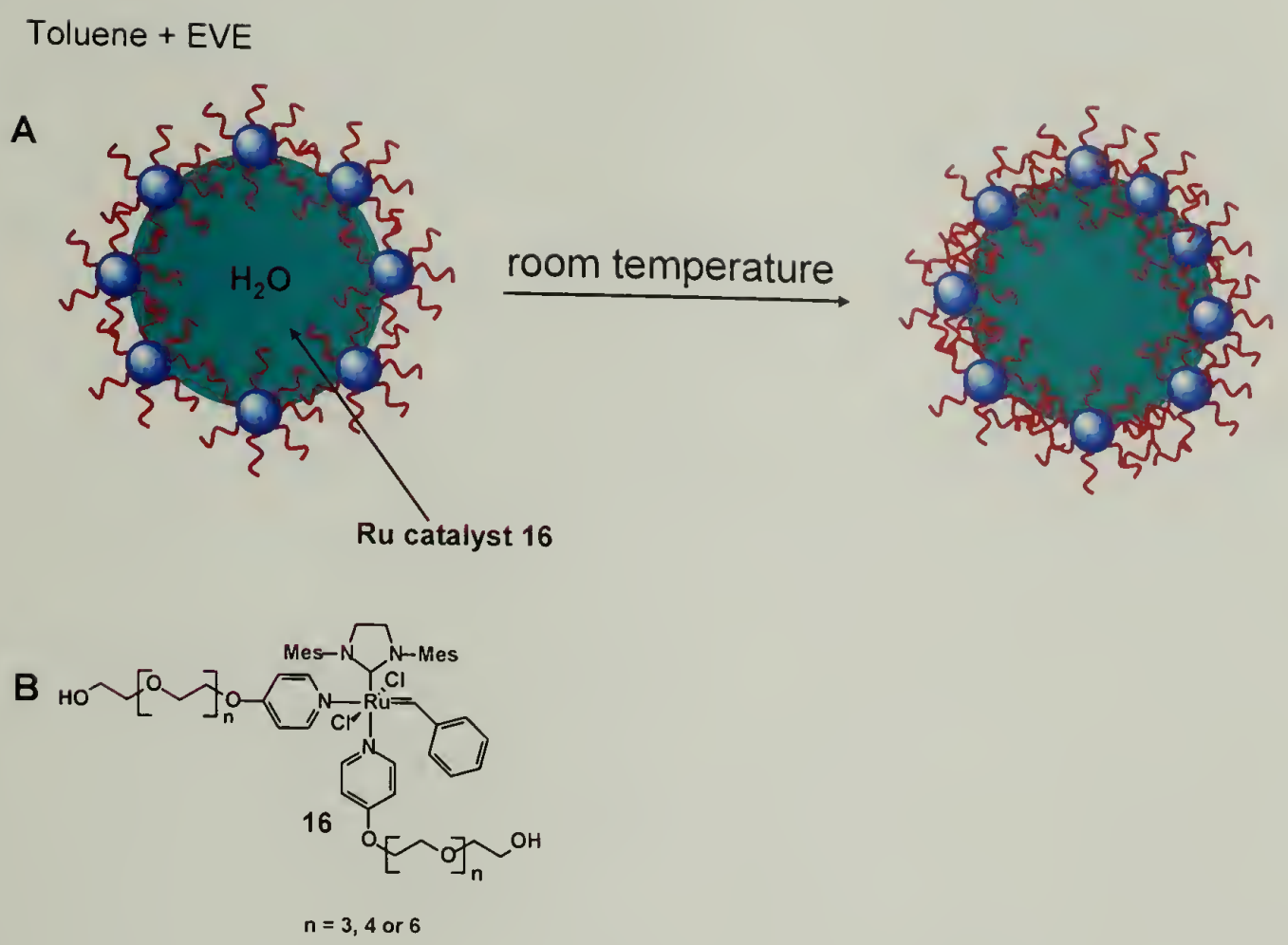

Figure 5.12: (A) Procedure for cross-linking **15**-functionalized CdSe/ZnS core/shell nanocrystals using a water-soluble ruthenium catalyst to give cross-linked nanocrystal capsules. (B) Structure of water soluble ring-opening metathesis catalyst **16**

nanocrystals was complete. The capsules were allowed to settle to the bottom of the toluene solution, then excess nanocrystals were removed by pipette and fresh toluene was added. The capsules were allowed to cross-link over a period of 30 minutes at room temperature.

Figure 5.13a shows fluorescence confocal images of micron size cross-linked nanocrystal capsules at the oil water interface. The nonspherical shape, Figure 5.13a, of the cross-linked capsules illustrate their more elastic properties, relative to the spherical shape found in uncross-linked samples. Cracks and holes seen in the capsules further demonstrates successful cross-linking. These holes and crack are not observed prior to

cross-linking because rapid interfacial diffusion of the nanocrystals prevents the formation of permanent defects. Figure 5.13b shows a crumpled capsule after removal of the interface by the addition of methanol. The crumpled nature of the capsule evident after removal of the oil-water interface further confirms successful cross-linking. Removal of the oil-water interface in assemblies that have not been cross-linked result in the precipitation and aggregation of the nanocrystals, an event not seen in Figure 5.13b.

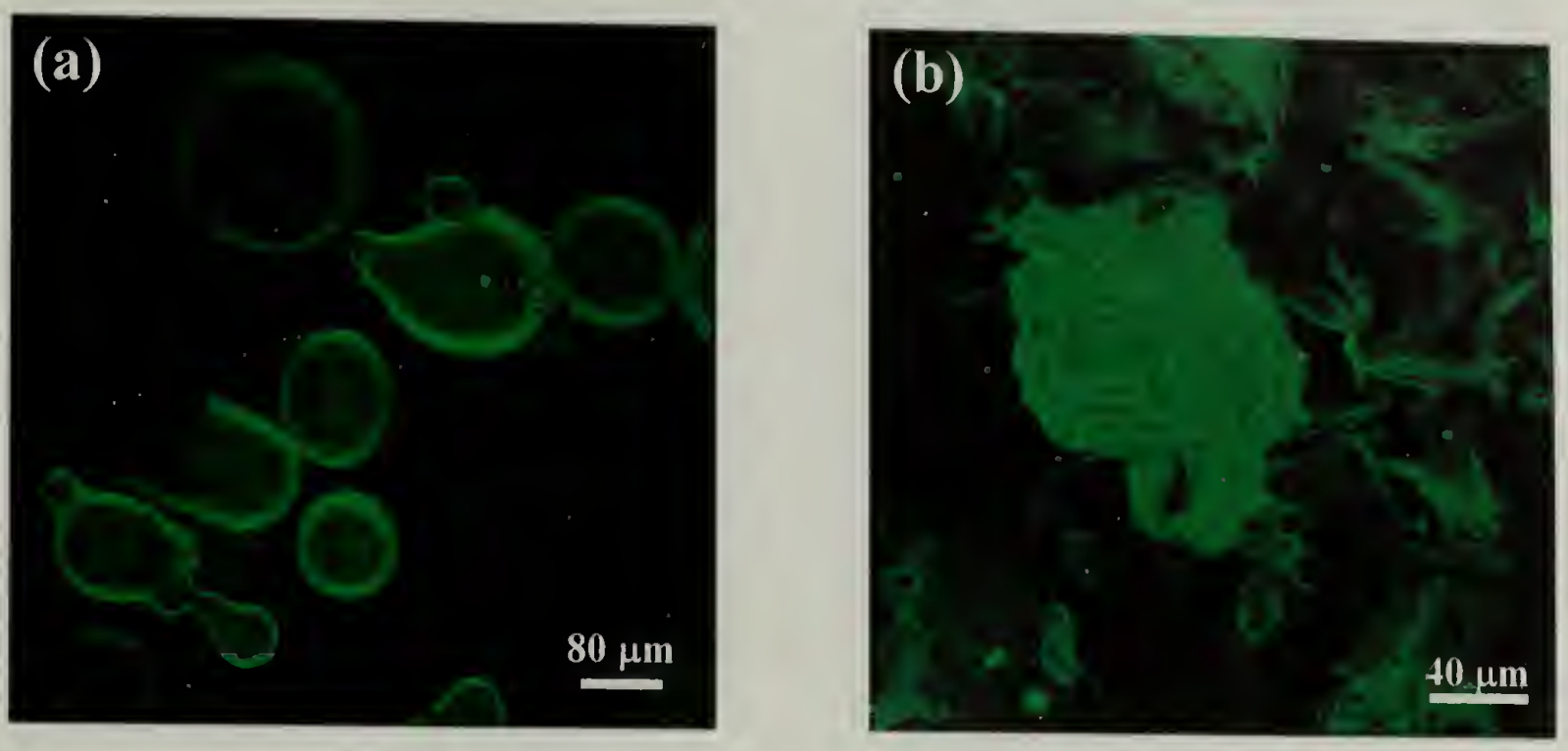

Figure 5.13: Confocal microscope images of cross-linked CdSe nanocrystals **(a)** assembled at the oil-water interface and **(b)** after the removal of the interface by addition of methanol (fragments of ruptures capsules can be seen in the background)

Transmission electron micrographs on solution cast samples of cross-linked nanocrystal capsules, in their dry state, as shown in Figure 5.14, illustrate key features of the capsules. The retention of the capsule shape subsequent to drying, shown in Figure 5.14a, is consistent with successful cross-linking. In addition, the liquid-like structure of the nanocrystals is shown in Figure 5.14b. Such structure is expected

considering prior work on these assemblies.[147] Finally, the inset of Figure 5.14b, an electron diffraction pattern taken of the dried capsule, confirms the presence of the nanocrystals. Figure 5.14b also shows that the nanoscopic features of the nanocrystals are maintained following the cross-linking chemistry. The nanoporous nature of the assemblies is evident from the interstitial spaces between the nanocrystals, and points to the possibility of using these membranes to restrict or control the flow of compounds from inside these capsules as was earlier demonstrated for the flat interface.[148]

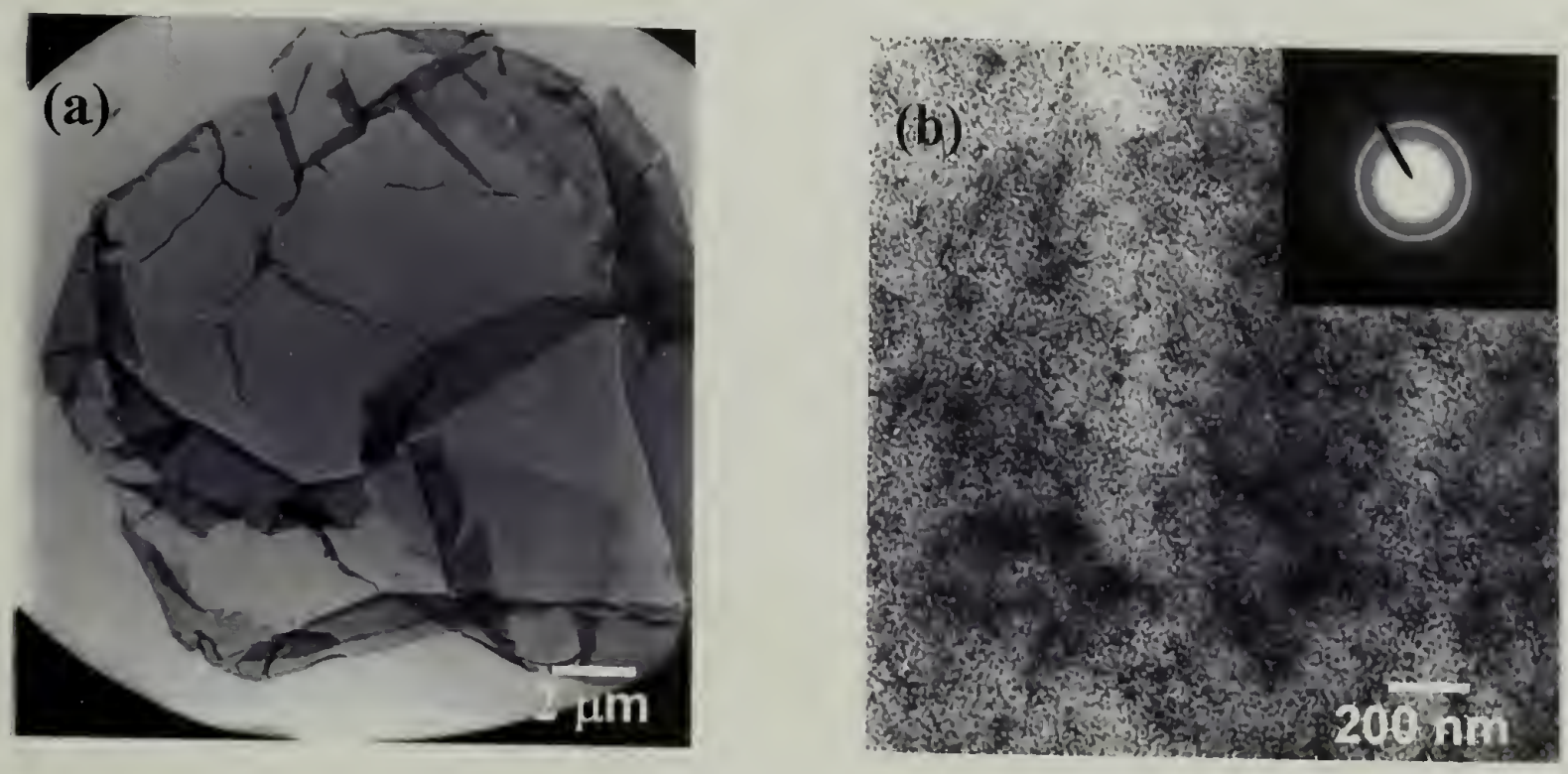

Figure 5.14: Transmission electron micrographs of cross-linked CdSe nanocrystal assemblies. **(a)** Low magnification image of a dried nanocrystal capsule showing the retention of the capsule shape after drying. **(b)** High magnification image of a region of the same capsule showing the liquid-like assembly of nanocrystals and the nanoporous nature of the capsule. The inset electron diffraction pattern in **(b)** confirms the presence of nanocrystals

In summary, this chapter has described an evolution of nanocrystal assembly, from the discovery of the liquid-liquid interfacial segregation, to the synthesis of stable, ultrathin nanocrystal capsules by cross-linking through the attached ligands. The

nanoporous nature of these capsules makes them ideal candidates to study precisely controlled release of encapsulated small molecules, *e.g.* drugs and dyes, and polymers.

5.3 Future Outlook

The successful cross-linking of CdSe nanocrystal assemblies using the techniques described in this chapter will lead to expanded studies of this technology and its applications to the to the encapsulation and controlled release of molecules such as dyes, fragrances, flavors, and drugs. The effect of nanoparticle size will be of interest to explore in such applications, as the larger the particle composing the assembly will create capsules with larger pore sizes because the interstitial space between these particles will be larger. Control over the pore size will allow for greater control and versatility over the type of encapsulant and the rate of its release. This control over the release of encapsulated molecule will, in turn, allow for more complex delivery systems. One can envision the encapsulation of two different size compounds, one small and one large. In this system, the smaller compound will diffuse through the nanoporous capsule at a faster rate than the larger molecule. This will result in a release profile with a fast release of the smaller compound and a slower and thus longer term release of the larger compound. This type of controlled release may be use in administration of for example, drug cocktails.

A second area of future study that to date has proven difficult is the cross-linking of one segment of the capsule shown in Figure 5.8, where different sized nanoparticles have phase-separated on the capsule surface. The selective cross-linking of these types of capsule morphologies will allow for the formation of capsules with,

pore sizes for highly variable transport studies of large molecular weight compounds such as polymers, *e.g.* proteins and DNA. The cross-linking procedure we have developed in **Section 5.3.2** is not suited for such desired selectivity, as this cross-linking occurs faster than the time needed for the phase separation. For this type of structure to be formed, a cross-linking procedure must be developed that can be triggered after the phase separation of the nanocrystals. A suitable trigger may be based on pH or on exposure to ultraviolet radiation. In either case, appropriately functionalized nanocrystals would be assembled at the oil-water interface and larger noncross-linkable nanocrystals would be added to the system. As described earlier, larger nanocrystals form more stable assemblies than smaller nanoparticles and thus they will displace the smaller ones at the interface. If performed correctly, a morphology as shown in Figure 5.7 will be achieved. The cross-linking can then be triggered, for example be UV irradiation, cross-linking the functional nanocrystals. Subsequent washing or dialysis results in the removal of larger, noncross-linked nanocrystals leaving large holes in the assembly. The diffusion of compounds in and out of these assemblies can then be studied by confocal microscopy. These types of systems may lend greater insight into the mobility and diffusion characteristics of polymers in confined areas.

CHAPTER 6

EXPERIMENTAL

6.1 Chapter 2 Experimental

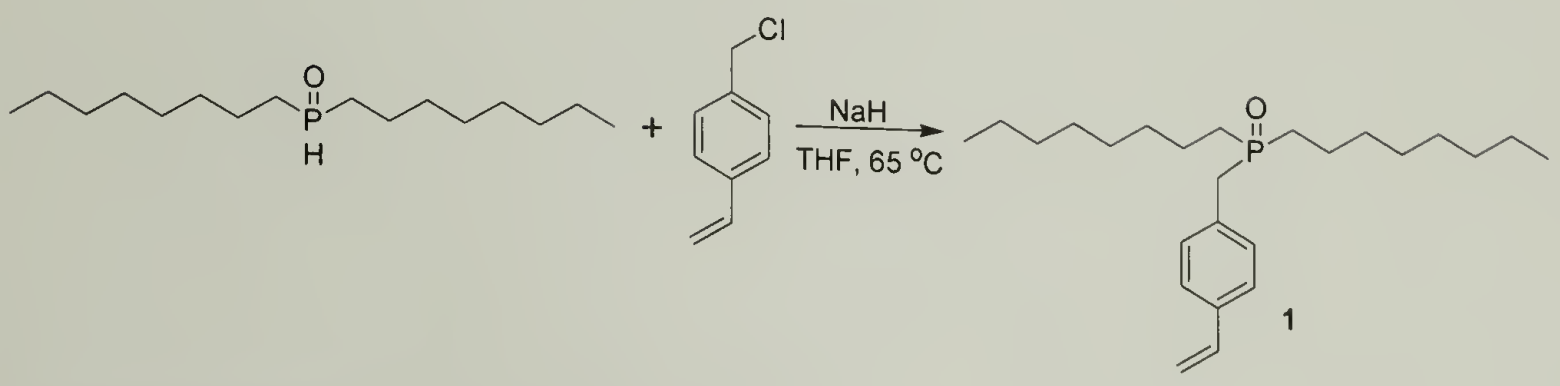

Preparation of *p*-vinylbenzyl-DOPO (1)

Sodium hydride (72 mg, 3.0 mmol) in THF (10 mL) was stirred at room temperature for 30 minutes. To this mixture was added a solution of di-*n*-octyl phosphine oxide[86] (0.50 g, 3.0 mmol) in THF (15 mL). The mixture was stirred for 30 min, then a solution of 4-vinylbenzylchloride (0.47 g, 3.0 mmol) in THF (5 mL) was added dropwise over 15 min. This mixture was stirred for 12 hrs at reflux. THF was then distilled off, and the solids were redissolved in CH_2Cl_2. The organic solution was then washed with water and brine, dried over $MgSO_4$, filtered, and concentrated to give a viscous liquid. This residue was crystallized from hexane to yield **1** (0.69 g, 62%); ^{1}H NMR (300 MHz, $CDCl_3$) δ 7.53 (d, 2H, aromatic), 7.21 (d, 2H, aromatic), 6.70 (dd, 1H, olefin), 5.70 (d, 1H, olefin), 5.22 (d, 1H, olefin), 3.10 (d, 2H, benzyl CH_2), 1.58 (br, 4 H, CH_2-P of *n*-octyl chains), 1.26 (br, 24 H), 0.88 (t, 6H, CH_3) ppm; ^{13}C NMR (75 MHz, $CDCl_3$) δ 138.6, 136.2, 131.9, 129.6, 126.5, 113.7, 36.3, 31.7, 30.9, 28.9, 27.7, 26.8, 22.6, 21.5, 14.0 ppm; ^{31}P (121 MHz, $CDCl_3$) δ 48.4 ppm; FTIR ν 2953, 2922, 2849, 1631, 1511, 1468, 1173, 1135, 988, 902, 864, 838, 721, 551, 471 cm^{-1}; HRMS Calcd. 390.3054; found 390.3013.

Preparation of 1-covered CdSe nanocrystals. TOPO-covered nanocrystals were prepared as described by Peng and co-workers,[149,150] then precipitated into anhydrous methanol and centrifuged. The supernate was discarded and the particles were dissolved in pyridine and allowed to stand at room temperature. The pyridine was partially removed under reduced pressure to give a viscous solution. The nanocrystals were precipitated into hexane and centrifuged. The supernate was discarded, and the precipitate (ca. 40 mg CdSe nanocrystals) was stirred as a suspension in freshly distilled, dry THF. Compound **1** (ca. 300 mg) was added, and the suspension was stirred for several hours at 55 °C, during which time the mixture became homogenous. Most of the THF was removed by distillation, and the remaining solution was twice precipitated with anhydrous methanol and centrifuged. The supernate was again discarded, and the **1**-covered nanocrystals were dissolved in freshly distilled, dry CH_2Cl_2 (ca. 2 mL).

Metathesis reaction of 1 and catalyst 2. A ^{1}H NMR spectrum was recorded of a solution of **2** (5 mg, 6 μmol) in $CDCl_3$ (0.8 mL). Compound **1** (4.7 mg, 12 μmol) was then added to the solution, and allowed to react for 20 min; a ^{1}H NMR spectrum was then recorded to confirm successful carbene exchange: key benzylidene resonances at δ 19.97 (s, 1H), 19.92 (s, 1H). Addition of cyclooctene (0.11 g, 1.0 mmol) to this solution resulted in full conversion to polymer in approximately 1 h, as observed by ^{1}H NMR.

Example preparation of polycyclooctene-CdSe composite. Polycyclooctene-CdSe composites were prepared first by alkylidene exchange of **1**-covered nanocrystals with catalysts **2** or **7**, for example by adding catalyst **2** (4 μmol) or catalyst **7** (0.3 μmol) to

the CH_2Cl_2-nanocrystal solution prepared as described above; the exchange process was monitored by ^1H NMR spectroscopy as depicted in the text. This solution was shaken vigorously and allowed to stand for 30 minutes. Into this solution was added cyclooctene (0.11 g, 1.0 mmol), and the mixture was shaken occasionally over two hours. Polymerization was terminated by addition of excess ethyl vinyl ether in CH_2Cl_2, and the product was precipitated by slow addition of methanol. The precipitate was dried under reduced pressure at room temperature, then dissolved in CH_2Cl_2. These CH_2Cl_2 solutions were used to spin and solution cast nanoparticle/polymer films, including those used for TEM analysis. The ^1H NMR spectrum of this composite material reveals the presence of polycyclooctene as major signals at δ 5.4 (multiplet), 2.0 (broad), and 1.3 (broad) ppm. No signals were present for the vinyl group of **1** (6.7 ppm), and a multiplet was found at 6.1-6.4 ppm, in the expected region for the protons of an olefin between a phenyl ring and an alkyl group, as in composite **6**.

Preparation of hydroxypropyl di-*n*-octylphosphine oxide (8)

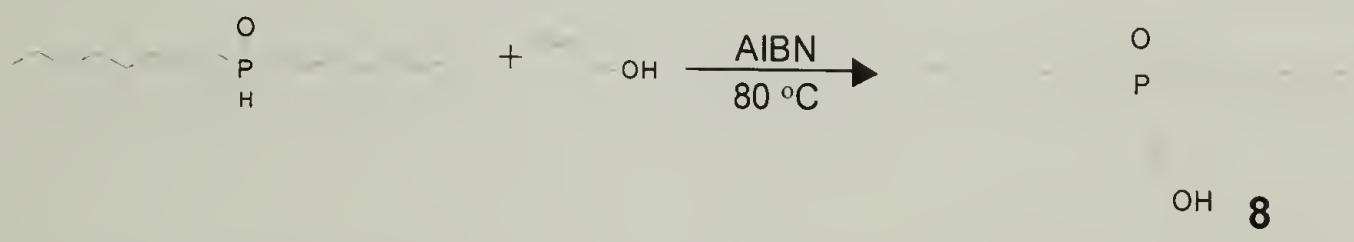

8

Di-*n*-octylphosphine oxide[86] (15.0g, 54.7 mmol), AIBN (1.35 g, 8.23 mmol), and allyl alcohol (3.49 g, 60.2 mmol) were stirred at 80 °C under a nitrogen atmosphere for 8 hrs. The product was purified by column chromatography (silica as the stationary phase) eluting with methanol:chloroform mixtures to yield **8** (15.1 g, 83%): ^1H NMR (300 MHz, $CDCl_3$) δ 4.75 (br, 1H, OH), 3.50 (t. 2H, $C\underline{H}_2$-OH), 1.66-1.12 (m, 32H, alkyl),

0.73 (t, 6H, CH_3) ppm; ^{13}C NMR (75 MHz, $CDCl_3$) δ 62.0, 61.9, 31.5, 30.9, 30.7, 28.8, 27.9, 27.0, 25.3, 25.0, 22.3, 21.4, 13.7 ppm; ^{31}P (121 MHz, $CDCl_3$) δ 52.2 ppm.

Preparation of ligand 10

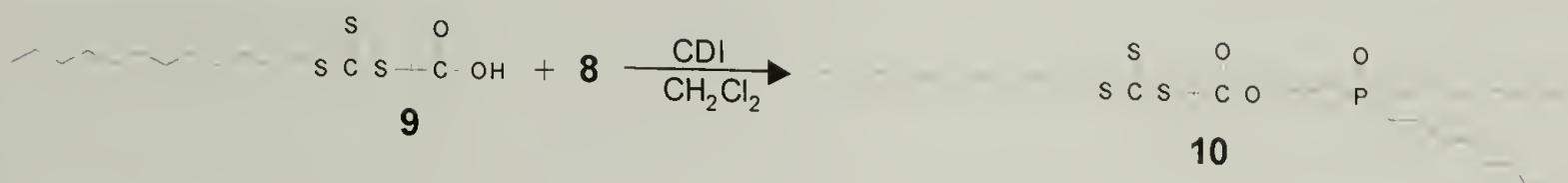

Compound **9**[90] (1.2 g, 3.3 mmol) in CH_2Cl_2 (5 mL) was stirred at room temperature under nitrogen atmosphere. A solution of CDI (0.53 g, 3.3 mmol) in CH_2Cl_2 (5 mL) was added, and the mixture was stirred for 1 hr. Compound **8** (1.2 g, 3.6 mmol) in CH_2Cl_2 (5 mL) was added, and the mixture was stirred for several days, until complete conversion was observed by ^{31}P NMR. CH_2Cl_2 was removed, and the residue was purified by column chromatography, using neutral alumina as the stationary phase, and eluting with methanol:chloroform mixtures to yield **10** (1.49 g, 67%): ^{1}H NMR (300 MHz, $CDCl_3$) δ 4.14 (t, 2H, CH_2O), 3.25 (t, 2H, CH_2S), 1.72 (s, 6H, *tert*-CH_3), 1.68-1.25 (br, 52H, alkyl), 0.88 (t, 9H, $CH_2C\underline{H}_3$) ppm; ^{13}C NMR (75 MHz, $CDCl_3$) δ 221.6, 206.8, 198.3, 172.7, 135.5, 131.3, 117.7, 66.0, 55.9, 51.0, 36.9, 31.8, 31.7, 29.5, 29.4, 29.3 29.1, 29.0, 28.9, 28.8, 25.3, 22.6, 22.5, 21.7, 14.1, 14.0 ppm; ^{31}P (121 MHz, $CDCl_3$) δ 49.0 ppm; HRMS calcd 678.4303, found 678.4333.

Preparation of 10-covered CdSe nanoparticles. TOPO-covered CdSe nanocrystals were prepared,[149,150] precipitated into anhydrous methanol, and centrifuged. The supernatant was discarded and the particles were dissolved in pyridine and stirred at 50 °C for 8 hrs. Pyridine was partially removed under reduced pressure to give a viscous solution. The nanocrystals were then precipitated into hexane and isolated by centrifugation. The supernatant was discarded, and the precipitate was stirred as a

suspension in dry THF. Compound **10** (ca. 250 mg) was added, and the suspension was stirred for several hours at 55 °C, during which time the mixture became homogenous. THF was removed by distillation, and the newly functionalized nanocrystals were dissolved in hexane. **10**-Covered nanocrystals were isolated from excess **10** using a centrifuge device (MWC 50,000). The isolated nanocrystals were then redissolved in toluene or benzene.

General polymerization. To a solution of **10**-covered CdSe nanocrystals (20 mg) in 1 mL toluene was added the monomer (8.7 mmol) and *t*-butyl peroxide (63.0 mg, 0.43 mmol). Freeze-pump-thaw was performed. The mixture was then heated to 70 °C under nitrogen atmosphere for 24 hours. The polymer-CdSe composite material was precipitated into methanol, isolated by filtration, and dried in a vacuum oven. For GPC analysis, the polymers were removed for the nanocrystals surface by stirring the product in a THF solution of hexylphosphonic acid at 50 °C, followed by fractional precipitation.

6.2 Chapter 3 Experimental

Preparation of pyridine terminated 4-hexaethylene glycol (11)

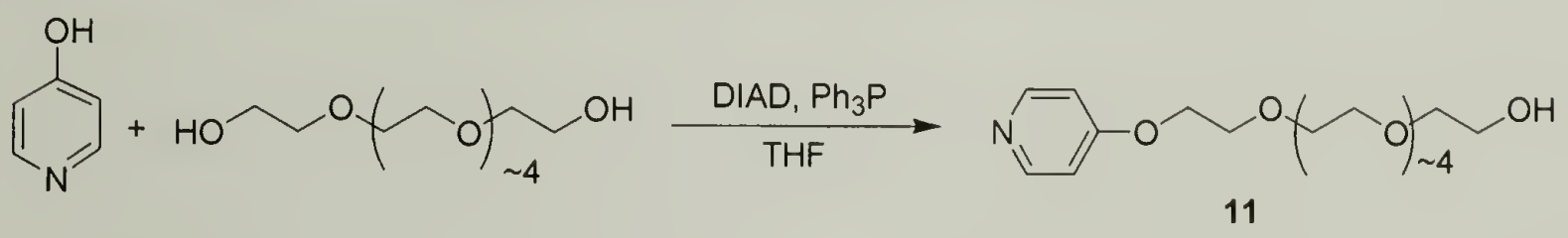

11

4-Hydroxypyridine (4.0 g, 42 mmol), triphenylphosphine (13.1 g, 50 mmol), and diisopropyl azodicarboxylate (10.1 g, 50 mmol) in THF (500 mL) were stirred at room temperature under nitrogen for 30 min. Hexaethylene glycol (51.6 g, 105 mmol) was added, and the mixture was stirred for 12 hours. THF was removed under vacuum, and

the residue was purified by column chromatography eluting with chloroform: acetone: methanol mixtures to yield **11** (8.4 g, 56%): ^{1}H NMR (300 MHz, $CDCl_3$) δ 8.36 (d, aromatic), δ 6.78 (d, aromatic), 4.12 (t, pyr-O-C$\underline{H_2}$-CH_2), 3.82 (t, pyr-O-CH_2-C$\underline{H_2}$), 3.59 (br, CH_2) ppm; ^{13}C NMR (75 MHz, $CDCl_3$) δ 164.7, 150.8, 110.2, 72.4, 70.7, 70.44, 70.38, 70.36, 70.2, 69.1, 67.1, 61.4 ppm; HRMS, calcd. 359.1942; Found M+H 360.2022.

Preparation of pyridine terminated 4-hexadecylethylene glycol monomethylether (12)

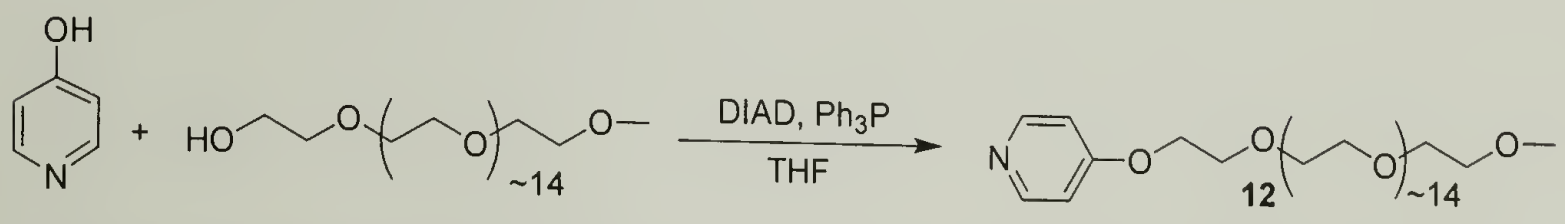

4-Hydroxypyridine (2.0 g, 22 mmol), triphenylphosphine (6.3 g, 24 mmol), and diisopropyl azodicarboxylate (4.8 g, 24 mmol) in THF (250 mL) were stirred at room temperature under nitrogen for 30 min.; hexadecylethylene glycol monomethylether (14.3 g, 20 mmol) was added, and the mixture was stirred overnight. THF was removed under vacuum, and the residue was purified by column chromatography eluting with chloroform : acetone : methanol mixtures to yield **12** (12.0 g, 78%). ^{1}H NMR (300 MHz, $CDCl_3$) δ 8.42 (d, aromatic), 6.82 (d, aromatic), 4.15 (t, pyr-O-C$\underline{H_2}$-CH_2), 3.86 (t, pyr-O-CH_2-C$\underline{H_2}$), 3.66 (br, CH_2), 3.37 (s, CH_3) ppm; ^{13}C NMR (75 MHz, $CDCl_3$) δ 164.7, 150.9, 110.2, 72.6, 71.8, 70.8, 70.4, 70.1, 67.1, 69.2, 58.9 ppm; HRMS calcd. 769.4441; Found M-H 768.4385.

General procedure to afford pegylated CdSe nanocrystals covered with 11 or 12. TOPO-covered nanocrystals were prepared as described by Peng and co-workers,[149,150] then precipitated into anhydrous methanol and centrifuged twice. The supernatant was

discarded and the nanocrystals were dispersed in pyridine and allowed to stand overnight. The nanocrystals were precipitated in hexanes and centrifuged. To this precipitate was added a solution of **11** or **12** (c.a. 200 mg) in either 2 mL of THF or MilliQ water. The solution became optically clear immediately. Alternatively, to a solution of TOPO-covered CdSe nanocrystals (c.a. 10 mg) in 3 mL of THF was added 200 mg of **11** or **12**. The solution was allowed to stand at room temperature overnight, after which the CdSe nanocrystals were precipitated in hexanes and centrifuged. The supernate was discarded and the precipitate was redissolved in MilliQ water, and centrifuged to remove any insoluble material. The supernate was removed and stored, giving an optically clear solution of CdSe nanocrystals in water.

6.3 Chapter 4 Experimental

Preparation of *p*-bromobenzyl-DOPO (13)

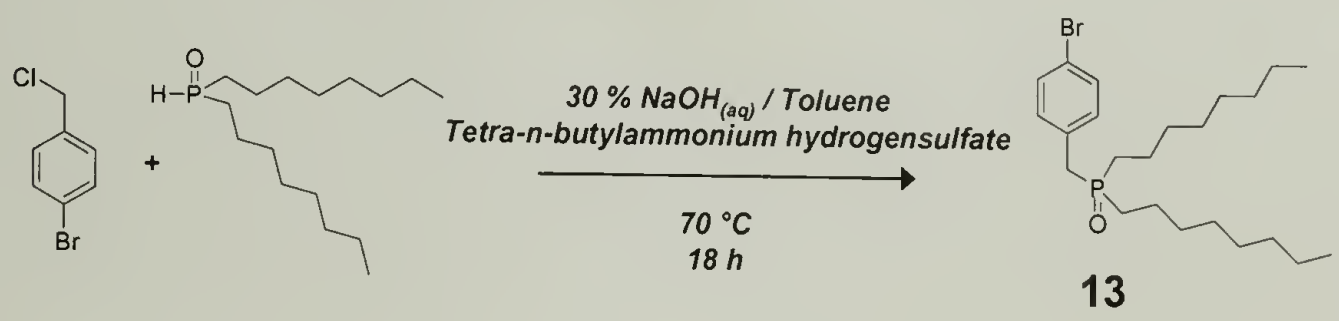

13

To a solution of di-*n*-octylphosphine oxide[86] (21.9 g, 80.0 mmol), 4-bromobenzyl chloride (18.5 g, 90.0 mmol), and tetra-*n*-butyl ammonium hydrogen sulfate (2.9 g) in toluene (330 mL) was added 120 mL of 30 wt% NaOH solution. The reaction was stirred overnight at 65 °C. The product was extracted with CH_2Cl_2 twice and the organic portions were combined and washed with water and brine, dried over $MgSO_4$, filtered, and concentrated to give a viscous liquid. The residue was crystallized twice

from hexane to yield **13** (24.7 g, 85%) as a white solid: (mp 70-71 °C). IR ν_{max}: 2956, 2922, 2853, 1486, 1466, 1241, 1205, 1160, 1131, 1071, 1013, 861, 832, 746, 717 cm^{-1}; ^1H NMR (300 MHz, $CDCl_3$) δ 0.88 (t, J_{HH}= 7.1 Hz, CH_3, 6 H), 1.32 (m, CH_2, 24 H), 1.58 (m, P-CH_2-CH_2, 4 H), 3.05 (d, J_{HH}= 13.8 Hz, Ar-CH_2-P, 2 H), 7.13 (d-d, J_{HH}= 8.5, 6.4 Hz, Ar-*H*, 2H), 7.45 (d, J_{HH}= 8.2 Hz, Ar-*H*) ppm. ^{13}C NMR (75 MHz, $CDCl_3$, δ) 14.28, 21.83 (d), 22.81, 27.69 (d), 29.20, 29.26, 31.27 (d), 31.95, 35.90 (d), 121.07 (d), 131.32 (d), 131.68 (d), 132.08 (d) ppm. HRMS-FAB (m/z): $[M+H]^+$ calcd for $C_{23}H_{41}BrOP$, 443.2078; found, 443.2080.

Preparation of 1,4-di-*n*-octyl-2,5-divinylbenzene

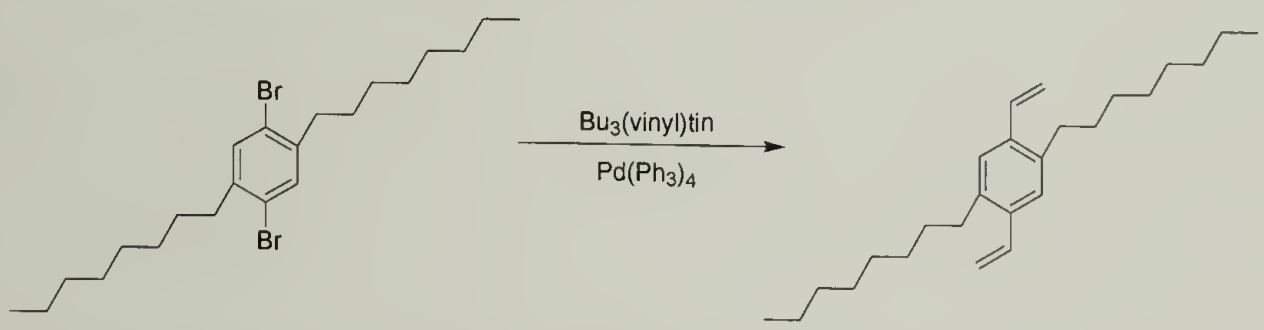

1,4-dibromo-2,5-di-*n*-octylbenzene[117] (2.0 g, 4.4 mmol), tetrakis(triphenyl phosphine) palladium (0) (0.20 g, 0.17 mmol), and a few crystals of 2,6-di-*tert*-butyl-4-methylphenol were dissolved in anhydrous dioxane (40 mL) and stirred at room temperature under an inert atmosphere. Tri-*n*-butyl vinyl tin (3.1 g, 9.8 mmol) was added to the stirring solution, and the reaction was refluxed for 12 hours. The product was extracted with ether and washed with water, saturated ammonium chloride solution, brine, and dried over $MgSO_4$. The solvent was removed under reduced pressure and the crude product was purified by flash chromatography eluting with hexanes to yield the desired compound (1.34g, 87%). ^1H NMR (300 MHz, $CDCl_3$, δ) 0.88 (t, J_{HH}= 6.9 Hz, CH_3, 6 H), 1.27 (m, CH_2, 24 H), 1.54 (quint, J_{HH}= 7.4 Hz, Ar-CH_2-CH_2, 4 H), 2.63 (t, J_{HH}=7.7 Hz, Ar-CH_2, 2 H), 5.25 (d-d, J_{HH}=11.0, 1.4 Hz, CH=CH_2, 2 H), 5.64 (d-d, J_{HH}=

17.4, 1.4 Hz, CH=CH_2, 2 H), 6.94 (d-d, J_{HH}=17.4, 11.0 Hz, CH=CH$_2$, 2 H), 7.24 (s, Ar-H, 2 H). ^{13}C NMR (75 MHz, $CDCl_3$, δ) 14.35, 22.92, 29.53, 29.71, 29.92, 31.56, 32.14, 33.32, 114.85, 126.80, 134.62, 135.81, 138.22.

Synthesis of 13-covered CdSe nanocrystals. To a 3-neck, 25 mL round bottom flask equipped with reflux condenser, Ar inlet, septum, and thermocouple probe was added **13** (4.48 g, 10.1 mmol), cadmium acetate (0.21 g), 1-*n*-hexadecylamine (2.78 g), and *n*-hexylphosphonic acid (0.45 g). The mixture was heated to 270 °C under Ar atmosphere until a homogeneous, colorless solution was observed. A solution of selenium (0.20 g) in tri-*n*-octyl phosphine (4 g) was injected quickly into this hot solution. The color of the solution gradually changed from yellow to red, and during this time the heating mantle was removed when an orange solution was observed. The solution was allowed to cool to room temperature, and **13**-covered nanocrystals were precipitated into anhydrous methanol (10 mL). The solution was centrifuged and the supernate decanted. The resulting solid was purified by dissolution in a minimal amount of THF, precipitation into methanol, and centrifugation. The red powder isolated from this process was dried under a purge of nitrogen gas, and stored as a THF or hexanes solution.

Preparation of PPV-CdSe composite materials. To a 7 mL reaction vial equipped with a stirbar and septum was added **13**-functionalized CdSe nanocrystals (5.5 mg) as a hexanes solution. The solvent was removed under reduced pressure, and 1,4-di-*n*-octyl-2,5-divinylbenzene (0.12 g, 0.33 mmol), 1,4-dibromo-2,5-di-*n*-octylbenzene (0.15 g, 0.33 mmol), and tris(dibenzylideneacetone)dipalladium (1.6 mg, 1.65 μmol) were added to the vial. The vial was evacuated for 30 minutes, and the system backfilled with N_2.

N-methyldicyclohexylamine (0.14 g, 0.72 mmol), tri-*t*-butylphosphine (0.7 mg, 3.3 μmol), and THF (0.5 mL) were added in sequence, and the mixture was stirred at 50 °C for 12 hours. The CdSe-PPV composite was isolated as a solid by precipitation into ethanol, then redissolved in any of a variety of organic solvents for analysis.

6.4 Chapter 5 Experimental

Deposition of CdSe nanocrystals in block copolymer templates. Templates were prepared by anchoring a random copolymer of PS and PMMA containing 58% styrene onto a silicon wafer onto which a 60-100 nm layer of SiO was evaporated; the coated templates were then annealed for 3 days. Excess brush was rinsed from the surface, and a very thin film of P(S-b-MMA) diblock copolymer with a thickness of L_o was spin-coated, on to this surface, then annealed at 170°C overnight. The film was then exposed to UV light under vacuum, and immersed in glacial acetic acid to selectively remove the degraded PMMA from the PS matrix. Subsequent inspection by AFM showed hexagonally ordered cylindrical pores normal to the substrate. These templates were then dipped vertically into heptane solutions of nanoparticles at various nanoparticle concentrations. The withdrawal rates varied from fast (ca. 20 cm/s) to slow (~2 cm/s). The impregnated templates were cut into small pieces, and removed from the silicon wafer by etching and floating on 5% HF in water.

Self-assembly of CdSe nanocrystals in block copolymer thin film. P(S-*r*-MMA) was anchored onto a ~ 100 nm layer of evaporated SiO by spin coating 1 % (w/w) solution in toluene and subsequently annealing under vacuum at 170 °C for 3 days. Solutions of the block copolymers and **11** and **12**- covered nanocrystals were separately prepared in

toluene and the two solutions were mixed prior to spin coating. 20 μL of a 10 mg/mL solution of nanocrystals was added to 90 μL of a 20 mg/mL polymer solution, giving 10% (w/w) nanocrystal to polymer. A subsequent addition of 70 μL of toluene made a final concentration of polymer 10 mg/mL relative to toluene. The mixture was stirred for 1 h and spin coated at 3000 rpm onto the P(S-*r*-MMA) coated substrate. The composite film (~30 nm) of P(S-*b*-MMA) and nanocrystals was annealed under vacuum at 170 °C for 1 day. Sections of the composite film were floated on 5% HF solution in deionized water and picked up with 400 mesh copper grids for transmission electron microscopy (TEM).

Preparation of norbornene thioacetate (14)

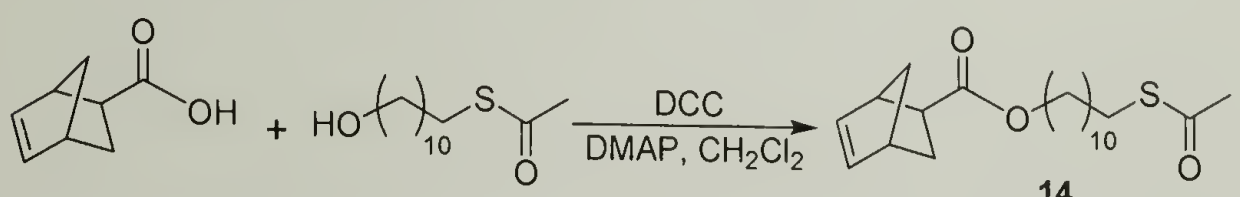

14

5-norbornene-2-carboxylic acid (1.00 g, 7.20 mmol), 11-thioacetate undecanol[145] (2.14 g, 8.70 mmol), dicyclohexylcarbodiimde (1.79 g, 8.70 mmol), and 4-(dimethylamino)pyridine (0.53g, 4.40 mmol) were dissolved in CH_2Cl_2 (20 mL). The reaction was stirred at room temperature under an inert atmosphere for 1 hr. The reaction mixture was filtered and the solvent was removed under reduced pressure to give a viscous liquid. The product was purified by column chromatography eluting with $CHCl_3$:hexane mixtures to yield **14** (1.93, 89%). ^{1}H NMR (300 MHz, $CDCl_3$) δ 6.20-5.91 (m, 2H), 4.04 (m, 2H), 3.21 (br s, 1H), 2.91 (m, 4H), 2.32 (s, 3H), 1.94-1.2 (m, 24H) ppm; ^{13}C NMR (75 MHz, $CDCl_3$) δ 196.0, 174.8, 138.0, 132.3, 64.5, 64.3, 55.7, 49.6, 46.6, 46.3, 45.7, 43.3, 43.2, 42.5, 41.6, 34.9, 30.6, 30.3, 29.5, 29.4, 29.3 ppm.

Preparation of thiol-functionalized norbornene (15)

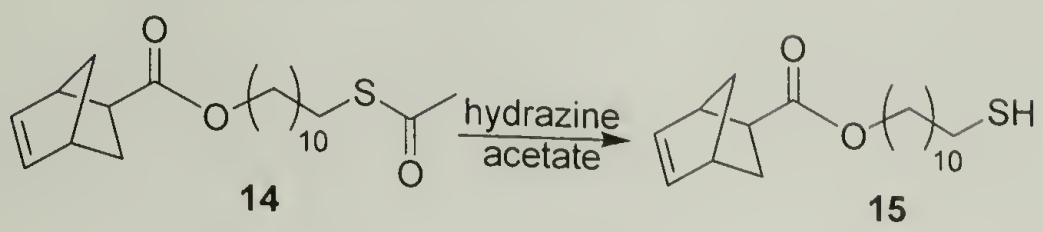

14 **15**

Compound **14** (1.0 g, 2.7 mmol) was dissolved in DMF (15 mL) and stirred at room temperature under an inert atmosphere. Hydrazine acetate (0.75g, 8.1 mmol) was added to the solution and allowed to react for 20 min. The reaction mixture was filtered and the solvent was removed under reduced pressure to yield **15** (0.68g, 97%). ^{1}H NMR (300 MHz, $CDCl_3$) δ 6.20-5.91(m, 2H), 4.02 (m, 2H), 3.21 (br s, 1H), 2.89 (m, 4H), 2.50 (t, 2H), 2.30 (br, 1H), 1.63-1.26 (m, 20H) ppm; ^{13}C NMR (75 MHz, $CDCl_3$) 174.8, 138.0, 132.3, 64.3, 46.6, 46.3, 45.7, 43.3, 43.1, 42.5, 41.6, 34.0, 29.4, 29.1, 29.0, 28.6, 28.3, 25.9, 24.6 ppm.

Preparation of 15-functionalized CdSe/ZnS nanocrystals. TOPO-covered CdSe/ZnS nanocrystals were prepared as described by Rosenzweig.[144] The particles were dissolved in pyridine and refluxed overnight under an inert atmosphere. The pyridine was partially removed under reduced pressure to give a viscous solution. The nanocrystals were precipitated by the addition of hexane and centrifuged. The supernate was discarded, and the precipitate (ca. 20 mg CdSe nanocrystals) was stirred as a suspension in freshly distilled, dry THF. Compound **15** (ca. 150 mg) was added, and the suspension was stirred for several hours at 50 °C. The THF was partially removed by distillation, and the remaining solution was precipitated with anhydrous methanol and centrifuged. The supernate was again discarded, and the **15**-covered nanoparticles were dissolved in freshly distilled toluene (7 mL).

General procedure for the preparation of cross-linked nanoparticle capsules. 300 μL of **15**-functionalized CdSe/ZnS nanocrystals (ca. 2 mg/1 mL) in toluene and 25 μL of ethyl vinyl ether were added to a eppendorf tube. 25 μL aqueous solution of catalyst **16** (1 mg/1 mL) was added to the nanocrystal solution and shaken vigorously. The nanocrystal capsules were allowed to settle to the bottom of the solution and the excess nanocrystal solution was removed and fresh toluene was added.

REFERENCES

(1) Klabunde, K. J. *Nanoscale Materials in Chemistry*; John Wiley & Sons, 2001.
(2) Hummel, R. E. *Electronic Properties of Materials*; 2 ed.; Springer-Verlag, 1993.
(3) Bosman, A. W.; Heumann, A.; Klaerner, G.; Benoit, D.; Fréchet, J. M. J.; Hawker, C. J. *J. Am. Chem. Soc.* **2001**, *123*, 6461-6462.
(4) Tully, D. C.; Wilder, K.; Fréchet, J. M. J.; Trimble, A. R.; Quate, C. F. *Adv. Mater* **1999**, *11*, 314-318.
(5) Townsend, P.; Olivares, J. *Appl. Surf. Sci.* **1997**, *110*, 275-282.
(6) Calander, N.; Willander, M. *Phys. Rev. Lett.* **2002**, *89*, 143603.
(7) Boal, A. K.; Ilhan, F.; DeRouchey, J. E.; Thurn-Albrecht, T.; Russell, T. P.; Rotello, V. M. *Nature* **2000**, *404*, 746-748.
(8) Haw, M. D.; Poon, W. C. K.; Pusey, P. N. *Physical Review E* **1997**, *56*, 1918-1933.
(9) Bunning, T. J.; Kirkpatrick, S. M.; Natarajan, L. V.; Tondiglia, V. P.; Tomlin, D. W. *CHem. Mater.* **2000**, *12*, 2842.
(10) Brott, L. L.; Naik, R. R.; Pikas, D. J.; Kirkpatrick, S. M.; Tomlin, D. W.; Whitlock, P. W.; Clarson, S. J.; Stone, M. O. *Nature* **2001**, *413*, 291-293.
(11) Htoo, M. S., Ed. *Microelectronic Polymers*; M. Dekker, 1989.
(12) Sneh, O.; Clark-Phelps, R. B.; Londergan, A. R.; Winkler, J.; Seidel, T. E. *Thin Solid Films* **2002**, *402*, 248-261.
(13) Townsend, P.; Olivares, J. *Applied Surface Science* **1997**, *110*, 275-282.
(14) Hong, L.; Vilar, R. M.; Wang, Y. M. *J. Mater. Sci.* **1997**, *32*, 5545-5550.
(15) Brown, T. L.; Swaminathan, S.; Chandrasekar, S.; Compton, W. D.; King, A. H.; Trumble, K. P. *J. Mater. Sci.* **2002**, *17*, 2484-2488.
(16) Bawendi, M. G.; Wilson, W. L.; Rothberg, L.; Carroll, P. J.; Jedju, T. M.; Steigerwald, M. L.; Brus, L. E. *Phys. Rev. Lett.* **1990**, *65*, 1623-1626.
(17) Brus, L. *Applied Physics a-Materials Science & Processing* **1991**, *53*, 465-474.
(18) Brus, L. E.; Szajowski, P. F.; Wilson, W. L.; Harris, T. D.; Schuppler, S.; Citrin, P. H. *J. Am. Chem. Soc.* **1995**, *117*, 2915-2922.
(19) Chen, C. C.; Herhold, A. B.; Johnson, C. S.; Alivisatos, A. P. *Science* **1997**, *276*, 398-401.
(20) Chestnoy, N.; Hull, R.; Brus, L. E. *J. Chem Phys.* **1986**, *85*, 2237-2242.
(21) Empedocles, S. A.; Bawendi, M. G. *Science* **1997**, *278*, 2114-2117.
(22) Empedocles, S.; Bawendi, M. *Acct. Chem. Res.* **1999**, *32*, 389-396.
(23) Nirmal, M.; Dabbousi, B. O.; Bawendi, M. G.; Macklin, J. J.; Trautman, J. K.; Harris, T. D.; Brus, L. E. *Nature* **1996**, *383*, 802-804.
(24) Nirmal, M.; Brus, L. *Acct. Chem. Res.* **1999**, *32*, 407-414.
(25) Shim, M.; Wang, C. J.; Guyot-Sionnest, P. *J. Phys. Chem.B* **2001**, *105*, 2369-2373.
(26) Shim, M.; Guyot-Sionnest, P. *Phys. Rev. B* **2001**, *6424*, art. no.-245342.
(27) Shim, M.; Wang, C. J.; Norris, D. J.; Guyot-Sionnest, P. *Mrs Bulletin* **2001**, *26*, 1005-1008.
(28) Gaponenko, S. v. *Optical Porperties of Semiconductor Nanocrystals*; Cambridge University Press: New York, 1998.

(29) Brus, L. *J. Phys. Chem. Sol.* **1998**, *59*, 459-465.
(30) Alivisatos, A. P.; Harris, T. D.; Brus, L. E.; Jayaraman, A. *J. Chem Phys.* **1988**, *89*, 5979-5982.
(31) De Schryver, F. C. *Pure and Applied Chemistry* **1998**, *70*, 2147.
(32) Li, L. S.; Hu, J. T.; Yang, W. D.; Alivisatos, A. P. *Nano Letters* **2001**, *1*, 349-351.
(33) Marcus, M. A.; Flood, W.; Stiegerwald, M.; Brus, L.; Bawendi, M. *J. Phys. Chem.* **1991**, *95*, 1572-1576.
(34) Rabani, E.; Hetenyi, B.; Berne, B. J.; Brus, L. E. *J. Chem. Phys.* **1999**, *110*, 5355-5369.
(35) Rossetti, R.; Ellison, J. L.; Gibson, J. M.; Brus, L. E. *J. Chem. Phys.* **1984**, *80*, 4464-4469.
(36) Steigerwald, M. L.; Alivisatos, A. P.; Gibson, J. M.; Harris, T. D.; Kortan, R.; Muller, A. J.; Thayer, A. M.; Duncan, T. M.; Douglass, D. C.; Brus, L. E. *J. Am. Chem. Soc.* **1988**, *110*, 3046-3050.
(37) Steigerwald, M. L.; Brus, L. E. *Annl. Rev. Mater. Sci.* **1989**, *19*, 471-495.
(38) Fojtik, A.; Weller, H.; Koch, U.; Henglein, A. *Berichte Der Bunsen-Gesellschaft-Physical Chemistry Chemical Physics* **1984**, *88*, 969-977.
(39) Murray, C. B.; Norris, D. J.; Bawendi, M. G. *J. Am. Chem. Soc.* **1993**, *115*, 8706-8715.
(40) Peng, X. G.; Schlamp, M. C.; Kadavanich, A. V.; Alivisatos, A. P. *J. Am. Chem. Soc.* **1997**, *119*, 7019-7029.
(41) Dabbousi, B. O.; RodriguezViejo, J.; Mikulec, F. V.; Heine, J. R.; Mattoussi, H.; Ober, R.; Jensen, K. F.; Bawendi, M. G. *J. Phys. Chem. B* **1997**, *101*, 9463-9475.
(42) Qu, L. H.; Peng, Z. A.; Peng, X. G. *Nano Letters* **2001**, *1*, 333-337.
(43) Peng, Z. A.; Peng, X. G. *J. Am. Chem. Soc.* **2001**, *123*, 183-184.
(44) Peng, Z. A.; Peng, X. G. *J. Am. Chem. Soc.* **2002**, *124*, 3343-3353.
(45) Qu, L. H.; Peng, X. G. *J. Am. Chem. Soc.* **2002**, *124*, 2049-2055.
(46) Becerra, L. R.; Murray, C. B.; Griffin, R. G.; Bawendi, M. G. *Journal of Chemical Physics* **1994**, *100*, 3297-3300.
(47) Guzelian, A. A.; Katari, J. E. B.; Kadavanich, A. V.; Banin, U.; Hamad, K.; Juban, E.; Alivisatos, A. P.; Wolters, R. H.; Arnold, C. C.; Heath, J. R. *J. Phys. Chem.* **1996**, *100*, 7212-7219.
(48) Wang, Y. A.; Li, J. J.; Chen, H.; Peng, X. G. *J. Am. Chem. Soc.* **2002**, *124*, 2293-2298.
(49) Balazs, A.; Ginzburg, V. V.; Qui, F.; Peng, G.; Jasnow, D. *J. Phys. Chem. B* **2000**, *104*, 3411-3422.
(50) Colvin, V. L.; Schlamp, M. C.; Alivisatos, A. P. *Nature* **1994**, *370*, 354-357.
(51) Dameron, C. T.; Reese, R. N.; Mehra, R. K.; Kortan, A. R.; Carroll, P. J.; Steigerwald, M. L.; Brus, L. E.; Winge, D. R. *Nature* **1989**, *338*, 596-597.
(52) Gerion, D.; Pinaud, F.; Williams, S. C.; Parak, W. J.; Zanchet, D.; Weiss, S.; Alivisatos, A. P. *J. Phys. Chem. B* **2001**, *105*, 8861-8871.
(53) Godovsky, D. Y. In *Biopolymers/Pva Hydrogels/Anionic Polymerisation Nanocomposites*, 2000; Vol. 153, pp 163-205.
(54) Harrison, M. T.; Kershaw, S. V.; Burt, M. G.; Rogach, A. L.; Kornowski, A.; Eychmuller, A.; Weller, H. *Pure and Applied Chemistry* **2000**, *72*, 295-307.

(55) Huynh, W. U.; Peng, X. G.; Alivisatos, A. P. *Adv. Mater.* **1999**, *11*, 923.
(56) Huynh, W. U.; Dittmer, J. J.; Alivisatos, A. P. *Science* **2002**, *295*, 2425-2427.
(57) Lee, J.; Sundar, V. C.; Heine, J. R.; Bawendi, M. G.; Jensen, K. F. *Adv. Mater.* **2000**, *12*, 1311-1311.
(58) Michalet, X.; Pinaud, F.; Lacoste, T. D.; Dahan, M.; Bruchez, M. P.; Alivisatos, A. P.; Weiss, S. *Single Molecules* **2001**, *2*, 261-276.
(59) Pathak, S.; Choi, S. K.; Arnheim, N.; Thompson, M. E. *J. Am. Chem. Soc.* **2001**, *123*, 4103-4104.
(60) Salafsky, J. S. *Solid-State Electronics* **2001**, *45*, 53-58.
(61) Liu, J.; Tanaka, T.; Sivula, K.; Alivisatos, A. P.; Frechet, J. M. J. *J. Am. Chem. Soc.* **2004**, *126*, 6550-6551.
(62) Fogg, D. E.; Radzilowski, L. H.; Blanski, R.; Schrock, R. R.; Thomas, E. L. *Macromolecules* **1997**, *30*, 417-426.
(63) Moffitt, M.; McMahon, L.; Pessel, V.; Eisenberg, A. *Chem. Mater.* **1995**, *7*, 1185-1192.
(64) Zhao, H. Y.; Douglas, E. P.; Harrison, B. S.; Schanze, K. S. *Langmuir* **2001**, *17*, 8428-8433.
(65) Qi, L.; Colfen, H.; Antonietti, M. *Nano Letters* **2001**, *1*, 61-65.
(66) Gu, Y. D.; Nederberg, F.; Kange, R.; Shah, R. R.; Hawker, C. J.; Moller, M.; Hedrick, J. L.; Abbott, N. L. *Chem Phys Chem* **2002**, *3*, 448.
(67) Petrash, S.; Cregger, T.; Zhao, B.; Pokidysheva, E.; Foster, M. D.; Brittain, W. J.; Sevastianov, V.; Majkrzak, C. F. *Langmuir* **2001**, *17*, 7645-7651.
(68) Moller, M.; Nederberg, F.; Lim, L. S.; Kange, R.; Hawker, C. J.; Hedrick, J. L.; Gu, Y. D.; Shah, R.; Abbott, N. L. *J. Poly. Sci. A* **2001**, *39*, 3529-3538.
(69) Juang, A.; Scherman, O. A.; Grubbs, R. H.; Lewis, N. S. *Langmuir* **2001**, *17*, 1321-1323.
(70) Zhao, B.; Brittain, W. J. *Macromolecules* **2000**, *33*, 8813-8820.
(71) Rajagopalan, P.; McCarthy, T. J. *Macromolecules* **1998**, *31*, 4791-4797.
(72) Chen, W.; McCarthy, T. J. *Macromolecules* **1998**, *31*, 3648-3655.
(73) Carrot, G.; Scholz, S. M.; Plummer, C. J. G.; Hilborn, J. G.; Hedrick, J. L. *Chem. Mater.* **1999**, *11*, 3571-3577.
(74) Milliron, D. J.; Alivisatos, A. P.; Pitois, C.; Edder, C.; Frechet, J. M. J. *Adv. Mater.* **2003**, *15*, 58.
(75) Farmer, S. C.; Patten, T. E. *CHem. Mater.* **2001**, *13*, 3920-3926.
(76) Mamedov, A. A.; Belov, A.; Giersig, M.; Mamedova, N. N.; Kotov, N. A. *J. Am. Chem. Soc.* **2001**, *123*, 7738-7739.
(77) Yeh, S. W.; Wei, K. H.; Sun, Y. S.; Jeng, U. S.; Liang, K. S. *Macromolecules* **2003**, *36*, 7903-7907.
(78) Lin, Y.; Skaff, H.; Emrick, T.; Dinsmore, A. D.; Russell, T. P. *Science* **2003**, *299*, 226-229.
(79) Skaff, H.; Ilker, M. F.; Coughlin, E. B.; Emrick, T. *J. Am. Chem. Soc.* **2002**, *124*, 5729-5733.
(80) Watson, K. J.; Zhu, J.; Nguyen, S. T.; Mirkin, C. A. *Pure Appl. Chem.* **2000**, *72*, 67-72.
(81) Zhou, Q. Y.; Wang, S. X.; Fan, X. W.; Advincula, R.; Mays, J. *Langmuir* **2002**, *18*, 3324-3331.

(82) Bockstaller, M. R.; Lapetnikov, Y.; Margel, S.; Thomas, E. L. *J. Am. Chem. Soc.* **2003**, *125*, 5276-5277.
(83) Trnka, T. M.; Grubbs, R. H. *Acct. Chem. Res.* **2001**, *34*, 18-29.
(84) Novak, B. M.; Risse, W.; Grubbs, R. H. *Advances in Polymer Science* **1992**, *102*, 47-72.
(85) Skaff, H.; Ilker, M. F.; Coughlin, E. B.; Emrick, T. *J. Am. Chem. Soc.* **2002**, *124*, 5729-5733.
(86) Williams, R. H.; Hamilton, L. A. *J. Am. Chem. Soc.* **1952**, *74*, 5418.
(87) Schwab, P.; Grubbs, R. H.; Ziller, J. W. *J. Am. Chem. Soc.* **1996**, *118*, 100.
(88) Chiefari, J.; Chong, Y. K.; Ercole, F.; Krstina, J.; Jeffery, J.; Le, T. P. T.; Mayadunne, R. T. A.; Meijs, G. F.; Moad, C. L.; Moad, G.; Rizzardo, E.; Thang, S. H. *Macromolecules* **1998**, *31*.
(89) Rizzardo, E.; Chiefari, J.; Chong, B. Y. K.; Ercole, F.; Krstina, J.; Jeffery, J.; Le, T. P. T.; Mayadunne, R. T. A.; Meijs, G. F.; Moad, C. L.; Moad, G.; Thang, S. H. *Macromol. Symp.* **1999**, *143*, 291-307.
(90) Lai , J. T.; Filla, D.; Shea, R. *Macromolecules* **2002**, *35*, 6754-6756.
(91) Guo, W. H.; Li, J. J.; Wang, Y. A.; Peng, X. G. *J. Am. Chem. Soc.* **2003**, *125*, 3901-1909.
(92) Bruchez, M.; Maronne, M.; Gin, P.; Weiss, S.; Alivisatos, A. P. *Science* **1998**, *281*, 2013.
(93) Han, M.; Gao, X.; J.Z., S.; Nie, S. *Nature Biotechnology* **2001**, *19*, 631.
(94) Mattoussi, H.; Mauro, J. M.; Goldman, E. R.; Anderson, G. P.; Sundar, V. C.; Mikulec, F. V.; Bawendi, M. G. *J. Am. Chem. Soc.* **2000**, *122*, 12142-12150.
(95) Rosenthal, S. J.; Tomlinson, I.; Adkins, E. M.; Schroeter, S.; Adams, S.; Swafford, L.; McBride, J.; Wang, Y.; DeFelice, L. J.; Blakely, R. D. *J. Am. Chem. Soc.* **2002**, *124*, 4586.
(96) Murray, C. D.; Kagan, C. R.; Bawendi, M. G. *Annu. Rev. Mater. Sci.* **2000**, *30*, 545.
(97) Robelek, R.; Niu, L.; Schmid, E. L.; Knoll, W. *Anal. Chem.* **2004**, *76*, 6160-6165.
(98) Bowen Katari, J. E.; Colvin, V. L.; Alivisatos, A. P. *J. Phys. Chem.* **1994**, *98*, 4190.
(99) Murray, C. B.; Norris, D. J.; Bawendi, M. G. *J. Am. Chem. Soc.* **1993**, *115*, 8706-8715.
(100) Pathak, S.; Choi, S. K.; Arnheim, N.; Thompson, M. E. *J. Am. Chem. Soc.* **2001**, *123*, 4103-4104.
(101) Qi, L.; Colfen, H.; Antonietti, M. *Nano Lett.* **2001**, *1*, 61-65.
(102) Gerion, D.; Pinaud, F.; Williams, S. C.; Parak, W. J.; Zanchet, D.; Weiss, S.; Alivisatos, A. P. *J. Phys. Chem. B* **2001**, *105*, 8861-8871.
(103) Harris, J. M. *Poly(ethylene glycol) Chemistry: Biotechnical and Biomedical Applications*; Plenum Press: New York, 1992.
(104) Lin, Y.; Skaff, H.; Boker, A.; Dinsmore, A. D.; Emrick, T.; Russell, T. P. *J. Am. Chem. Soc.* **2003**, *125*, 12690-12691.
(105) Aldana, J.; Wang, A.; Peng, X. *J. Am. Chem. Soc.* **2001**, *123*, 8844.

(106) Parak, W. J.; Gerion, D.; Zanchet, D.; Woerz, A. S.; Pellegrino, T.; Michael, C.; Williams, S. C.; Seitz, M.; Bruehl, R. E.; Bryant, Z.; Bustamante, C.; Bertozzi, C. R.; Alivisatos, A. P. *Chem. Mater.* **2002**, *14*, 2113.
(107) Huynh, W. U.; Peng, S. G.; Alivisatos, A. P. *Adv. Mater* **1999**, *11*, 923.
(108) Huynh, W. U.; Dittmer, J. J.; Alivisatos, A. P. *Science* **2002**, *295*, 2425-2427.
(109) Leatherdale, C. A.; Kagan, C. R.; Morgan, N. Y.; Empedocles, S. A.; Kastner, M. A.; Bawendi, M. G. *Phys. Rev. B* **2000**, *62*, 2669-2680.
(110) Lee, J.; Sundar, V. C.; Heine, J. R.; Bawendi, M. G.; Jensen, K. F. *Adv. Mater* **2000**, *12*, 1311-1311.
(111) Gao, M. Y.; Richter, B.; Kirstein, S. *Adv. Mater.* **1997**, *9*, 802.
(112) Schlamp, M. C.; Peng, X. G.; Alivisatos, A. P. *J. Appl. Phys.* **1997**, *82*, 5837.
(113) Skaff, H.; Sill, K.; Emrick, T. *J. Am. Chem. Soc.* **2004**, *126*, 11322-11325.
(114) Fogg, D. E.; Radzilowski, L. H.; Blanski, R.; Schrock, R. R.; Thomas, E. L. *Macromolecules* **1997**, *30*, 417-426.
(115) Sankaran, V.; Cummins, C. C.; Schrock, R. R.; Cohen, R. E.; Silbey, R. J. *J. Am. Chem. Soc.* **1990**, *112*, 6858-6859.
(116) Littke, A. F.; Fu, G. C. *J. Am. Chem. Soc.* **2001**, *123*, 6989-7000.
(117) Rehahn, M.; Schluter, A. D.; Feast, W. J. *Synthesis* **1998**, 386.
(118) Gao, M. Y.; Richter, B.; Kirstein, S. *Adv. Mater.* **1997**, *9*, 802.
(119) Coe, S.; Woo, W. K.; Bawendi, M.; Bulovic, V. *Nature* **2002**, *420*, 800-803.
(120) Gao, M. Y.; Richter, B.; Kirstein, S. *Syn. Met.* **1999**, *102*, 1213-1214.
(121) Schlamp, M. C.; Peng, X. G.; Alivisatos, A. P. *J. Appl. Phys.* **1997**, *82*, 5837-5842.
(122) Murray, C. B.; Kagan, C. R.; Bawendi, M. G. *Science* **1995**, *270*, 1335-1338.
(123) Zehner, R. W.; Lopes, W. A.; Morkved, T. L.; Jaeger, H.; Sita, L. R. *Langmuir* **1998**, *14*, 241.
(124) Zehner, R. W.; Sita, R. *Langmuir* **1999**, *15*, 6139.
(125) Thompson, R. B.; Ginzburg, V. V.; Matsen, M. W.; Balazs, A. C. *Science* **2001**, *292*, 2469-2472.
(126) Förster, S.; Antonietti, M. *Adv. Mater.* **1998**, *10*, 195.
(127) Spatz, J. P.; Roescher, A.; Möller, M. *Adv. Mater.* **1996**, *8*, 337.
(128) Moffitt, M.; Eisenberg, A. *Macromolecules* **1997**, *30*, 4363.
(129) Lopes, W. A.; Jaeger, H. M. *Nature* **2001**, *414*, 735.
(130) Mansky, P.; Liu, Y.; Huang, E.; Russell, T. P.; Hawker, C. *Science* **1997**, *275*.
(131) Huang, E.; Rockford, L.; Russell, T. P.; Hawker, C. J. *Nature* **1998**, *395*, 757.
(132) Böker, A.; Lin, Y.; Chiapperini, K.; Horowitz, R.; Thompson, M.; Carreon, V.; Xu, T.; Abetz, C.; Skaff, H.; Dinsmore, A. D.; Emrick, T.; Russell, T. P. *Nat. Mater.* **2004**, *3*, 302 - 306.
(133) Widawski, G.; Rawiso, M.; Francois, B. *Nature* **1994**, *369*, 387.
(134) Srinivasarao, M.; Collings, D.; Philips, A.; Patel, S. *Science* **2001**, *292*, 79.
(135) Stenzel-Rosenbaum, M. H.; Davis, T. P.; Fane, A. G.; Chen, V. *Angew. Chem. Int. Ed.* **2001**, *40*, 3428.
(136) Misner, M. J.; Skaff, H.; Emrick, T.; Russell, T. P. *Adv. Mater* **2002**, *15*, 221-224.
(137) Yin, Y.; Lu, Y.; Gates, B.; Xia, Y. *J. Am. Chem. Soc.* **2001**, *123*, 8718.
(138) Gaudin, A. M. *Flotation*; McGraw Hill Inc.: York, 1957.

(139) Pieranski, P. *Phys. Rev. Lett.* **1980**, *45*, 569.
(140) Velev, O. D.; Furusawa, K.; Nagayama, K. *Langmuir* **1996**, *12*, 2374.
(141) Dinsmore, A. D.; Hsu, M. F.; Nikolaides, M. G.; Marquez, M.; Bausch, A. R.; Weitz, D. A. *Science* **2002**, *298*, 1006.
(142) Lin, Y.; Skaff, H.; Emrick, T.; Dinsmore, A. D.; Russell, T. P. *Science* **2003**, *299*, 226.
(143) Lobkovsky, A.; Gentges, S.; Li, H.; Morse, D.; Witten, T. *Science* **1995**, *270*, 1482.
(144) Chen, Y. F.; Ji, T. H.; Rosenzweig, Z. *Nano Letters* **2003**, *3*, 581-584.
(145) Barrientos, A. G.; de la Fuente, J. M.; Rojas, T. C.; Fernandez, A.; Penades, S. *Chemistry-a European Journal* **2003**, *9*, 1909-1921.
(146) A modification of the procedure developed by the Grubbs group was used to synthesize catalyst 3. More details on this synthesis will be discussed in a later publication.
(147) Lin, Y.; Böker, A.; Skaff, H.; Cookson, D.; Dinsmore, A. D.; Emrick, T.; Russell1, T. P. *Langmuir* **2004**, *in press*.
(148) Lin, Y.; Skaff, H.; Boker, A.; Dinsmore, A. D.; Emrick, T.; Russell, T. P. *J. Am. Chem. Soc.* **2003**, *125*, 12690-12691.
(149) Peng, Z. A.; Peng, X. G. *J. Am. Chem. Soc.* **2001**, *123*, 183-184.
(150) Peng, Z. A.; Peng, X. G. *J. Am. Chem. Soc.* **2002**, *124*, 3343-3353.

BIBLIOGRAPHY

Aldana, J.; Wang, A.; Peng, X. *J. Am. Chem. Soc.* **2001**, *123*, 8844.

Alivisatos, A. P.; Harris, T. D.; Brus, L. E.; Jayaraman, A. *J. Chem. Phys.* **1988**, *89*, 5979-5982.

Balazs, A.; Ginzburg, V. V.; Qui, F.; Peng, G.; Jasnow, D. *J. Phys. Chem. B* **2000**, *104*, 3411-3422.

Barrientos, A. G.; de la Fuente, J. M.; Rojas, T. C.; Fernandez, A.; Penades, S. *Chemistry-a European Journal* **2003**, *9*, 1909-1921.

Bawendi, M. G.; Wilson, W. L.; Rothberg, L.; Carroll, P. J.; Jedju, T. M.; Steigerwald, M. L.; Brus, L. E. *Phys. Rev. Lett.* **1990**, *65*, 1623-1626.

Becerra, L. R.; Murray, C. B.; Griffin, R. G.; Bawendi, M. G. *J. Chem. Phys.* **1994**, *100*, 3297-3300.

Boal, A. K.; Ilhan, F.; DeRouchey, J. E.; Thurn-Albrecht, T.; Russell, T. P.; Rotello, V. M. *Nature* **2000**, *404*, 746-748.

Bockstaller, M. R.; Lapetnikov, Y.; Margel, S.; Thomas, E. L. *J. Am. Chem. Soc.* **2003**, *125*, 5276-5277.

Böker, A.; Lin, Y.; Chiapperini, K.; Horowitz, R.; Thompson, M.; Carreon, V.; Xu, T.; Abetz, C.; Skaff, H.; Dinsmore, A. D.; Emrick, T.; Russell, T. P. *Nat. Mater.* **2004**, *3*, 302 - 306.

Bosman, A. W.; Heumann, A.; Klaerner, G.; Benoit, D.; Frechet, J. M. J.; Hawker, C. J. *J. Am. Chem. Soc.* **2001**, *123*, 6461-6462.

Bowen Katari, J. E.; Colvin, V. L.; Alivisatos, A. P. *J. Phys. Chem.* **1994**, *98*, 4190.

Brott, L. L.; Naik, R. R.; Pikas, D. J.; Kirkpatrick, S. M.; Tomlin, D. W.; Whitlock, P. W.; Clarson, S. J.; Stone, M. O. *Nature* **2001**, *413*, 291-293.

Brown, T. L.; Swaminathan, S.; Chandrasekar, S.; Compton, W. D.; King, A. H.; Trumble, K. P. *J. Mater. Res.* **2002**, *17*, 2484-2488.

Bruchez, M.; Maronne, M.; Gin, P.; Weiss, S.; Alivisatos, A. P. *Science* **1998**, *281*, 2013.

Brus, L. *J. Phys. Chem. Sol.* **1998**, *59*, 459-465.

Brus, L. *Appl. Phys- a Mater. Sci.& Proc.* **1991**, *53*, 465-474.

Brus, L. E.; Szajowski, P. F.; Wilson, W. L.; Harris, T. D.; Schuppler, S.; Citrin, P. H. *J. Am. Chem. Soc.* **1995**, *117*, 2915-2922.

Bunning, T. J.; Kirkpatrick, S. M.; Natarajan, L. V.; Tondiglia, V. P.; Tomlin, D. W. *Chem. Mater.* **2000**, *12*, 2842.

Calander, N.; Willander, M. *Phys. Rev. Lett.* **2002**, *89*, 143603.

Carrot, G.; Scholz, S. M.; Plummer, C. J. G.; Hilborn, J. G.; Hedrick, J. L. *Chem. Mater.* **1999**, *11*, 3571-3577.

Chen, C. C.; Herhold, A. B.; Johnson, C. S.; Alivisatos, A. P. *Science* **1997**, *276*, 398-401.

Chen, W.; McCarthy, T. J. *Macromolecules* **1998**, *31*, 3648-3655.

Chen, Y. F.; Ji, T. H.; Rosenzweig, Z. *Nano Lett.* **2003**, *3*, 581-584.

Chestnoy, N.; Hull, R.; Brus, L. E. *J. Chem. Phys.* **1986**, *85*, 2237-2242.

Chiefari, J.; Chong, Y. K.; Ercole, F.; Krstina, J.; Jeffery, J.; Le, T. P. T.; Mayadunne, R. T. A.; Meijs, G. F.; Moad, C. L.; Moad, G.; Rizzardo, E.; Thang, S. H. *Macromolecules* **1998**, *31*.

Coe, S.; Woo, W. K.; Bawendi, M.; Bulovic, V. *Nature* **2002**, *420*, 800-803.

Colvin, V. L.; Schlamp, M. C.; Alivisatos, A. P. *Nature* **1994**, *370*, 354-357.

Dabbousi, B. O.; RodriguezViejo, J.; Mikulec, F. V.; Heine, J. R.; Mattoussi, H.; Ober, R.; Jensen, K. F.; Bawendi, M. G. *J. Phys. Chem. B* **1997**, *101*, 9463-9475.

Dameron, C. T.; Reese, R. N.; Mehra, R. K.; Kortan, A. R.; Carroll, P. J.; Steigerwald, M. L.; Brus, L. E.; Winge, D. R. *Nature* **1989**, *338*, 596-597.

De Schryver, F. C. *Pure and App. Chem.* **1998**, *70*, 2147.

Dinsmore, A. D.; Hsu, M. F.; Nikolaides, M. G.; Marquez, M.; Bausch, A. R.; Weitz, D. A. *Science* **2002**, *298*, 1006.

Empedocles, S.; Bawendi, M. *Acct. Chem. Res.* **1999**, *32*, 389-396.

Empedocles, S. A.; Bawendi, M. G. *Science* **1997**, *278*, 2114-2117.

Farmer, S. C.; Patten, T. E. *Chem. Mater.* **2001**, *13*, 3920-3926.

Fogg, D. E.; Radzilowski, L. H.; Blanski, R.; Schrock, R. R.; Thimas, E. L. *Macromolecules* **1997**, *30*, 417-426.

Fojtik, A.; Weller, H.; Koch, U.; Henglein, A. *Berichte Der Bunsen-Gesellschaft-Physical Chemistry Chemical Physics* **1984**, *88*, 969-977.

Förster, S.; Antonietti, M. *Adv. Mater.* **1998**, *10*, 195.

Gao, M. Y.; Richter, B.; Kirstein, S. *Adv. Mater.* **1997**, *9*, 802.

Gao, M. Y.; Richter, B.; Kirstein, S. *Synthetic Metals* **1999**, *102*, 1213-1214.

Gaponenko, S. v. *Optical Porperties of Semiconductor Nanocrystals*; Cambridge University Press: New York, 1998.

Gaudin, A. M. *Flotation*; McGraw Hill Inc.: York, 1957.

Gerion, D.; Pinaud, F.; Williams, S. C.; Parak, W. J.; Zanchet, D.; Weiss, S.; Alivisatos, A. P. *J. Phys. Chem. B* **2001**, *105*, 8861-8871.

Gerion, D.; Pinaud, F.; Williams, S. C.; Parak, W. J.; Zanchet, D.; Weiss, S.; Alivisatos, A. P. *J. Phys. Chem. B* **2001**, *105*, 8861-8871.

Godovsky, D. Y. In *Biopolymers/Pva Hydrogels/Anionic Polymerisation Nanocomposites*, 2000; Vol. 153, pp 163-205.

Gu, Y. D.; Nederberg, F.; Kange, R.; Shah, R. R.; Hawker, C. J.; Moller, M.; Hedrick, J. L.; Abbott, N. L. *Chemphyschem* **2002**, *3*, 448.

Guo, W. H.; Li, J. J.; Wang, Y. A.; Peng, X. G. *J. Am. Chem. Soc.* **2003**, *125*, 3901-1909.

Guzelian, A. A.; Katari, J. E. B.; Kadavanich, A. V.; Banin, U.; Hamad, K.; Juban, E.; Alivisatos, A. P.; Wolters, R. H.; Arnold, C. C.; Heath, J. R. *J. Phys. Chem.* **1996**, *100*, 7212-7219.

Han, M.; Gao, X.; J.Z., S.; Nie, S. *Nature Biotechnology* **2001**, *19*, 631.

Harris, J. M. *Poly(ethylene glycol) Chemistry: Biotechnical and Biomedical Applications*; Plenum Press: New York, 1992.

Harrison, M. T.; Kershaw, S. V.; Burt, M. G.; Rogach, A. L.; Kornowski, A.; Eychmuller, A.; Weller, H. *Pure and Applied Chemistry* **2000**, *72*, 295-307.

Haw, M. D.; Poon, W. C. K.; Pusey, P. N. *Phys. Rev. E* **1997**, *56*, 1918-1933.

Hong, L.; Vilar, R. M.; Wang, Y. M. *J. Mater. Sci.* **1997**, *32*, 5545-5550.

Htoo, M. S., Ed. *Microelectronic Polymers*; M. Dekker, 1989.

Huang, E.; Rockford, L.; Russell, T. P.; Hawker, C. J. *Nature* **1998**, *395*, 757.

Hummel, R. E. *Electronic Properties of Materials*; 2 ed.; Springer-Verlag, 1993.

Huynh, W. U.; Dittmer, J. J.; Alivisatos, A. P. *Science* **2002**, *295*, 2425-2427.

Huynh, W. U.; Peng, X. G.; Alivisatos, A. P. *Adv. Mater* **1999**, *11*, 923.

Juang, A.; Scherman, O. A.; Grubbs, R. H.; Lewis, N. S. *Langmuir* **2001**, *17*, 1321-1323.

Klabunde, K. J. *Nanoscale Materials in Chemistry*; John Wiley & Sons, 2001.

Lai , J. T.; Filla, D.; Shea, R. *Macromolecules* **2002**, *35*, 6754-6756.

Leatherdale, C. A.; Kagan, C. R.; Morgan, N. Y.; Empedocles, S. A.; Kastner, M. A.; Bawendi, M. G. *Phys. Rev. B* **2000**, *62*, 2669-2680.

Lee, J.; Sundar, V. C.; Heine, J. R.; Bawendi, M. G.; Jensen, K. F. *Adv. Mater* **2000**, *12*, 1311-1311.

Li, L. S.; Hu, J. T.; Yang, W. D.; Alivisatos, A. P. *Nano Letters* **2001**, *1*, 349-351.

Lin, Y.; Böker, A.; Skaff, H.; Cookson, D.; Dinsmore, A. D.; Emrick, T.; Russell1, T. P. *Langmuir* **2004**, *in press*.

Lin, Y.; Skaff, H.; Boker, A.; Dinsmore, A. D.; Emrick, T.; Russell, T. P. *J. Am. Chem. Soc.* **2003**, *125*, 12690-12691.

Lin, Y.; Skaff, H.; Emrick, T.; Dinsmore, A. D.; Russell, T. P. *Science* **2003**, *299*, 226-229.

Littke, A. F.; Fu, G. C. *J. Am. Chem. Soc.* **2001**, *123*, 6989-7000.

Liu, J.; Tanaka, T.; Sivula, K.; Alivisatos, A. P.; Frechet, J. M. J. *J. Am. Chem. Soc.* **2004**, *126*, 6550-6551.

Lobkovsky, A.; Gentges, S.; Li, H.; Morse, D.; Witten, T. *Science* **1995**, *270*, 1482.
Lopes, W. A.; Jaeger, H. M. *Nature* **2001**, *414*, 735.

Mamedov, A. A.; Belov, A.; Giersig, M.; Mamedova, N. N.; Kotov, N. A. *J. Am. Chem. Soc.* **2001**, *123*, 7738-7739.

Mansky, P.; Liu, Y.; Huang, E.; Russell, T. P.; Hawker, C. *Science* **1997**, *275*.

Marcus, M. A.; Flood, W.; Stiegerwald, M.; Brus, L.; Bawendi, M. *J. Phy.Chem.* **1991**, *95*, 1572-1576.

Mattoussi, H.; Mauro, J. M.; Goldman, E. R.; Anderson, G. P.; Sundar, V. C.; Mikulec, F. V.; Bawendi, M. G. *J. Am. Chem. Soc.* **2000**, *122*, 12142-12150.

Michalet, X.; Pinaud, F.; Lacoste, T. D.; Dahan, M.; Bruchez, M. P.; Alivisatos, A. P.; Weiss, S. *Single Molecules* **2001**, *2*, 261-276.

Milliron, D. J.; Alivisatos, A. P.; Pitois, C.; Edder, C.; Fréchet, J. M. J. *Adv. Mater.* **2003**, *15*, 58.

Misner, M. J.; Skaff, H.; Emrick, T.; Russell, T. P. *Adv. Mater* **2002**, *15*, 221-224.

Moffitt, M.; Eisenberg, A. *Macromolecules* **1997**, *30*, 4363.

Moffitt, M.; McMahon, L.; Pessel, V.; Eisenberg, A. *Chem. Mater.* **1995**, *7*, 1185-1192.

Moller, M.; Nederberg, F.; Lim, L. S.; Kange, R.; Hawker, C. J.; Hedrick, J. L.; Gu, Y. D.; Shah, R.; Abbott, N. L. *J. of Polym. Sci. A* **2001**, *39*, 3529-3538.

Murray, C. B.; Kagan, C. R.; Bawendi, M. G. *Science* **1995**, *270*, 1335-1338.

Murray, C. B.; Norris, D. J.; Bawendi, M. G. *J. Am. Chem. Soc.* **1993**, *115*, 8706-8715.

Murray, C. D.; Kagan, C. R.; Bawendi, M. G. *Annu. Rev. Mater. Sci.* **2000**, *30*, 545.

Nirmal, M.; Brus, L. *Acct. Chem. Res.* **1999**, *32*, 407-414.

Nirmal, M.; Dabbousi, B. O.; Bawendi, M. G.; Macklin, J. J.; Trautman, J. K.; Harris, T. D.; Brus, L. E. *Nature* **1996**, *383*, 802-804.

Novak, B. M.; Risse, W.; Grubbs, R. H. *Adv. Poly. Sci.* **1992**, *102*, 47-72.

Parak, W. J.; Gerion, D.; Zanchet, D.; Woerz, A. S.; Pellegrino, T.; Michael, C.; Williams, S. C.; Seitz, M.; Bruehl, R. E.; Bryant, Z.; Bustamante, C.; Bertozzi, C. R.; Alivisatos, A. P. *Chem. Mater.* **2002**, *14*, 2113.

Pathak, S.; Choi, S. K.; Arnheim, N.; Thompson, M. E. *J. Am. Chem. Soc.* **2001**, *123*, 4103-4104.

Pathak, S.; Choi, S. K.; Arnheim, N.; Thompson, M. E. *J. Am. Chem Soc.*. **2001**, *123*, 4103-4104.

Peng, X. G.; Schlamp, M. C.; Kadavanich, A. V.; Alivisatos, A. P. *J. Am. Chem. Soc.* **1997**, *119*, 7019-7029.

Peng, Z. A.; Peng, X. G. *J. Am. Chem. Soc.* **2001**, *123*, 183-184.

Peng, Z. A.; Peng, X. G. *J. Am. Chem. Soc.* **2002**, *124*, 3343-3353.

Petrash, S.; Cregger, T.; Zhao, B.; Pokidysheva, E.; Foster, M. D.; Brittain, W. J.; Sevastianov, V.; Majkrzak, C. F. *Langmuir* **2001**, *17*, 7645-7651.

Pieranski, P. *Phys. Rev. Lett.* **1980**, *45*, 569.

Qi, L.; Colfen, H.; Antonietti, M. *Nano Letters* **2001**, *1*, 61-65.

Qu, L. H.; Peng, X. G. *J. Am. Chem. Soc.* **2002**, *124*, 2049-2055.

Qu, L. H.; Peng, Z. A.; Peng, X. G. *Nano Letters* **2001**, *1*, 333-337.

Rabani, E.; Hetenyi, B.; Berne, B. J.; Brus, L. E. *J. Chem. Soc,* **1999**, *110*, 5355-5369.

Rajagopalan, P.; McCarthy, T. J. *Macromolecules* **1998**, *31*, 4791-4797.

Rehahn, M.; Schluter, A. D.; Feast, W. J. *Synthesis* **1998**, 386.

Rizzardo, E.; Chiefari, J.; Chong, B. Y. K.; Ercole, F.; Krstina, J.; Jeffery, J.; Le, T. P. T.; Mayadunne, R. T. A.; Meijs, G. F.; Moad, C. L.; Moad, G.; Thang, S. H. *Macromol. Symp.* **1999**, *143*, 291-307.

Robelek, R.; Niu, L.; Schmid, E. L.; Knoll, W. *Anal. Chem.* **2004**, *76*, 6160-6165.

Rosenthal, S. J.; Tomlinson, I.; Adkins, E. M.; Schroeter, S.; Adams, S.; Swafford, L.; McBride, J.; Wang, Y.; DeFelice, L. J.; Blakely, R. D. *J. Am. Chem. Soc.* **2002**, *124*, 4586.

Rossetti, R.; Ellison, J. L.; Gibson, J. M.; Brus, L. E. *J. Chem . Phys.* **1984**, *80*, 4464-4469.

Salafsky, J. S. *Solid-State Electronics* **2001**, *45*, 53-58.

Sankaran, V.; Cummins, C. C.; Schrock, R. R.; Cohen, R. E.; Silbey, R. J. *J. Am. Chem. Soc.* **1990**, *112*, 6858-6859.

Schlamp, M. C.; Peng, X. G.; Alivisatos, A. P. *J. Appl. Phys.* **1997**, *82*, 5837.

Schwab, P.; Grubbs, R. H.; Ziller, J. W. *J. Am. Chem. Soc.* **1996**, *118*, 100.

Shim, M.; Guyot-Sionnest, P. *Phys. Rev. B* **2001**, *6424*, 245342.

Shim, M.; Wang, C. J.; Guyot-Sionnest, P. *J. Phys. Chem. B* **2001**, *105*, 2369-2373.

Shim, M.; Wang, C. J.; Norris, D. J.; Guyot-Sionnest, P. *Mrs Bulletin* **2001**, *26*, 1005-1008.

Skaff, H.; Ilker, M. F.; Coughlin, E. B.; Emrick, T. *J. Am. Chem. Soc.* **2002**, *124*, 5729-5733.

Skaff, H.; Sill, K.; Emrick, T. *J. Am. Chem. Soc.* **2004**, *126*, 11322-11325.

Sneh, O.; Clark-Phelps, R. B.; Londergan, A. R.; Winkler, J.; Seidel, T. E. *Thin Solid Films* **2002**, *402*, 248-261.

Spatz, J. P.; Roescher, A.; Möller, M. *Adv. Mater.* **1996**, *8*, 337.
Srinivasarao, M.; Collings, D.; Philips, A.; Patel, S. *Science* **2001**, *292*, 79.

Steigerwald, M. L.; Alivisatos, A. P.; Gibson, J. M.; Harris, T. D.; Kortan, R.; Muller, A. J.; Thayer, A. M.; Duncan, T. M.; Douglass, D. C.; Brus, L. E. *J. Am. Chem. Soc.* **1988**, *110*, 3046-3050.

Steigerwald, M. L.; Brus, L. E. *Annual Review of Materials Science* **1989**, *19*, 471-495.

Stenzel-Rosenbaum, M. H.; Davis, T. P.; Fane, A. G.; Chen, V. *Angew. Chem. Int. Ed.* **2001**, *40*, 3428.

Thompson, R. B.; Ginzburg, V. V.; Matsen, M. W.; Balazs, A. C. *Science* **2001**, *292*, 2469-2472.

Townsend, P.; Olivares, J. *Appl. Surf. Sci.* **1997**, *110*, 275-282.

Trnka, T. M.; Grubbs, R. H. *Acct. Chem. Res.* **2001**, *34*, 18-29.

Tully, D. C.; Wilder, K.; Frechet, J. M. J.; Trimble, A. R.; Quate, C. F. *Adv. Mater* **1999**, *11*, 314-318.

Velev, O. D.; Furusawa, K.; Nagayama, K. *Langmuir* **1996**, *12*, 2374.

Wang, Y. A.; Li, J. J.; Chen, H.; Peng, X. G. *J. Am. Chem. Soc.* **2002**, *124*, 2293-2298.

Watson, K. J.; Zhu, J.; Nguyen, S. T.; Mirkin, C. A. *Pure Appl. Chem.* **2000**, *72*, 67-72.

Widawski, G.; Rawiso, M.; Francois, B. *Nature* **1994**, *369*, 387.

Williams, R. H.; Hamilton, L. A. *J. Am. Chem. Soc.* **1952**, *74*, 5418.

Yeh, S. W.; Wei, K. H.; Sun, Y. S.; Jeng, U. S.; Liang, K. S. *Macromolecules* **2003**, *36*, 7903-7907.

Yin, Y.; Lu, Y.; Gates, B.; Xia, Y. *J. Am. Chem. Soc.* **2001**, *123*, 8718.

Zehner, R. W.; Lopes, W. A.; Morkved, T. L.; Jaeger, H.; Sita, L. R. *Langmuir* **1998**, *14*, 241.

Zehner, R. W.; Sita, R. *Langmuir* **1999**, *15*, 6139.

Zhao, B.; Brittain, W. J. *Macromolecules* **2000**, *33*, 8813-8820.

Zhao, H. Y.; Douglas, E. P.; Harrison, B. S.; Schanze, K. S. *Langmuir* **2001**, *17*, 8428-8433.

Zhou, Q. Y.; Wang, S. X.; Fan, X. W.; Advincula, R.; Mays, J. *Langmuir* **2002**, *18*, 3324-3331.